Okinawa Institute of Science and Technology

Graduate University

Thesis submitted for the degree of

Doctor of Philosophy

Study on Alteration of Cellular Phenotypes and Processes in Cancer Using Exogenous Biological Agents

by

Hong Huat Hoh

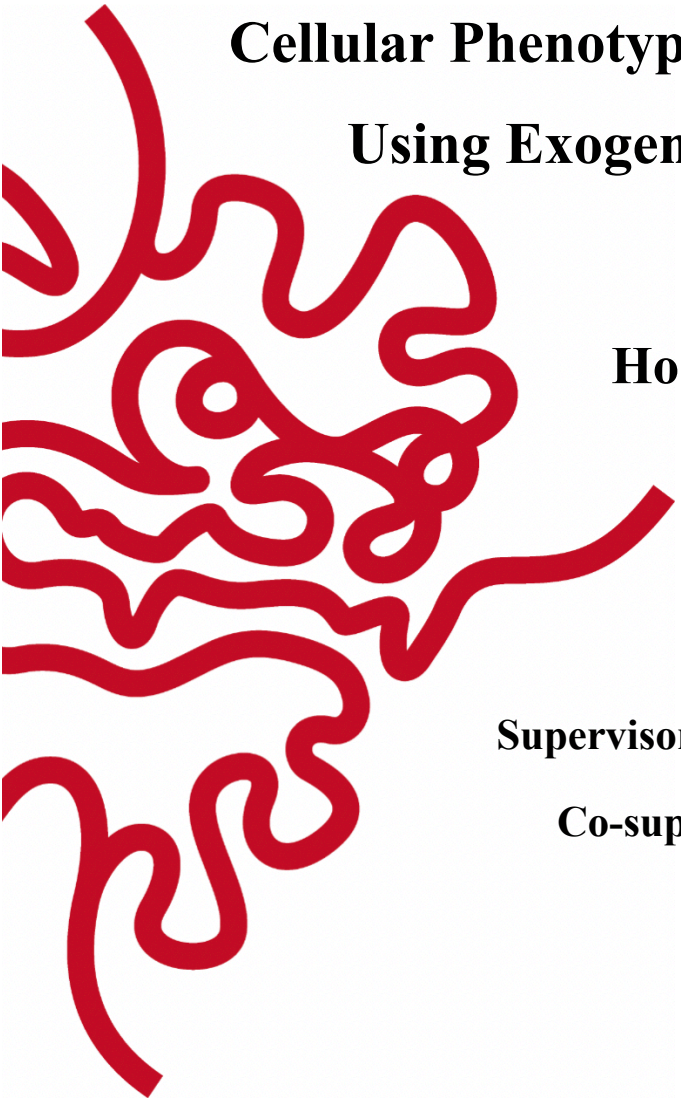

Supervisor: Tadashi, Yamamoto

Co-supervisor: Ye, Zhang

August 2020

Declaration of Original and Sole Authorship

I, **Hong Huat Hoh**, declare that this thesis entitled '**Study on Alteration of Cellular Phenotypes and Processes in Cancer Using Exogenous Biological Agents**' and the data presented in it are original and my own work.

I confirm that:

- This work was done solely while I am a candidate for the research degree at the Okinawa Institute of Science and Technology Graduate University, Japan.
- No part of this work has previously been submitted for a degree at this or any other university.
- References to the work of others have been clearly acknowledged. Quotations from the work of others have been clearly indicated, and attributed to them.
- In cases where others have contributed to part of this work, such contribution has been clearly acknowledged and distinguished from my own work.
- None of this work has been previously published elsewhere.

Signature: 

Date: August 14, 2020

Dedication

This thesis is dedicated to the late Dr. MARIUSZ GAJDA,

my dearest Professor from Kraków, Poland.

You had deeply inspired and introduced me to the world of biomedical research. I am forever indebted to the support, motivation, and encouragement you had showered me from afar.

You will be missed forever.

Abstract

Cellular and genetic heterogeneity contributes to the complexity of cancer which poses challenges for cancer therapy. For instance, epithelial-to-mesenchymal transition (EMT) is a physiological phenomenon that was adopted to neoplasm to describe the possibility of carcinoma cells in acquiring mesenchymal traits, leading to invasion and metastatic dissemination. These EMT-induced tumor cells acquire cancer stem cells (CSCs) properties and contribute to heterogeneity within a tumor microenvironment. My thesis is set out to tackle the abovementioned phenomenon, with a common goal of investigating the potential of using exogenous biological agents in modifying the cellular phenotypes and processes of cancer. Firstly, I demonstrated the molecular mechanism and the ability of altering the stem cell property of breast cancer cells by downregulating CD44 molecules using exogenous miRNAs. Secondly, I investigated the potential of bioinspired laminin-derived self-assembling peptides to alter the microenvironment and cellular processes including metabolism of cancer cells for anti-metastatic treatment in pancreatic cancer. Both studies utilized comprehensive molecular biology approaches in elucidating the functional changes and mechanisms behind the therapeutic effects of biological agents using relevant cancer cell lines and animal xenotransplantation models. This thesis provides insights into cancer cell plasticity which can be harnessed for cancer therapy.

Disclaimer

Due to the collaborative nature of the research work, this thesis is presented in the following order. I apologize in advance for the occasional incoherence and gaps in the presentation.

1. Literature review presenting the overview and introduction to the common thesis research theme, focusing on breast and pancreatic cancer (**Chapter 1**)

2. Research findings for the first part of the thesis (**Chapter 2 & 3**) on cancer stem cell regulation in breast cancer (This part of the thesis was conducted under the supervision of Professor Tadashi Yamamoto)

3. Research findings for the second part of the thesis (**Chapter 4**) on preclinical therapeutic investigation of self-assembling peptides in pancreatic cancer (This part of the thesis was conducted under the supervision of Professor Ye Zhang)

Acknowledgements

I am forever grateful for the amazing peers I have met during the course of my Ph.D. study. In particular, Shukla Sarkar and Sandrine Burriel were my constant source of support who had repeatedly and unconditionally lent me their hands when I needed the most. With their incessant encouragement, the road to obtaining a Ph.D. was never a lonely journey.

Chee Wai Chua, Principal Investigator from Shanghai Jiao Tong University affiliated Renji Hospital whom I met at a workshop at Cold Spring Harbor Laboratory, New York in 2016 had been generous in providing me advice and guidance on my research.

I am thankful to my advisors, Tadashi Yamamoto and Ye Zhang for providing me the opportunities to carry out independent research in their laboratories. I would like to express my words of gratitude to the lab members, especially, Taku Ito-Kureha, Ken Matsuura, Akinori Takahashi, Saori Nishijima, Tiziana Paganini, Atsuko Sato, Nao Ohmine, Risa Ishida and Miho Tokumasu of the Cell Signal Unit and Dingze Mang of the Bioinspired Soft Matter Unit who had assisted and taught me valuable experimental techniques and approaches to answering research questions. I also thank Haojing Zou and Prof. Jian Li from the Beijing University of Chinese Medicine for the assistance in running the RNA sequencing sample preparation.

I am grateful to the Dean of Graduate School who also served in my thesis committee, Ulf Skoglund, Vice Dean of Graduate School, Misaki Takabayashi, and my academic mentor, Hidetoshi Saze for smoothly taking care of my academic matters during time of difficulties. I thank each and every graduate school staff, special thanks goes to Chiaki Chibana who supported me and made the end of my Ph.D. journey a more enduring one. I thank the Japan Society for the Promotion of Science and the Okinawa Institute of Science and Technology Graduate University for providing generous fellowship and funding for my Ph.D.

I owe thanks most of all, to my parents and family who have supported me to pursue such an unconventional path and offered words of encouragements throughout the journey.

List of Abbreviations

3'UTR	3'-untranslated region
BM	Basement membrane
bp	base pairs
CAF	Cancer-associated fibroblast
CD44s	CD44 standard isoform
CD44v	CD44 splice variant isoform
CSC	Cancer stem cell
ECM	Extracellular matrix
EGF	Epidermal growth factor
FAK	Focal adhesion kinase
GO	Gene Ontology
HB-EGF	Heparin-binding epidermal growth factor
HIF	Hypoxia-inducible factor
LDSA	Laminin-derived self-assembling
MAPK	Mitogen-activated protein kinase
miR/miRNA	microRNA
MMP	Matrix metalloproteinase
mRNA	Messenger RNA
PanIN	Pancreatic intraepithelial neoplasia
PDAC	Pancreatic ductal adenocarcinoma
PDX	Patient-derived tumor xenograft
PI3K/Akt	Phosphoinositide 3-kinase/protein kinase B
ROCK1	Rho-associated coiled-coil containing protein kinase 1
RT-PCR	real-time Polymerase Chain Reaction

SD	Standard deviation
SEM	Standard error of mean
siRNA	Small interfering RNA
TME	Tumor microenvironment
TNBC	Triple negative breast cancer
TSS	Transcription start site

Table of Contents

List of Figures

List of Tables

Chapter 1

Introduction to tumor heterogeneity and cellular plasticity in breast and pancreatic cancer

1.1 Tumor heterogeneity as a hallmark of cancer

Cancer is a highly complex and dynamic disease. One reason for its complexity is that during the course of disease, the cellular makeup of the tumor becomes more and more heterogenous as the cancer attempts to evolve for survival. As a result of the dynamic process of cancer evolution, a bulk tumor is often made up of cells harboring distinct molecular signatures, termed intratumor heterogeneity (Dagogo-Jack and Shaw, 2018) which have important clinical and therapeutic implications.

Many inherent traits of a tumor cannot be traced back to individual tumor cell and the genotype they possess, challenging the traditional notion of cell-autonomous malignant transformation that was proposed in early twentieth century (Kleppe and Levine, 2014). Though the contribution of essential somatic alterations in oncogenes or tumor suppressors in a stepwise malignant transformation still largely holds true, there is increasing evidences illuminating the diversity in the genome of cells within a tumor, thanks to the advent and widespread use of next-generation sequencing. Consequently, the dynamic of a tumor genome also brought about an emergence of a diverse microenvironment to help sustain the tumor survival and progression. Intratumor heterogeneity is now recognized as a common feature of human malignancies for its contribution to the major hallmarks of cancer, including emerging characteristics like avoiding immune destruction, deregulating cellular energetic, genome instability, and tumor-promoting inflammation (Hanahan and Weinberg, 2000, 2011). Due to its complexity, tumor heterogeneity poses a key challenge for cancer treatment.

Though genomic diversity in tumors was proposed back in 1956 (Huxley, 1956), it is not until the introduction of next-generation sequencing that more comprehensive evidence emerged to highlight the heterogenous sub-clone of cells bearing a variety of genomic alterations within a tumor. To align with the theme of this thesis research, I will review the intratumor genetic heterogeneity in the context of breast cancer and pancreatic cancer as follow.

1.2 Genomic diversity is a common feature of intratumor heterogeneity in breast and pancreatic cancers

Breast cancer has been broadly classified based on their histology or molecular characteristics. Histologically, they are categorized into in situ carcinoma and invasive carcinoma. In situ carcinoma is further subclassified into ductal (DCIS) or lobular carcinoma in situ (LCIS) while invasive carcinoma is subclassified into infiltrating ductal, invasive lobular, ductal/lobular, mucinous, tubular, medullary and papillary carcinomas (Malhotra et al., 2010). On the other hand, breast cancer is also stratified according to their molecular markers such as estrogen receptor (ER), progesterone receptor (PR) and ErbB2 (Her2/neu) receptor into the following subtypes: basal-like, ErbB2^{+}, normal breast like, Luminal Type A, Luminal Type B and claudin-low (Perou et al., 2000; Sørlie et al., 2001; Prat et al., 2010). These major classifications had driven development of specific therapeutic strategies that tailor to the tumor subtype, for instance, hormonal therapies, HER2-targeting agents, and cytotoxic chemotherapy for triple-negative subtype (tumors that do not express ER, PR and ErbB2). No matter how successful the therapies are for these tumors, some patients still relapse and present with resistance to chemotherapy, especially common among triple-negative breast cancer (TNBC) patients. This had led to a surge of investigations into the intratumor heterogeneity of breast cancer during tumor progression.

Early study using comparative genomic hybridization demonstrated that tumor subpopulations consists of diverse patterns of chromosomal alterations including focal amplifications and deletions in the primary breast tumors and during tumor progression to lymph node metastases (Torres et al., 2007; Navin et al., 2010). Further studies into the evolution of breast cancer by whole genome analysis revealed that breast tumors generally follow a sub-clonal diversification route with a characteristic dominant lineage which undergo subsequent mutational processes before expansion happens (Nik-Zainal et al., 2012a, 2012b).

On the other hand, by applying a more rigorous approach of combining whole-genome and targeted sequencing to multiple regions of breast tumor samples, Yates and colleagues found that there is profound sub-clonal diversification with high number of point mutations and rearrangement within a tumor and suggested that chemotherapy targeting actionable mutations might expose the resistant clones that initially exist in the primary lesion (Yates et al., 2015).

The revolutionary development of single-cell genome sequencing that combines flow-sorting, whole genome amplification and next-generation sequencing offers a much closer look into the genome profile of individual cells, and provides new perspectives on tumor evolution (Navin, 2015; Zhang et al., 2016). Using single-cell sequencing, researchers found that no two individual breast tumor cells are genetically identical; chromosomal aberrations occurred through short punctuated bursts early in tumor evolution, followed by point mutations that evolved over a long period of time to generate an expansive of diverse sub-clones (Navin et al., 2011; Wang et al., 2014; Gao et al., 2016). Metastatic cells also emerged through a punctuated clonal evolution with few intermediates, challenging the conventional paradigm of a gradual clonal expansion model of tumor progression. In addition, using single-cell RNA sequencing analysis, Lee *et. al.* reported that there is significant heterogeneity, including specific RNA variants involved in microtubule stabilization and organization among individual cells that are resistant to chemotherapeutic agent (paclitaxel) in a triple-negative metastatic breast cancer cell line (Lee et al., 2014).

While examining the intratumor heterogeneity, one must also notice that tumors cells present with a dynamic plasticity in adapting to new signaling pathways under various growth and therapeutic stress conditions. Cellular plasticity which generally refers to changes in cell identity and property is a collective term used to describe the ability of tumors cells to undergo molecular and phenotypic changes during cancer progression where there is a dynamic change in genetic and epigenetic alterations, or in response to the volatile microenvironmental cues

and treatment (Yuan et al., 2019). For instance, it has been shown in a mouse tumor xenograft study that not only non-dominant sub-clone of cells are capable of stimulating growth of all tumor cells in a non-cell autonomous manner via a tumor-promoting microenvironmental signal like Interleukin-11, they can also be outgrown by a sub-clone with a higher proliferative index (Marusyk et al., 2014). The genomic landscape of metastatic lesions also underwent significant remodeling including *de novo* mutations from the primary tumor xenografts, displaying a temporal pattern of cellular plasticity during cancer progression (Ding et al., 2010). Therapeutic intervention such as chemotherapy similarly induces changes in the tumor cells. As reported by Balko and colleagues, the genomic landscape of residual tumors of TNBC after neoadjuvant treatment differed largely from their matched pre-treatment specimens (Balko et al., 2014). Another evidence of cellular plasticity is depicted by the observation of a stochastic change of tumor cells into a stem-like state from normal and neoplastic mammary epithelial cells, giving rise to a unique subpopulation of cells called cancer stem cells (CSCs) through dedifferentiation (Chaffer et al., 2011; Gupta et al., 2011). A more detailed review on breast CSCs will be presented in the following section of this chapter. Overall, these studies underscore the complex heterogeneity of breast tumors, both in spatial and temporal terms which may explain the therapeutic challenges occurred during tumor relapse or metastasis.

Similar to breast cancer, pancreatic cancer is a well-established model to study intratumor heterogeneity. The main reason for studying pancreatic cancer is the fact that it remains one of the deadliest malignancies with a dismal 5-year survival rate of less than 10%. Among the reasons that lead to its aggressiveness and poor survival rate are late detection due to the retroperitoneum anatomical position of pancreas, rapidly growing feature of the tumor mass, and most importantly, the lack of effective treatment (Hidalgo, 2010). In contrast to other malignancies, it is predicted that pancreatic cancer incidence rate will continue to rise and eventually become the second most common cause of cancer-related death worldwide before

2030 if no improvement in treatment is achieved. The mainstay of pancreatic cancer treatment is surgery whereby it is only curative in early stage or for locally advanced tumors. Chemo-radiation is the alternative treatment option when the cancer has advanced to higher stage where invasion or metastasis has had taken place. The dismal prognosis of pancreatic cancer had raised immediate attention among the cancer research community to look into the genetics and biology of pancreatic cancer.

Pancreatic adenocarcinoma (PDAC) which arises from the exocrine part of the pancreas is the most common histological type, representing approximately 85 percent of the pancreatic tumor cases. PDAC, the most aggressive phenotype was thought to progress from a neoplastic, noninvasive precursor lesion called pancreatic intraepithelial neoplasia (PanIN) (Hruban et al., 2001) through a series of acquisition of common mutations in oncogenes or tumor suppressors, including *KRAS*, *CDKN2A*, *SMAD4*, *TP53* and *BRCA2* (Hruban et al., 2000; Yamano et al., 2000). The development of genome-wide studies in the recent decades had advanced our understanding of the divergence of pancreatic cancer development and the tumor heterogeneity of PDAC. As such, exome-based stratification of PDAC samples revealed a complex and wide intertumoral heterogeneity in altered signaling pathways, chromosomal rearrangements and structural variations, copy number variations, and genetic mutations that contribute to disease progression and metastasis (Jones et al., 2008; Campbell et al., 2010; Collisson et al., 2011; Biankin et al., 2012; Waddell et al., 2015; Witkiewicz et al., 2015; Bailey et al., 2016). For instance, Campbell *et. al.* discovered that the ubiquitous *KRAS* activating mutation found in PDAC has an amplified copy numbers at specific metastatic sites like peritoneum or lung, but not in the primary tumor or other metastatic locations, indicating that heterogeneity within the core *KRAS* signaling pathway exists (Campbell et al., 2010). This finding was later reinforced by another gene-expression study using large-scale microarray data which delineated PDAC molecularly into three subtypes, namely classical, quasi-mesenchymal, and exocrine-like with

varying prognosis, and found that an array of human PDAC cell lines are represented by either classical (*KRAS*-dependent) or quasi-mesenchymal (partial or less *KRAS*-dependent) with differing sensitivity to epidermal growth factor receptor inhibitor (erlotinib) or conventional chemotherapeutic drug for PDAC (gemcitabine, a nucleoside analog) (Collisson et al., 2011). A more recent whole-genome sequencing study analyzing 100 PDAC samples reported that only one-fifth of the tested tumors are classified as 'stable', carrying less than 50 structural variations, and are often presenting with widespread aneuploidy, while the majority of the samples exhibited greater number of structural variations and non-random chromosomal damage (Waddell et al., 2015).

Apart from genetic heterogeneity, efforts looking into the epigenome landscape also yielded significant understanding in the epigenetic reprogramming in PDAC: diverse DNA methylation pattern, distinct histone marks, and alteration of the enhancer landscape in different subtypes of PDAC which drive specific malignant heterogeneity, clinical outcome and therapeutic response (Nones et al., 2014; Silverman and Shi, 2016; McDonald et al., 2017; Lomberk et al., 2018, 2019). Intriguingly, a few studies pointed out that tumor microenvironment (TME) or the tumor stroma contribute to the genetic and epigenetic heterogeneity. As such, a specific basal subtype of PDAC with an activated stroma gene expression profile was determined (Collisson et al., 2011; Moffitt et al., 2015). This basal subtype tumors were found to be associated with upregulation of a gene responsible for chemo-resistance, CYP3A5 (Noll et al., 2016), and possess a distinct epigenetic landscape around genes that are highly oncogenic and are related to epithelial-to-mesenchymal transition (EMT) (Lomberk et al., 2018). Overall, these studies not only provided insights into the remarkable intratumor genetic and epigenetic heterogeneity of PDAC, they also highlighted the challenge of therapeutic difficulty and relevance of personalized medicine for PDAC.

It is important to note that the phenotypic heterogeneity of most cancers cannot be solely attributed to the diverse genetic or epigenetic make-up of tumors. Two models provide further explanation for the phenotypic and functional heterogeneity among cancer cells in certain tumors: 1) cancer stem cell model and 2) diversity of tumor microenvironment (TME). I will discuss these two models further using breast and pancreatic cancer as the representative example for each model.

1.3 Cancer stem cells contribute to the intratumor heterogeneity and cellular plasticity of breast cancer

Cancer stem cells (CSCs) or tumor-initiating cells constitute a small portion of the bulk of tumor. They were first described in human acute myeloid leukemia in 1994 (Lapidot et al., 1994), but it was not until 2003 where the first identification of CSCs in solid tumor, i.e., breast cancer was reported (Al-Hajj et al., 2003). Serial tumor transplantation assay combined with limiting dilution assay are the gold standards to identify the cell-of-origin of cancers and to assess the CSCs' self-renewal property as well as tumorigenic potential by testing their ability to regenerate new tumors and to maintain tumor propagation in mice. By transplanting increasingly diluted single-cell preparations, limiting dilution assay enables the determination of minimum CSC frequency that can regenerate a xenograft tumor. Like adult tissue stem cells, CSCs can be identified and isolated based on specific antigen profiles. Most of these markers are also present on human embryonic stem cells or adult tissue stem cells. For breast cancer, CSCs were initially characterized by surface markers $CD44^{+}/CD24^{low/-}$ and had since been established as the minimum requirement for isolating breast CSCs (Al-Hajj et al., 2003). A plethora of other markers were later identified, including CD133, epithelial cell adhesion molecule (EpCAM), CD49f, CXCR4, and ALDH1, that are also commonly used to define CSC population in other tumors (Ginestier et al., 2007; Meyer et al., 2010; Kim and Ryu, 2017).

CD44 is a transmembrane glycoprotein that engages with many ECM proteins for tissue adhesion and migration. It has a molecular weight of 85-200 kDa and is expressed ubiquitously throughout the body tissues. Other than hyaluronan, a glycosaminoglycan which serves as the major ligand, proteins like collagen, laminin, fibronectin, osteopontin, and matrix metalloproteinases were also found to bind CD44 in various cell types (Jalkanen and Jalkanen, 1992; Underhill, 1992; Weber et al., 1996; Yu and Stamenkovic, 1999). Its interaction with these proteins had been implicated for tumor progression. Unsurprisingly, breast tumors that highly express CD44 are linked to a malignant phenotype and have significantly worse prognosis and overall survival (Tse et al., 2005; Mayer et al., 2008). CD24, on the other hand, is a 38-70 kDa mucin-type glycoprotein that is bound to the cell membrane via a glycosylphosphatidylinositol (GPI)-anchor. It binds to P-selectin, which is often found on the surfaces of endothelial cells and platelets, to regulate cell adhesion and proliferation (Aigner et al., 1995, 1997). In breast cancer, the exact role of CD24 in driving tumorigenesis and metastasis remains controversial. On the one hand, CD24 was found to be overexpressed by most primary breast carcinoma, and are associated with tumor growth and metastasis (Fogel et al., 1999; Kristiansen et al., 2003; Baumann et al., 2005). On the other hand, downregulation of CD24 both in messenger RNA (mRNA) and protein levels was associated with an invasive phenotype; cells expressing low levels of CD24 had higher tumorigenic potential in immunocompromised mice (Schindelmann et al., 2002; Schabath et al., 2006). One possible explanation to this conflicting evidence is that CD24 expression level inversely correlates with ER status, which explains the high expression of CD24 in triple-negative breast cancer cells in contrast to their ER-positive counterparts (Kaipparettu et al., 2008). Therefore, it is important to assess the relevance of the individual CSC markers before they are used to define the CSC population in different tumor subtypes. Nevertheless, the high prevalence of $CD44^{+}/CD24^{low/-}$

phenotype in breast cancer signals tumor aggressiveness and may predict poor prognosis, particularly in triple-negative breast cancer (Idowu et al., 2012; Wang et al., 2017).

Due to extensive similarities between normal stem cells and cancer stem cells, it was postulated that CSCs are derived from stem cells of normal breast tissues with deregulated signaling pathways, including Notch, WNT, Hippo, and Hedgehog signaling. However, this hierarchical model of explanation was challenged when some evidence emerged to suggest that breast CSCs and non-CSCs are interconvertible, and that phenotypic transition is common among cancer cells (Meyer et al., 2009; Chaffer et al., 2011; Gupta et al., 2011; Iliopoulos et al., 2011; Kim et al., 2013). The underlying mechanism of such interconversions can be attributed to a process called epithelial-mesenchymal transition (EMT), a key embryonic developmental program that also orchestrates cancer invasion and metastasis (*Figure 1.1*). EMT is often driven by a set of transcription factors which include Snail, Slug, TWIST1, ZEB1 and ZEB2, resulting in a loss of epithelial cell polarity and cellular adhesions (loss of E-cadherin) and an acquisition of a mesenchymal, motile phenotype (expression of vimentin and N-cadherin) (Nieto et al., 2016). Indeed, EMT was found to be responsible for the generation of breast CSCs as revealed by the high expression of EMT-associated genes in $CD44^{+}/CD24^{low/-}$ cells and an increase of CSCs in mice with an activated EMT program (Mani et al., 2008; Morel et al., 2008). Other studies analyzing the role of EMT transcription factors supported this hypothesis that an activation of EMT in cooperation with other stem cell-related transcription factors like Sox9 led to breast cancer cell plasticity and enhanced tumorigenicity (Guo et al., 2012; Chaffer et al., 2013; Hollier et al., 2013; Ye et al., 2015).

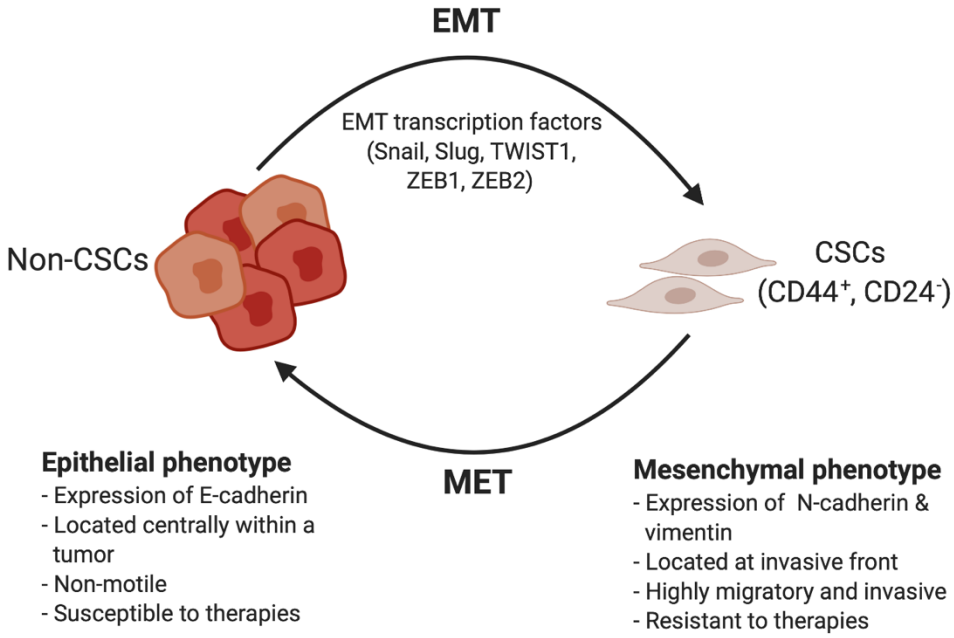

Figure 1.1 Epithelial-to-mesenchymal transition and cancer stem cells' fate transition
The transition of non-cancer stem cells (non-CSCs) to CSCs is triggered by a transcriptional program called epithelial-to-mesenchymal transition (EMT) via a set of transcription factors to drive loss of epithelial characteristics and acquisition of mesenchymal markers and traits. In breast cancer, CSCs are marked with $CD44^+$ and $CD24^-$. (*Created with BioRender.com*)

To complicate the picture further, breast CSCs were found to transition between epithelial and mesenchymal states with each occupied anatomically distinct locations- central versus tumor invasive front within a tumor, and played disparate functions in proliferation or invasion, respectively (Liu et al., 2014). The association between EMT program and CSCs can also explain the enhanced tumor colonization, invasion, and metastasis of CSCs that is equivalent to an acquired mesenchymal phenotype. It was proposed that the transition of non-CSCs into CSCs after EMT program activation may serve as the entry point for CSCs to disseminate to distant tissues and to initiate metastatic growths (Lawson et al., 2015; del Pozo Martin et al., 2015; Schmidt et al., 2015). Last but not least, it has also been discovered that breast CSCs with a distinct genetic program and residing in a unique stem cell niche are resistant to conventional chemotherapy and radiotherapy (Phillips et al., 2006; Li et al., 2008;

Creighton et al., 2009; Gómez-Miragaya et al., 2017). In particular, Creighton and colleagues demonstrated that $CD44^{+}/CD24^{low/-}$ cells retain an increased expression of mesenchymal markers in residual tumors after endocrine therapy and chemotherapy, highly suggesting the close links between EMT, CSCs and therapy resistance (Creighton et al., 2009). The unique characteristics of breast CSCs and the dynamic transition of cellular states governed by EMT program in breast cancer have undeniably posed a significant challenge for clinical treatment of metastatic and tumor relapse of breast cancers.

1.4 Desmoplastic stroma is an example of malignant tumor microenvironment best represented by pancreatic cancer

In normal tissue, the collective complex surrounding the tissue called 'stroma' is made up of cellular components (fibroblasts and immune cells), vasculatures and interstitial extracellular matrix (ECM). The stroma plays a major role in maintaining normal tissue homeostasis and architecture, controlling the dynamic of cell growth and proliferation, and is involved in signal transduction. Similarly, tumor surrounding is also composed of a microenvironment that consists of both neoplastic and non-neoplastic cells as well as a dynamic ECM to sustain tumor survival, progression and metastasis (Bissell and Hines, 2011).

One of the striking biological characteristic of PDAC in comparison to other tumor types is the extensive desmoplastic reaction around the tumor mass which make up the stroma and constitutes tumor microenvironment (Whatcott et al., 2015a). Desmoplastic reaction or desmoplasia is a pathological term used to describe the excessive stromal and fibrotic reaction as a result of inflammation that occurs around a tissue leading to a change in the extracellular architecture. In essence, desmoplasia in a tumor is analogous to a wound that does not heal, which is characterized by an activation of myofibroblasts involved in wound healing processes and extracellular matrix reorganization (Dvorak, 1986).

PDAC tumor microenvironment consists of a heterogeneous assortment of extracellular matrix proteins like collagen, fibronectin, laminin, proteoglycans and hyaluronan (*Figure 1.2*) (Feig et al., 2012; Neesse et al., 2019).

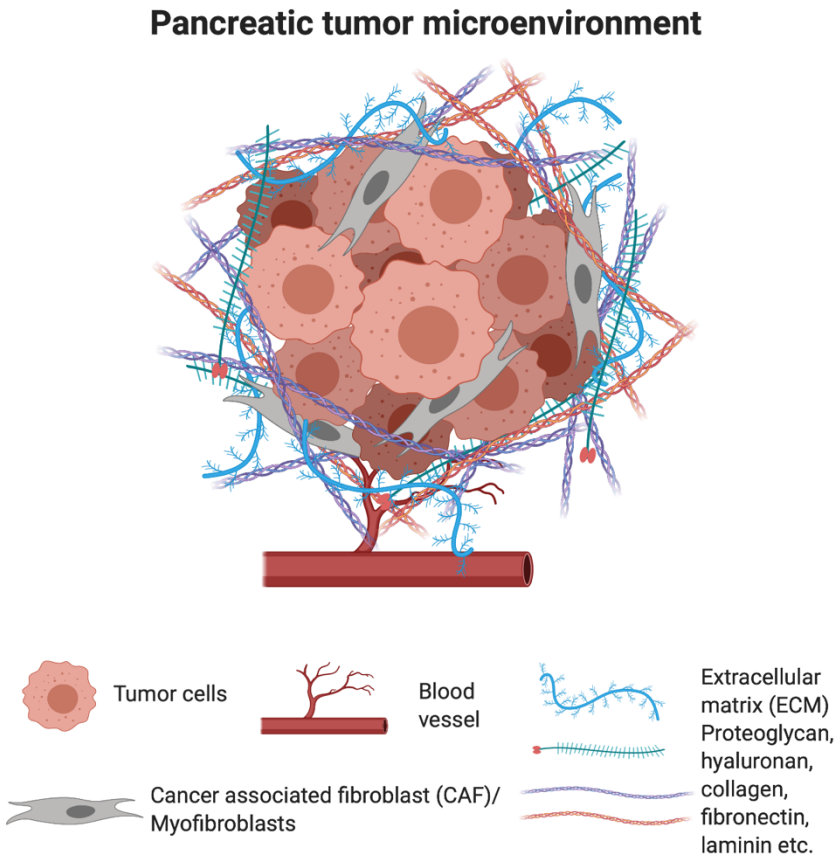

Figure 1.2 Illustration of pancreatic adenocarcinoma's tumor microenvironment (TME) Pancreatic adenocarcinomas are often surrounded by a thick layer of matrix proteins consisting of collagen, fibronectin, laminin, hyaluronan, proteoglycans, produced by activated fibroblasts, called cancer associated fibroblasts (CAFs) or myofibroblast. (*Created with BioRender.com*)

Similar to inflammatory breast tumors, fibroblasts, immune cells and blood vessels that nourishes the tumor are the cellular components that are ubiquitously found within the TME of a pancreatic tumor (*Figure 1.2*). What differentiates the TME of PDAC from other tumors is the abundance of stromal fibroblasts, known as pancreatic stellate cells or myofibroblasts. In cancer, they are often referred to as cancer associated fibroblasts (CAFs). Pancreatic stellate cells were found to be present in both normal and diseased human pancreas (Bachem et al.,

1998, 2005). They are thought to be originated from the bone marrow (Sparmann et al., 2010; Scarlett et al., 2011). In healthy pancreas, pancreatic stellate cells are considered quiescent, and present in low abundance adjacent to the basolateral sides of pancreatic acinar cells or along the pancreatic ducts and in between acini (Watari et al., 1982; Naoki, 1990; Apte et al., 1998; Bachem et al., 1998). However, when activated during acute and chronic inflammatory diseases (Apte et al., 1999), pancreatic stellate cells secrete collagen into the surrounding that drives pancreatic fibrosis (Haber et al., 1999) and progression of PDAC (Apte et al., 2004).

On the other hand, hyaluronan, a glycosaminoglycan highly accumulated in the PDAC stroma (Fries et al., 1994; Theocharis et al., 2000), which binds to cell surface receptor CD44 (Abetamann et al., 1996), is excessively synthesized and secreted by PDAC cells (Mahlbacher et al., 1992) or as a result of interaction with CAFs (Knudson et al., 1984). One particular study showed that forced expression of hyaluronan synthase 3 (HAS3) in PDAC and accumulation of extracellular hyaluronan promoted tumor growth via EMT program (Kultti et al., 2014). In addition, excess hyaluronan deposition in the TME raised tumor interstitial pressure and impaired vascular perfusion, which compromised drug delivery to the tumor (Provenzano et al., 2012; Jacobetz et al., 2013), and led to a poor prognosis for patients bearing hyaluronan-rich PDAC tumors (Cheng et al., 2013). Indeed, more evidence unveiled that a dense desmoplastic stroma in PDAC acts as a physical barrier to the delivery of chemotherapeutic drugs or to protect cancer cells from radiotherapy (Olive et al., 2009; Mantoni et al., 2011; Provenzano et al., 2012; Jacobetz et al., 2013). Another study reported that inhibition of the crosstalk between CAFs and PDAC cells via Vitamin D receptor reduced tissue inflammatory fibrotic reaction and enhanced responsiveness to the cytotoxic agent (gemcitabine) (Sherman et al., 2014). Furthermore, CAFs were also found to induce adaptive transcriptional programs in PDAC cells involving cell cycle, DNA replication, and metabolic pathway via histone acetylation, which in turn drive cancer progression (Sherman et al., 2017). In patients, an

activated stroma index, which measures the ratio of area stained for smooth muscle actin of stromal fibroblasts to the area stained for collagen or a high expression of fibroblast activation protein (FAP) in the stroma adjacent to the tumor, are indicative of poor prognosis in PDAC (Erkan et al., 2008; Cohen et al., 2008). Collectively, these findings had led to the emergence of anti-stromal therapy as a promising approach for PDAC.

However, contradictory evidence emerged later which suggested that targeting the tumor stroma by depleting the CAFs or stroma compartments in PDAC transgenic mouse models led to a more undifferentiated, aggressive phenotype (Özdemir et al., 2014; Rhim et al., 2014), arguing the rationale of targeting the tumor stroma for PDAC. This may partly explain the lack of benefits in terms of clinical outcomes of using stromal inhibitors, including hedgehog inhibitors and hyaluronidase in combination with conventional chemotherapeutic drug in metastatic PDAC, as evidenced by two recently failed clinical trials (De Jesus-Acosta et al., 2020; Tempero et al., 2020). These results caution the approach of anti-stromal strategy in PDAC treatment and demand a more comprehensive understanding of the tumor stroma using appropriate experimental approaches.

1.5 Problem statements and aims

While a great deal of knowledge had been uncovered about tumor heterogeneity and cellular plasticity, in reality, this does not align with the improvement in cancer treatment. It is clear that both CSCs and tumor microenvironment contribute to the complexity of tumor biology, and that they have important implications for clinical treatment. As shown in the example of breast cancer, dynamic transition between non-CSCs and CSCs further complicates the simplistic notion of targeting CSCs which explains the impartial efficiency of anti-CSC therapies despite years of research into them. Targeting the tumor heterogeneity as a whole would be out of the scope of this thesis, I would however take on a reductionist approach to

target the breast CSCs, an important component that brings about the tumor heterogeneity. One practical approach may involve the understanding of transcriptional regulation of CSCs and harnessing the power of transcriptional control to alter the CSCs' phenotype into a less aggressive and more differentiated state, by taking advantage of the cellular plasticity governing the transition between CSC and non-CSC state. Such approach is analogous to the successful example of differentiation therapy with all-trans retinoic acid (ATRA) in acute promyelocytic leukemia (APL). To address this hypothesis, the following aims had been set out:

Aim 1: To investigate the transcriptional control of CSC's surface marker, CD44 by microRNA (miRNA)

Aim 2: To study the effects of overexpression or inhibition of miRNAs in CSCs' control by harnessing the ability of miRNA to regulate gene transcription

Aim 3: To elucidate molecular mechanisms of the action of miRNA in altering CSCs' and non-CSCs' phenotypes

Meanwhile, the understanding of TME is paramount for the treatment of pancreatic cancer. Previous conflicting studies and failure of clinical trials of using anti-stromal therapies had taught us that we are still far from fully comprehending the PDAC's complex TME. The advent and proper optimization of physiologically relevant *in vitro* and *in vivo* PDAC models may circumvent this problem. However, these models are still hard to come by, therefore in order to preliminary test certain biological agents for their feasibility to modulate the TME as a potential PDAC treatment at a preclinical level, cancer cell lines still offer a less expensive and less time-consuming alternative. For this part of the thesis, I tested a designed biomaterial made up of biological peptides on PDAC cell lines with the following aim in mind:

Aim 4: To investigate the functional effects and mechanisms of action of an ECM-derived synthetic peptide to alter PDAC cells' phenotype

Upon addressing these aims, this thesis will provide insights into the potential approaches for modulating cellular plasticity due to CSCs and TME in hard-to-treat cancers.

Chapter 2

Role of microRNA-96 (miR-96) in controlling breast cancer stem cells

2.1 Introduction

2.1.1 Expression and role of CD44 in breast cancer stem cells

CD44 is a cell adhesion molecule that primarily functions by tethering cells to extracellular matrix ligands to activates intracellular signaling cascades. CD44, which belongs to the family of transmembrane glycoprotein, binds hyaluronan as its main ligand (Aruffo et al., 1990), but also interacts with other extracellular ligands and components of extracellular matrix to direct cell behaviors in response to the cellular environment (Ponta et al., 2003). Due to its binding to various ligands and matrix proteins, it is widely expressed in mammalian cells including lymphocytes, endothelial cells, epithelial cells, fibroblasts, and keratinocytes to regulate tissue homeostasis and function.

The cellular functions are highly dependent on the expression of CD44 variants and posttranslational modifications such as N- and O-glycosylation. Though CD44 proteins are encoded by a single, highly conserved gene containing 20 exons spanning a length of 60 kilobases, extensive alternative splicing of *CD44* transcripts between exon 5 and 14 results in an array of CD44 variant isoforms (CD44v) on top of the standard CD44 isoform (CD44s), which is devoid of all variable exons (Screaton et al., 1992). It has been reported that the variant exons are present in the stem structure of extracellular portion of CD44, and their inclusion is controlled by mitogenic signal such as mitogen-activated protein kinase (MAPK) pathway that regulates alternative splicing (König et al., 1998; Matter et al., 2002; Weg-Remers et al., 2001). The large CD44 splice variants that are often found in cancer cells have important functional significance in tumorigenesis and cancer progression. The first evidence of correlation between CD44v and metastatic potential was found in metastasizing rat pancreatic tumor and mammary adenocarcinoma cell lines in 1991 (Günthert et al., 1991). This finding was followed by the development of an anti-CD44v monoclonal antibody that effectively blocked metastatic spread into lymph nodes and lungs in a highly malignant tumor cell line (Seiter et al., 1993). Indeed,

a multitude of reports demonstrated that the expression of CD44v isoforms indicate tumor aggressiveness, high metastatic potential, and poor prognosis in breast cancer (Dall et al., 1995; Iida and Bourguignon, 1995; Kaufmann et al., 1995; Rodriguez et al., 1995).

Interestingly, plasticity between CD44 splice isoforms also exists, and it brings about significant influence on cellular activities. Comprehensive analysis of CD44 revealed that though generally overexpressed, there is a heterogenous expression pattern of CD44 isoforms found across different molecular subtypes and among CSCs that are marked by $CD44^{+}/CD24^{low/-}$ or ALDH1 (Olsson et al., 2011a). CD44 splice variants are able to undergo isoform switching to CD44s to activate Akt signaling during EMT in breast epithelial and tumor cells (Brown et al., 2011). Further studies showing the effect of EMT transcription factors, Snail, in repressing splicing factor (Reinke et al., 2012), reinforced the relationship between isoform switching of CD44 and EMT, which modulates cellular phenotype and drives breast cancer metastasis (Shapiro et al., 2011; Xu et al., 2014). Similar isoform switching mechanism was also observed in metastatic mouse mammary cells and human $CD44^{+}/CD24^{low/-}$ CSCs, but in an opposite manner from CD44s to CD44v, which led to increased lung metastases, suggesting that CD44v correlates with poor prognosis in breast cancer patients (Yae et al., 2012; Hu et al., 2017). A more recent study using data from RNA sequencing also reported that alternative splicing centrally regulates CD44 isoform expression in human breast CSCs. The researchers reported that CD44s is the predominant isoform expressed in CSCs, and is upregulated in triple-negative breast cancer; they functionally govern tumor initiation process via an activation of platelet-derived growth factor receptor beta (PDGFRβ) signaling pathway (Zhang et al., 2019a). The use of distinct experimental models, cancer cell lines versus human bulk tumor data from The Cancer Genome Atlas (TCGA) or intravenous tumor xenotransplantation versus HER2/neu breast cancer mouse model might have accounted for the conflicting findings. Nonetheless, it is well established that

overexpression of CD44 in general plays a role in tumor formation and metastasis in breast carcinoma.

Other than the presence of CD44 variant isoforms, the encoded CD44 peptide can also be post-translationally modified by N- and O-linked glycosylation. CD44v3, in particular, possesses unique motif that allows the addition of heparan sulfate and chondroitin sulfate, which in return bind growth factors like heparin-binding epidermal growth factors (HB-EGF) and basic fibroblast growth factors (bFGF) (Bennett et al., 1995; Jackson et al., 1995; Greenfield et al., 1999). As revealed by multiple molecular studies, CD44v3 also functions by interacting with coreceptors such as matrix metalloproteinase 9 (MMP-9), Tiam1, and RhoA-specific guanine nucleotide exchange factor (p115RhoGEF) that activates cytoskeleton-related Rho family of GTPase, Rac and Rho to mediate breast tumor cell migration and invasion (Bourguignon et al.,1998, 1999, 2000, 2003; Kalish et al., 1999). It is therefore not surprising that the expression of CD44v3 in breast carcinomas correlates with metastases to the lymph nodes (Ryś et al., 2003). Other studies had also demonstrated that the interaction between hyaluronan, osteopontin or matrix metalloproteinases with CD44 triggers a variety of downstream signaling molecules including phosphoinositide 3-kinase (PI3K), MAPK, transforming growth factor-β (TGF-β), and Rho GTPases that result in cancer cell growth, migration, invasion, angiogenesis, bone metastasis, and chemoresistance (Senbanjo and Chellaiah, 2017; Chen et al., 2018).

2.1.2 miRNAs are dysregulated in breast cancer

It is known that CD44 expression is regulated by various transcription factors including well-known tumor suppressor p53 (Godar et al., 2008) and epigenetic mechanism like DNA methylation (Müller et al., 2010; Rauscher et al., 2015). However, there is also a number of reports that investigated the regulation of CD44 by miRNAs. MicroRNAs are a family of

evolutionary conserved, short, single-stranded, non-coding RNAs typically made up of 19 to 25 nucleotides that can bind to the 3'-untranslated region (3'UTR) of target mRNAs to cause translational suppression and mRNA degradation (Ha and Kim, 2014). Briefly, their biogenesis involves a transcription by RNA polymerase II/III (Lee et al., 2004; Borchert et al., 2006) to generate the primary transcripts (pri-miRNAs), which are later processed by a microprocessor complex, Drosha-DGCR8 to form a hairpin structure called precursor transcripts (pre-miRNAs) (Lee et al., 2003; Gregory et al., 2004; Han et al., 2004, 2006; Morlando et al., 2008). Next, the pre-miRNAs are transported from nucleus into the cytoplasm to undergo loop-cleavage by Dicer, a RNase III (Hutvágner et al., 2001; Ketting et al., 2001; Lee et al., 2002; Basyuk et al., 2003) to generate mature miRNA/miRNA duplexes, which are loaded into an Agonaute (Ago) protein to form a RNA-induced silencing complex (RISC) where the passenger strand is cleaved leaving one mature miRNA strand (Hammond et al., 2000; Matranga et al., 2005; Miyoshi et al., 2005; Leuschner et al., 2006; Kawamata et al., 2009; Yoda et al., 2010). Once the effector complex termed miRNA-containing RNA-induced silencing complex (miRISC) containing mature miRNA, Ago protein, glycine-tryptophan protein of 182 kDa (GW182), and other proteins is formed, the mature miRNA can then exert its effect by binding to the 3'UTR of target mRNAs complementary to the miRNA's seed sequence (nucleotide 2 to 8 from the 5'-end of miRNA) (Lai, 2002; Lewis et al., 2003; Eulalio et al., 2008; Filipowicz et al., 2008; Fabian and Sonenberg, 2012). As a result of this interaction, deadenylase complex CCR4-NOT or PAN2-PAN3 is recruited to shorten the poly(A) tail of target mRNA to induce mRNA degradation or translational repression (Yamashita et al., 2005; Wu et al., 2006). Due to the short seed sequence of miRNA and their imperfect complementarity to target mRNAs in inducing translational repression (Saxena et al., 2003; Zeng et al., 2003; Doench and Sharp, 2004), it is not uncommon that a single miRNA can bind multiple target mRNAs and vice versa (Lewis et al., 2005; Lim et al., 2005). The complementary base pairing of a miRNA with

multiple mRNAs had prompted the development of computational approaches to identity putative target mRNAs of documented miRNAs (Lewis et al., 2003; John et al., 2004; Kiriakidou et al., 2004; Krek et al., 2005).

Because of the complex interaction between a miRNA and multiple mRNAs, any dysregulation in miRNA expression can lead to functional impairment of tissues causing diseases like cardiovascular disorders and cancers (Hwang and Mendell, 2006; Mendell and Olson, 2012). In human cancers, it was discovered that majority (> 50%) of miRNA genes are frequently located at cancer-associated genomic regions or fragile sites such as regions of deletion, amplification or chromosomal rearrangement (Calin et al., 2004). Two comprehensive expression studies had uncovered that there is a global dysregulation of miRNAs in human tumors, and identified common cancer-associated miRNA signatures across various human cancers (Lu et al., 2005; Volinia et al., 2006). By developing a bead-based flow cytometric profiling which uses fluorescently-labeled oligonucleotide-capture probes complementary to miRNAs of interest and coupled with polymerase chain reaction (PCR) to systematically analyzed the miRNA expression, Lu and colleagues found that miRNAs are generally downregulated in tumors compared with normal tissues, and that the clusters of miRNA profiles recapitulated the developmental origin and differentiation status of tumors (Lu et al., 2005). On the other hand, using a large-scale microarray analysis, Volinia and colleagues identified 36 overexpressed miRNAs and 21 downregulated miRNAs in tumors when compared to normal tissues; their aberrant expression correlated well with the expression of known oncogenes or tumor suppressors in each cancer type (Volinia et al., 2006). For instance, the reduced expression of miR-20a coincided with increased expression of transforming growth factor β receptor II (TGFBR2) in breast cancer which signals a poor prognosis in TNBC patients (Buck et al., 2004; Volinia et al., 2006). In parallel, a microarray expression study involving 76 human breast cancer samples that encompass various clinicopathologic states and

10 normal breast samples reported 29 deregulated miRNAs, of which 15 of them can be used as a signature to distinguish tumor from normal breast tissues and a few aberrantly expressed miRNAs, for instance, miR-21 (upregulated), let-7, miR-145 and miR-9-3 (downregulated) could suggest cancer progression to high tumor grade or metastasis (Iorio et al., 2005). Numerous studies have also found other miRNAs that are differentially expressed in breast cancer and depending on the role of target genes in tumorigenesis, they can be generally subdivided into either oncogenic miRNAs (oncomiRs) or tumor suppressor miRNAs. These miRNAs have profound influence on cancer processes including cell proliferation, cell cycle regulation, metastasis and invasion, control of cell death, and angiogenesis (Loh et al., 2019).

In breast CSCs, miRNA expression is also dysregulated. A few such miRNAs where their functions in breast CSCs had been elucidated are worth to be mentioned. For instance, a widely-studied downregulated miR-200 family members (miR-141, miR-200a, b and c, and miR-429) in breast cancers were found to modulate the expression of stem cell and EMT-related genes such as Krüppel-like factor family (*KLF4*) (Wellner et al., 2009), polycomb complex protein *BMI1* (Shimono et al., 2009), suppressor of zeste 12 (*SUZ12*) (Iliopoulos et al., 2010), and *ZEB1/ZEB2* (Burk et al., 2008; Gregory et al., 2008; Korpal et al., 2008; Park et al., 2008), leading to activation of EMT program and increased breast CSCs (Shimono et al., 2009; Polytarchoua et al., 2012; Knezevic et al., 2015). Similarly, let-7 is significantly downregulated in breast CSCs and restoration of let-7 expression resulted in decreased cell proliferation, *in vitro* mammosphere formation, *in vivo* tumor formation and metastasis in an immunosuppressed mouse model (Yu et al., 2007). Another tumor suppressor miR-34a, a direct downstream effector of p53 (He et al., 2007), that are often inactivated by promoter methylation (Lodygin et al., 2008), plays key roles in cell fate commitment in mammary gland progenitors and breast cancer cell differentiation; they control breast CSCs by targeting WNT and Notch signaling (Kang et al., 2015; Bonetti et al., 2019). These findings are in line with

other studies reporting roles of miR-34 in CSCs in other cancers. For example, miR-34 suppresses prostate cancer, pancreatic cancer, and medulloblastoma CSCs by repressing CD44 or Notch signals (Ji et al., 2009; de Antonellis et al., 2011; Liu et al., 2011). Conversely, oncomiRs like miR-31 (Lv et al., 2017), miR-155 (Zuo et al., 2018) and miR-221/222 (Stinson et al., 2011; Li et al., 2016) are often found to be upregulated in breast CSCs to promote CSCs' self-renewal, tumorigenesis, and metastasis.

2.1.3 Pathological roles of miR-96 in breast cancer and CSCs

Other than the miR-200 family that was extensively investigated, another miRNA cluster, miR-183-96-192, hereafter called miR-183 cluster, was also reported to be significantly downregulated in human breast CSCs ($CD44^{+}/CD24^{low/-}$ subpopulation), normal human and murine mammary stem cells compared to non-tumorigenic cancer cells and normal breast epithelial cells (Shimono et al., 2009). It was confirmed that miR-183 cluster cooperates with miR-200 and miR-203 in repressing stem cell factors, like BMI1 in pancreatic and colorectal cancer cells, and their expressions are tightly regulated by the EMT activator, ZEB1 (Wellner et al., 2009). This was further reinforced by another study which showed that loss of p21, a downstream effector of p53, induces EMT by downregulating miR-183 cluster (Li et al., 2014b). Conversely, when miR-183 and miR-96 without miR-182 were reintroduced to the p21-deficient colorectal cancer cells, EMT-related genes, such as ITGB1, KLF4, SLUG and ZEB1 were repressed, which led to inhibition of cell migration and invasion (Li et al., 2014b). However, there has not been any follow-up studies that specifically investigated and elucidated the roles of miR-183-96-182 in breast CSCs which serves as the main rationale of this study.

The miR-183 cluster is made up of paralogous miR-183, miR-96 and miR-182 that share sequence homology and chromosomal proximity (Weston et al., 2006; Xu et al., 2007). It is highly conserved, and its expression is tightly regulated during normal development and

maturation of sensory organs (Pierce et al., 2008; Sacheli et al., 2009; Weston et al., 2011). They have also been reported to be critically upregulated in cancers (Lehmann et al., 2010; Lin et al., 2010; Hannafon et al., 2011; Giricz et al., 2012; Zhang et al., 2013). The upregulation of miR-183 cluster in breast cancer was found to be correlated with poor clinical presentation and prognosis (Song et al., 2016). Although generally all three miRNAs within the cluster were invariably upregulated in breast tumor tissues, there is growing evidence hinting that the roles played by each miRNA within the cluster might differ in breast cancer (Zhang et al., 2013). This is partly due to the fact that the 3 miRNAs of miR-183 cluster have similar but slightly different seed sequences (Wang et al., 2012), despite having overlapping sets of target mRNAs (Fogerty et al., 2019). To investigate this using a reductionist approach, I have chosen to look into and summarize the literatures published on miR-96 or miR-96 in combination with miR-182 and/or miR-183 in breast cancer (*Table 1*).

Table 1 List of gene targets and functions of miR-96 in breast cancer

miRNA	Target Genes	Function	Reference
miR-96, 182	*FOXO1*	Promote cell viability and proliferation	(Guttilla and White, 2009)
miR-96	*FOXO3a*	Promote growth by enhancing G1/S transition	(Lin et al., 2010a)
miR-96	*RAD51, REV1*	Decrease homologous recombination and improve sensitivity to cisplatin and PARP inhibition	(Wang et al., 2012)
miR-96	*RECK*	Promote proliferation and invasion	(Zhang et al., 2014)
miR-96, 182, 183	*RAB*	Promote proliferation and migration	(Li et al., 2014a)
miR-96, 182, 183	*BRMS1L, GHR*	Promote EMT and invasion stimulated by human growth hormone	(Zhang et al., 2015)
miR-96, 182	*PALLD*	Inhibit migration and metastasis	(Gilam et al., 2016)
miR-96	*PTPN9*	Promote proliferation, migration, and invasion	(Hong et al., 2016)

miR-96-5p	*FOXO*	Promote proliferation by inhibiting autophagy and apoptosis, enhance migration and invasion	(Shi et al., 2017)
miR-96	*ABCA1*	Promote proliferation by suppressing apoptosis	(Moazzeni et al., 2017)
miR-96	*MTSS1*	Promote migration	(Xie et al., 2018)
miR-96-5p	*CTNNB1*	Inhibit proliferation and invasion	(Gao et al., 2020)

Given the conflicting data presented, it is impossible to deduce that miR-96 plays its role either as an oncogene or a tumor suppressor in breast cancer. The use of different miRNA mimic or inhibitor, cell lines or clinical breast tumor tissue samples, and experimental approaches may have contributed to the discrepancies in findings. However, it is rather interesting to find that when it is common consensus that miR-183 cluster is upregulated in breast cancer, its expression is ironically downregulated in breast CSCs (Shimono et al., 2009), suggesting that miR-96 plays distinct roles in regulating CSCs' self-renewal and breast cancer oncogenesis. To understand this phenomenon, I set out to investigate how miR-96 controls breast CSCs by paying particular attention on the expression of CD44 which governs the stem cell function.

2.2 Materials and Methods

Cell culture

All cell lines were obtained from ATCC®. MCF7 and SK-BR3 cells were cultured in RPMI 1640 medium containing 10% fetal bovine serum (FBS) (GIBCO) and 1% penicillin/streptomycin. MDA-MB231, MDA-MB468, ZR-75-1, and HEK293T cells were cultured in high-glucose DMEM with 10% FBS and 1% penicillin/streptomycin. MCF10A cells were cultured in DMEM/F12 (Invitrogen) containing 5% horse serum, 20 ng/mL EGF, 0.5 mg/mL hydrocortisone, 100 ng/mL cholera toxin, 10 μg/mL insulin, and 1% penicillin/streptomycin. Cells were maintained at 37°C and 5% CO_2.

Transfection

Cells were plated in 6-well plates at a density of 200,000 cells/well. Transfection reagents were prepared by mixing 5 µL Lipofectamine® RNAiMax reagent (Thermo Fisher Scientific) in 250 µL of reduced serum medium OPTI-MEM (Thermo Fisher Scientific). mirVana™ miR-96 mimic (miRbase ID: hsa-miR-96-5p)- a small, double-stranded RNA that mimics endogenous precursor miRNAs or inhibitor (anti-miR™ miRNA Inhibitor)- a single-stranded, RNA oligonucleotide that binds to and inhibits the activity of endogenous miRNAs (Ambion) was diluted to a final concentration of 16 nM in OPTI-MEM. The mixture of miR-96 mimic/inhibitor and RNAiMax was incubated at room temperature for 10 min before adding it to the cell mixture in culture medium. Untreated and mock-treated samples (cells that were transfected with Lipofectamine® RNAiMax only) without the miR-96 mimic or inhibitor were used as controls.

Staining and flow cytometry analysis

After treatment for 72 h, cells were detached by trypsinization and centrifuged. Cell pellets were resuspended in PBS with 2% FBS containing anti-human FITC-conjugated CD44 (clone BJ18) antibodies (Biolegend®) and PE-conjugated anti-human CD24 (clone ML5) antibodies (Biolegend®) at a concentration of 1:1000. Anti-human IgG antibodies were used to determine the positive subsets of cells from background staining. Cells were incubated on ice in the dark for 30 min. Cells were washed 3 times with PBS before being analyzed by flow cytometry. 1 µg/mL 7-AAD was used as a viability dye (Sigma). Analysis was performed using a FACSAria™ III cell sorter system (BD Biosciences, San Jose, CA, USA) and data was plotted and quantified using FlowJo™ software Version 10 (Becton, Dickinson and Company, 2019).

Sphere formation assay

Cells were harvested and dissociated by trypsinization after treatment for 72 h. Single cells (100 cells/well) were plated on 24-well ultra-low attachment tissue culture plates (Corning). Briefly, cells were cultured in Mammary Epithelial Basal Medium (Lonza) containing 10 ng/mL EGF, 10 ng/mL bFGF, and B27 up to 14 days. Tumorspheres were measured and imaged using a Nikon Eclipse TS100 inverted microscope (Nikon Instruments, Tokyo, Japan) with a 4x objective lens. The number of tumorspheres over 50 μm was counted.

Determination of miRNA and mRNA expression levels

Total RNA was extracted using ISOGEN-II (Nippon Gene, Japan) reagent. For mRNA quantification, cDNA was synthesized from 1 μg of total RNA with Prime Script™ RT reagent (TAKARA, Japan). For miRNA quantification, miRNAs were extracted using an miRVANA™ miRNA Isolation Kit (Life Technologies) following the manufacturer's instructions. Reverse transcription and quantitative real-time PCR were performed using Taqman® Small RNA Assays (Applied Biosystems) following the manufacturer's protocol. Quantitative real-time PCR (RT-PCR) was performed on a ViiA 7 Real-Time PCR System (Thermo Fisher Scientific) using SYBR Premix Ex Taq II Master Mix (TAKARA, Japan). *GAPDH* expression level was used for mRNA normalization while *U6 snRNA* was used for miRNA normalization. Primers employed in quantitative RT-PCR are listed in *Table 4* in Chapter 3.2.

Mouse xenotransplantation and tumorigenicity assay

Animal experiments were performed in accordance with protocol approved by the Animal Experiment Review Committee of Okinawa Institute of Science and Technology Graduate University. Untreated, mock and miR-96 mimic-treated cells were harvested using trypsinization and centrifugation. $1x10^6$ cells were resuspended in 150 μL 100% Matrigel

before being injected subcutaneously into the flanks of 8-week old female BALB/c nu/nu nude mice. Three mice were used for each group. Four weeks after transplantation, mice were euthanized, and tumors were harvested. Tumor size and mass were measured with calipers and a precision balance, respectively, before they were lysed with lysis buffer from miRVANA™ miRNA Isolation Kit (Life Technologies) for RNA extraction. Tumor volume (mm^3) was calculated using the formula: $(xy)^{(\frac{3}{2})} \times \frac{\pi}{6}$.

DNA or plasmid constructs and luciferase assays

For luciferase reporter assays, the full-length 3'UTR and promoter region, 2000 and 1000 base pairs (bp) upstream of transcription start site (TSS), of *CD44* were amplified from human genomic DNA and cloned upstream of *Firefly* luciferase vector, *Luc2* (Promega). The primer sequences used for cloning are presented in *Table 2*. HEK 293T cells were first transfected with 8 nM miR-96 mimic or inhibitor. A day later, they were then transfected with 50 ng of *Luc2* constructs containing *CD44* 3'UTR or promoters, together with 10 ng of *Renilla* Luciferase reporter plasmid as a control. Twenty-four hours later, culture media containing transfection reagents was removed and cells were washed twice with PBS. Luciferase activities were analyzed following the Promega Dual-Luciferase® Reporter Assay's (Promega) protocol and measured by Centro XS^3 LB 960 Microplate Luminometer (Berthold Technologies, Wildbad, Germany). Relative luciferase activities were calculated as ratios of *Firefly* to *Renilla* luciferase index.

Table 2 Primers used for luciferase reporter vector cloning

Gene	Forward primer	Reverse primer
CD44 3'UTR	AATCTCTAGACACCTACACCATTATC TTG	AATCTCTAGAATGTTAGCCTTTTA ATAT
CD44 promoter (2000 bp upstream of TSS)	AATCAAGCTTTGGCATAGCTTACACC TTGT	AATCAAGCTTTGGGTTCAGCCTTT GGCCTC
CD44 promoter (1000 bp upstream of TSS)	AATCAAGCTTAGATAGATATAGAGTT ATC	AATCAAGCTTTGGGTTCAGCCTTT GGCCTC
HB-EGF 3'UTR	AATCTAGAGAGAGACTTGTGCTCAAG GA	AATCTCTAGATGGAATAAGGGTTA TCTTTATTTG

Statistics

Results are presented as means ± SD for at least three repeated individual experiments for each group. Statistically significant differences between mean values were determined using two-tailed Student's *t*-test (***$p < 0.001$, **$p < 0.01$ and *$p < 0.05$), unless otherwise specified.

2.3 Results

2.3.1 miR-96 is differentially expressed in various breast cancer cell lines and in breast CSCs

Compared to MCF10A (a normal mammary epithelial cell line), all studied human breast cancer cell lines that encompass various histological types and molecular signatures, including estrogen and progesterone status, except for MDA-MB231, showed significantly increased expression of miR-96 (*Figure 2.1*). MCF7, an ErbB2/HER2 negative, estrogen and progesterone receptor-positive cell line, and SK-BR3, an ErbB2/HER2-positive cell line, demonstrated exceptionally high expression of miR-96.

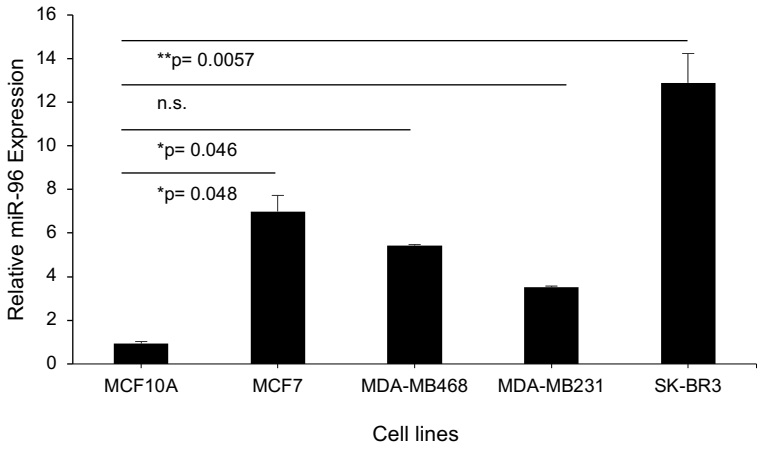

Figure 2.1 miR-96 is highly expressed across various breast cancer cell lines

miR-96 expressions were measured by quantitative RT-PCR in breast cancer cell lines derived from various histological subtypes and molecular signatures (MCF7 ($ER^+/PR^+/HER2^-$), MDA-MB468 (TNBC), MDA-MB231 (TNBC), and SK-BR3 ($HER2^+$)) compared to normal mammary epithelial cells, MCF10A. Results are presented relative to *U6 snRNA* expression. Data represent three independent experiments (**$p < 0.01$, *$p < 0.05$, and n.s- not significant). Error bars represent means of three independent experiments ± S.D. (N=3).

Next, I isolated CSCs by surface expression of CD44 and CD24 using flow cytometry from the following three cell lines expressing high miR-96 level: MCF7, MDA-MB468, and SK-BR3. When the CSCs ($CD44^+/CD24^{low/-}$ subpopulation) were assessed for their expression of miR-96 by quantitative real-time PCR after RNA extraction, I found significant reduction of miR-96 copies in CSCs as compared to their non-CSCs counterpart across all three cell lines (*Figure 2.2*). The difference in the level of miR-96 expression between CSCs and non-CSCs was especially great in MCF7 cells. Following this observation, I hypothesized that miR-96 downregulation is needed for CSCs' functions and hence further upregulation of miR-96 can potentially reduce CSCs population within breast cancer. In order to address the effect of miR-96 on tumorigenesis, I have selected MCF7 ($CD44^{low}$) and MDA-MB468 ($CD44^{high}$) for further investigation.

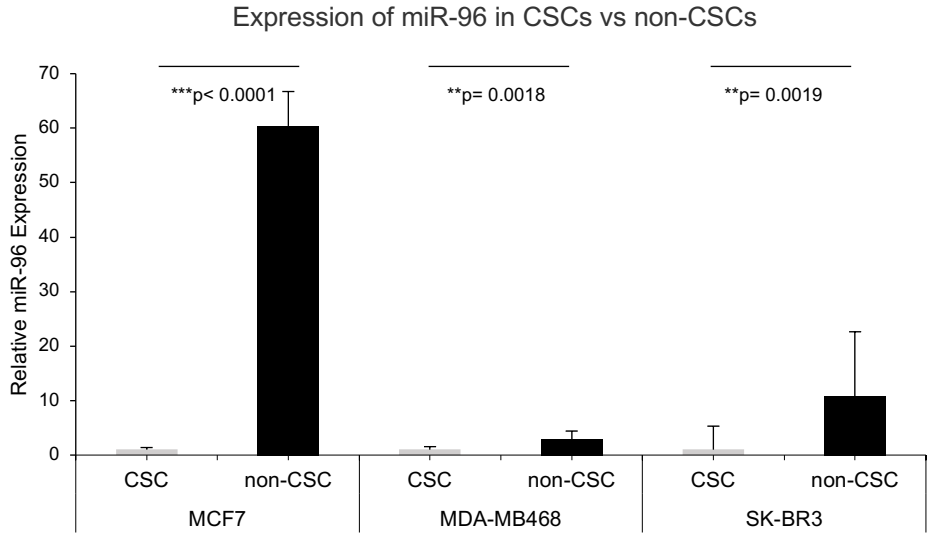

CSC (CD44^{high}, CD24$^{low/-}$); non-CSC (CD44^{-}, CD24^{high})

Figure 2.2 Expression of miR-96 in CSCs versus non-CSCs

Expression of miR-96 was measured between CSCs (CD44^{+}/CD24$^{low/-}$) and non-CSCs (CD44^{-}/CD24^{high}) of three breast cancer cell lines isolated by flow cytometry based on CD44 and CD24 expression. Results are presented relative to *U6 snRNA* expression. Data represent three independent experiments (***$p < 0.001$, **$p < 0.01$ (*t*-test, two-tailed)). Error bars represent means of three independent experiments ± S.D. (N=3).

2.3.2 Overexpression of miR-96 reduced the breast CSCs population

First of all, I optimized the concentration of miR-96-5p mimic (precursor miRNA) or inhibitor (anti-miR) and found that 16 nM sufficiently enhanced or repressed, respectively, the miR-96 level in both MCF7 and MDA-MB468 cells (*Figure 2.3a & b*). These treatments were highly specific in modifying miR-96 levels without affecting expression of other miRNAs in the same cluster, miR-182 and miR-183 (*Figure 2.3c*).

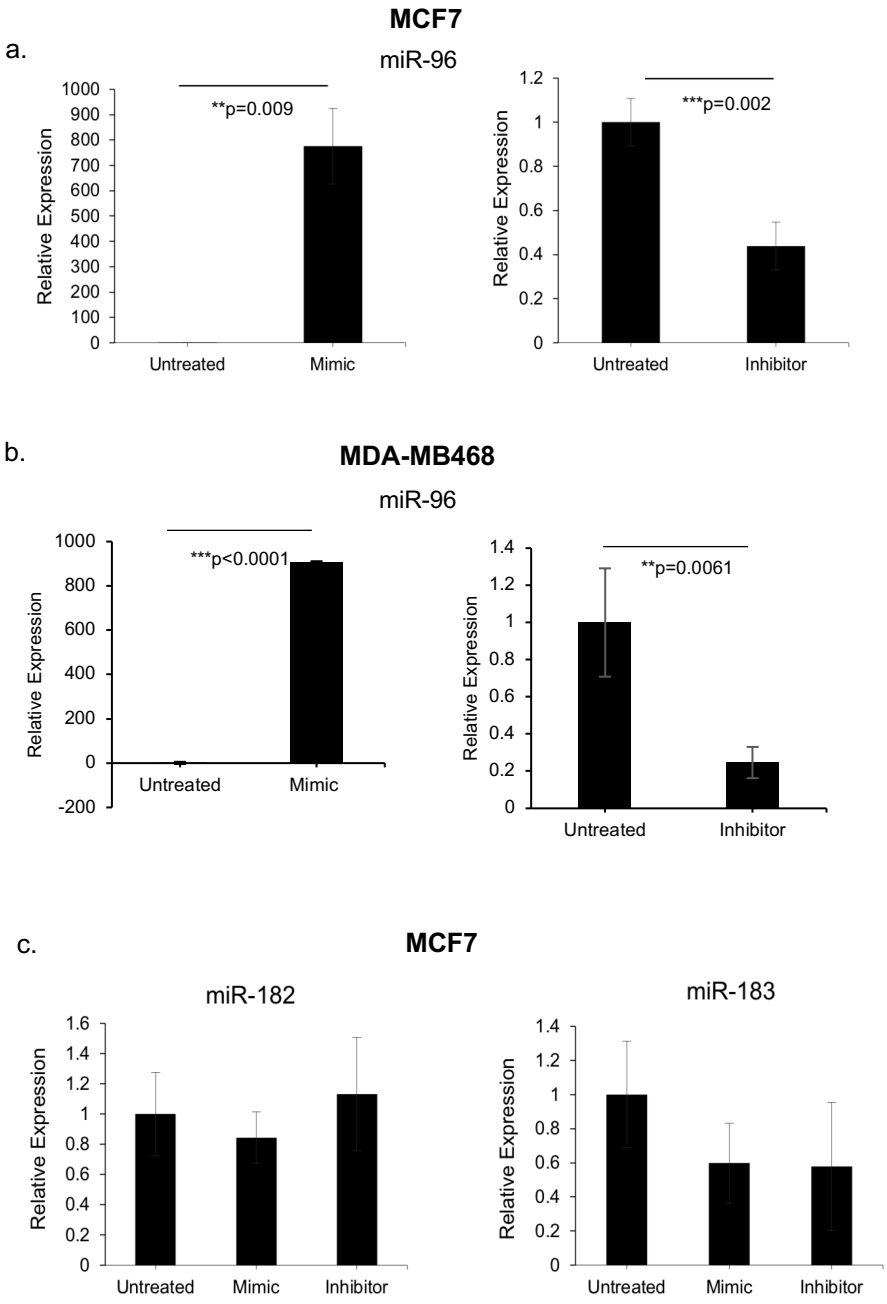

Figure 2.3 Confirmation of miR-96, 182 and 183 levels upon treatment with miR-96 mimic and inhibitor

miR-96 expression, as measured by quantitative RT-PCR in **a.** MCF7 and **b.** MDA-MB468 cells transfected with miR-96 mimic and inhibitor. **c.** miR-182 (*left*) and miR-183 (*right*) expressions were also quantified in miR-96 mimic- and inhibitor-treated MCF7 cells. Results are presented relative to *U6 snRNA* expression. Error bars represent means of three independent experiments ± S.D. (N=3). (***$p < 0.00$, **$p < 0.01$ (*t*-test, two-tailed)).

To probe the effects of these molecules on the expression of breast CSC markers, upon treatment with miR-96 mimic or inhibitor, staining of cells with anti-CD44 and CD24 antibodies followed by flow cytometry analysis were carried out. Results revealed a significant reduction in the CSC population ($CD44^+$, $CD24^-$) in MCF7 cells treated with an miR-96 mimic, while a tremendous increase of CSCs occurred in those transfected with miR-96 inhibitor (*Figure 2.4a*). For $CD44^{high}$ cell line, MDA-MB468, I focused on the CD44 level after transfection and found that there was also a partial reduction in the expression after miR-96 mimic treatment (*Figure 2.4b*).

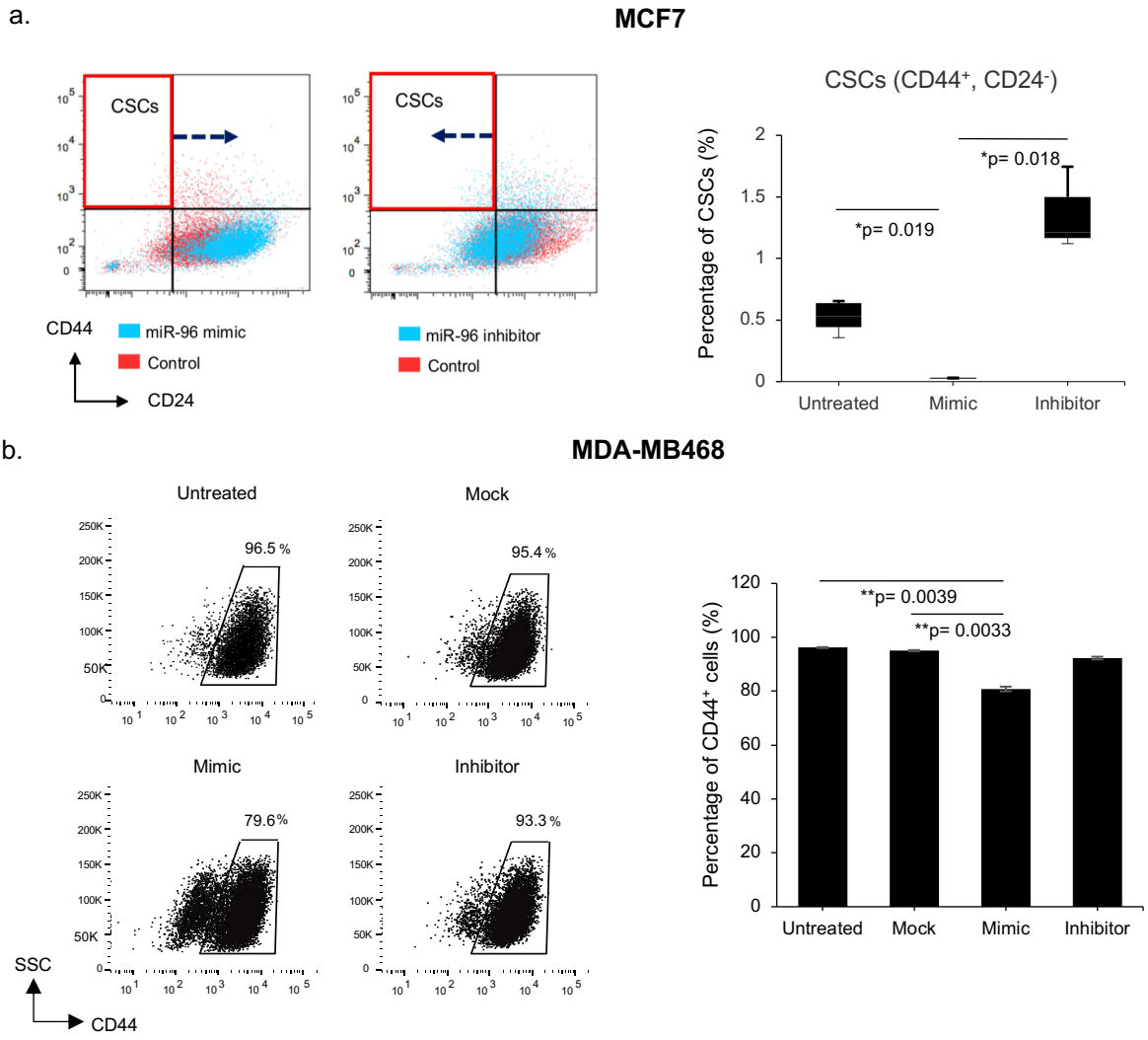

Figure 2.4 Surface expression of CD44 upon transfection with miR-96 mimic or inhibitor

a. Surface staining of CD44 and CD24 on MCF7 cells analyzed by flow cytometry after treatment with miR-96 mimic or inhibitor for 72 h. Numbers in outlined areas indicate the cells

in CSC populations. Arrows show the shift of treated cells (*blue dots*) away from or towards CSC populations in relation to untreated/control cells (*red dots*). Average percentage of CSCs ($CD44^+$, $CD24^-$) in each group was quantified and presented using a box and whisker plot on the right. **b.** Dot plots showing surface staining of CD44 on triple-negative MDA-MB468 breast cancer cells after treatment with miR-96 mimic or inhibitor for 72 h. $CD44^+$ population is marked in the box and the percentage of $CD44^+$ cells is shown on top of the box. Average percentage of $CD44^+$ cells were quantified in each group and presented in the bar chart on the right. Data represent three independent experiments (**$p < 0.001$, *$p < 0.05$ (t-test, two-tailed)).

In conjunction with this finding, a sphere formation assay was performed to investigate the potential of tumor growth *in vitro*. Consistent with flow cytometry results, after 14 days of culture under serum-free and ultra-low attachment conditions, tumorspheres generated from miR-96 mimic-treated cells were much smaller and fewer in number compared to untreated or inhibitor-treated tumorspheres (*Figure 2.5a & b*). In contrast to MCF7, the sphere forming ability of MDA-MB468 was not as effective under such culture condition.

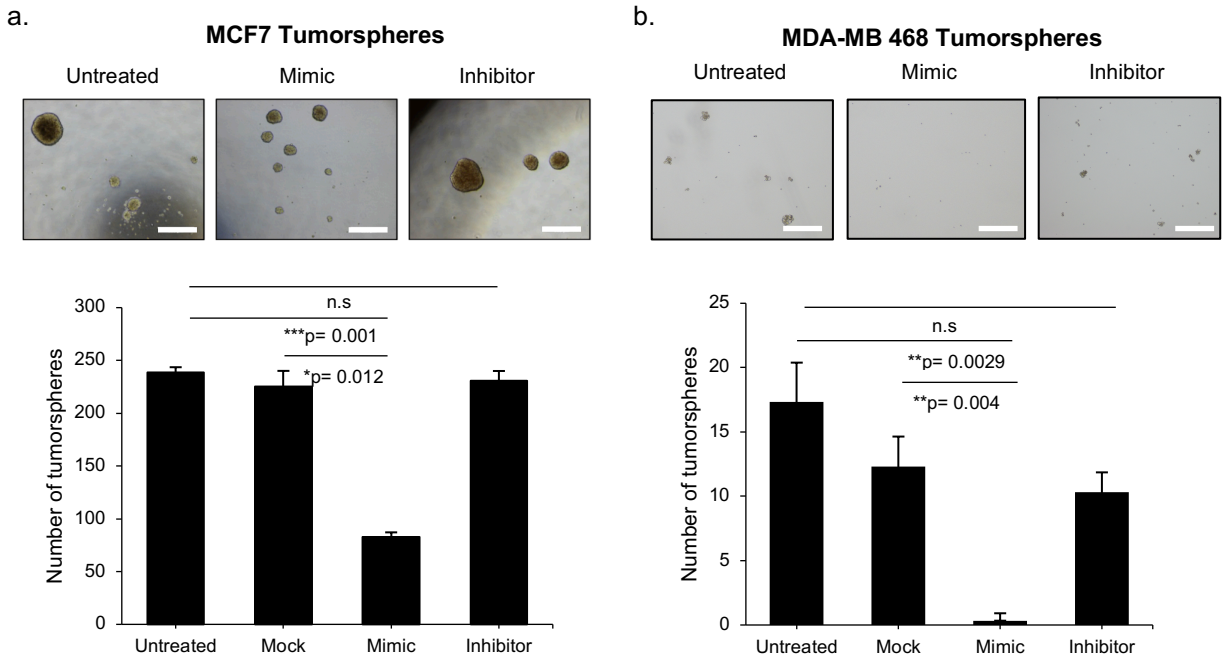

Figure 2.5 Sphere forming ability of cells transfected with miR-96 mimic or inhibitor

Representative images of **a.** MCF7 and **b.** MDA-MB468 tumorspheres. The sphere forming ability was evaluated by culturing the 72 h-mimic or inhibitor-transfected cells in serum-free medium for 14 days. Scale bar represents 200 µm. Number of tumorspheres over 50 µm was quantified in each group and presented in the bar charts below the images. Data represent three independent experiments (***$p < 0.001$, **$p < 0.01$, *$p < 0.05$, and n.s- not significant (*t*-test, two-tailed)).

2.3.3 *In vivo* tumor growth was stunted by cells overexpressing miR-96

To verify the *in vitro* findings, I expanded the study by subcutaneously grafting miR-96 mimic-treated MCF7 and MDA-MB468 cells into immunocompromised nude mice for an *in vivo* tumor growth assay. After a course of 28 days, tumors were excised and examined (*Figure 2.6a*). The effect of transfection- upregulation of miR-96 by mimic was sustained as revealed by miR-96 expression analysis using quantitative RT-PCR (*Figure 2.6b*). However, the inhibitor did not sufficiently suppress the miR-96 level in growing tumors and so, the tumors were not assessed further. Both miR-96 mimic-treated MCF7 and MDA-MB468 cells had significantly smaller tumor volumes and masses in comparison to untreated or mock-treated samples (*Figure 2.6c & d*). Taken together with *in vitro* results, this suggests that while miR-96 is naturally downregulated in breast CSCs, its forced overexpression led to a reduction of CSCs, which subsequently restricted tumor growth *in vivo*, implying that miR-96 potentially regulates breast CSCs.

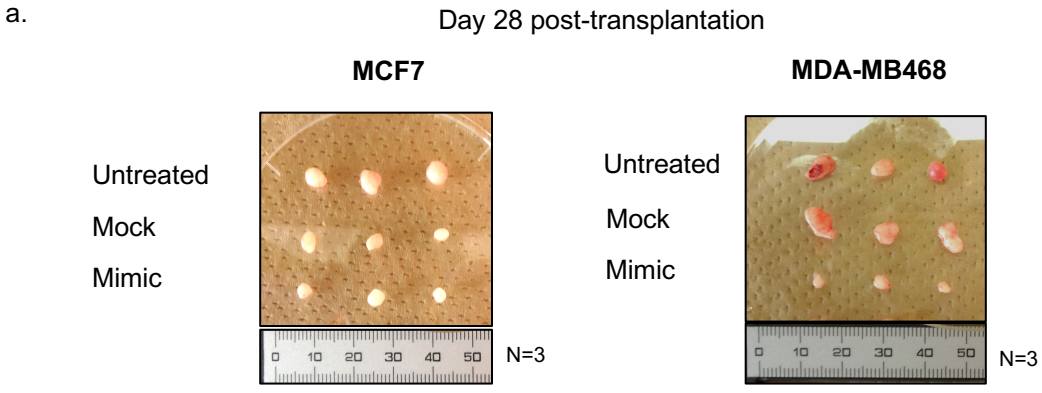

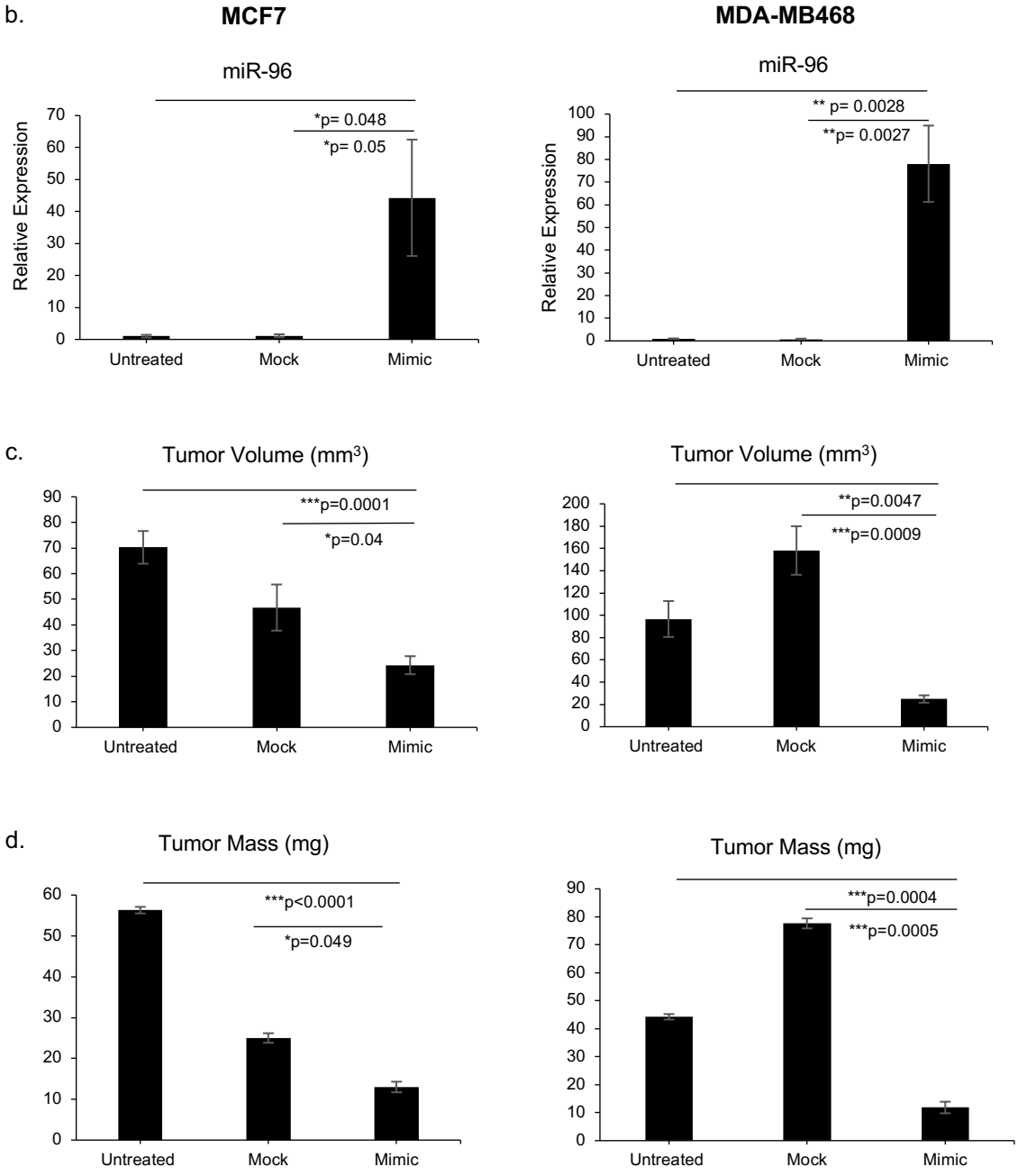

Figure 2.6 *In vivo* xenotransplantation of untreated, mock-treated, and miR-96 mimic-treated breast cancer cells

a. Images of untreated, mock-treated, and miR-96 mimic-treated MCF7 (*left*) and MDA-MB468 (*right*) tumors formed after xenografted subcutaneously into nude mice and excised for examination 28 days post-transplantation. **b.** miR-96 expression level of tumors from each experimental group as analyzed by quantitative RT-PCR. RNAs were isolated from homogenized tumors after excision. Results are presented relative to *U6 snRNA* expression. **c.** Tumor volume (mm^3) was calculated based on the width (x) and length (y) of each tumor

measured with calipers. Average tumor volume from three biological replicates were quantified. **d.** Average tumor mass of each experimental group (***$p < 0.001$, **$p < 0.0$, *$p < 0.05$ (*t*-test, two-tailed)).

2.3.4 miR-96 suppressed CD44 expression via transcriptional control

I was intrigued by the significant reduction of CD44 in both $CD44^{high}$ and $CD44^{low}$ cell lines after overexpression of miR-96. As discussed earlier, CD44 is a well-known stem cell marker that participates in mediating EMT and stem cell renewal. The current findings coupled with other studies that had reported the low expression of miR-96 in $CD44^{high/+}$ CSCs subpopulation point that miR-96 potentially regulates CD44 expression. To test this hypothesis, I first performed quantitative RT-PCR to verify that *CD44* mRNA was suppressed upon treatment with miR-96 in both MCF7 and MDA-MB468 cells (*Figure 2.7*). The splice variant of CD44, *CD44v3* mRNA, commonly found in aggressive type breast tumors was also significantly downregulated by miR-96 (*Figure 2.7*).

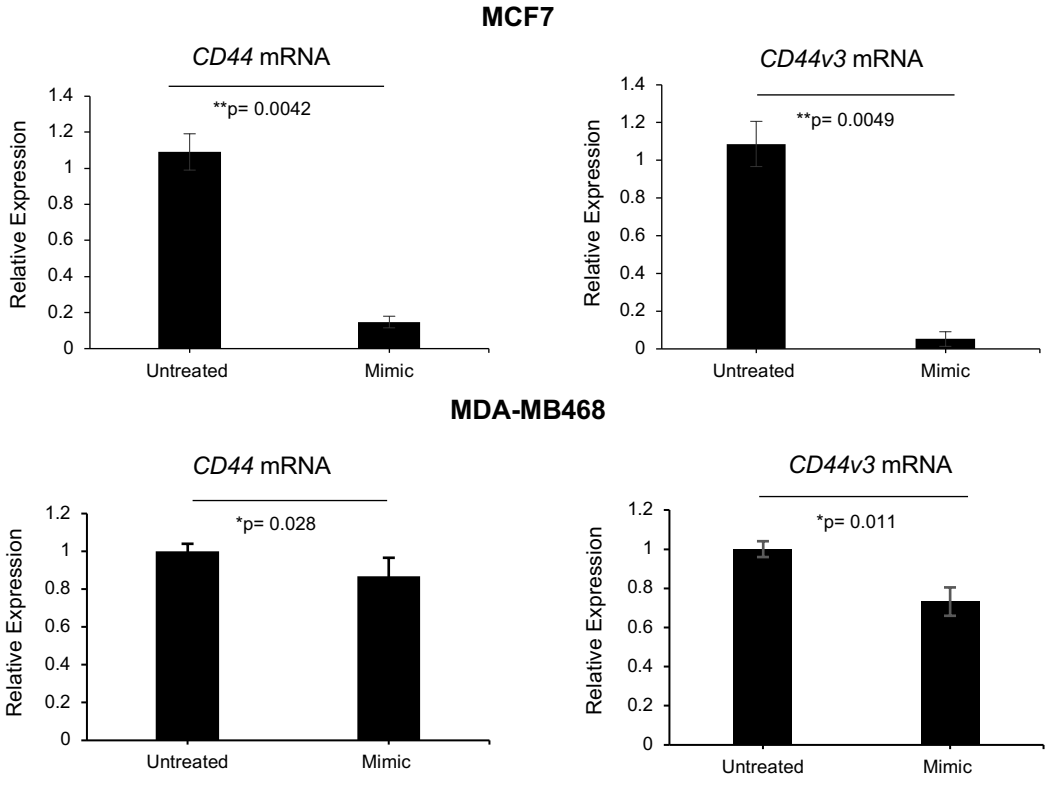

Figure 2.7 miR-96 suppressed *CD44* and *CD44v3* mRNA levels

Quantitative RT-PCR analysis of *CD44* and *CD44v3* mRNA in miR-96 mimic-treated MCF7 (*upper panel*) and MDA-MB468 (*lower panel*) cells. Results are presented relative to *GAPDH* expression. Error bars represent means of three independent experiments ± S.D. (N=3) (**$p <$ 0.0, *$p < 0.05$ (*t*-test, two-tailed)).

In order to identify the possibility that *CD44* mRNA is a direct target of miR-96, I performed luciferase assays by cloning the full length *CD44* 3'UTR into the pGL4.10 luciferase reporter vector. The pGL4.10-CD44 3'UTR vector, together with the control luciferase vector, pRL-TK *Renilla* luciferase vector, and miR-96 mimics were co-transfected into HEK293T cells that express miR-96 weakly. Surprisingly, the luciferase activity was not suppressed by the miR-96 mimic (*Figure 2.8a*). This result verified the finding from the TargetScan (a miRNA targets' computational prediction tool developed based on sequence evolutionary conservation) (Lewis et al., 2005; Agarwal et al., 2015) that predicts the 3'UTR of *CD44* does not harbor a target site complementary to the seed sequence of miR-96-5p.

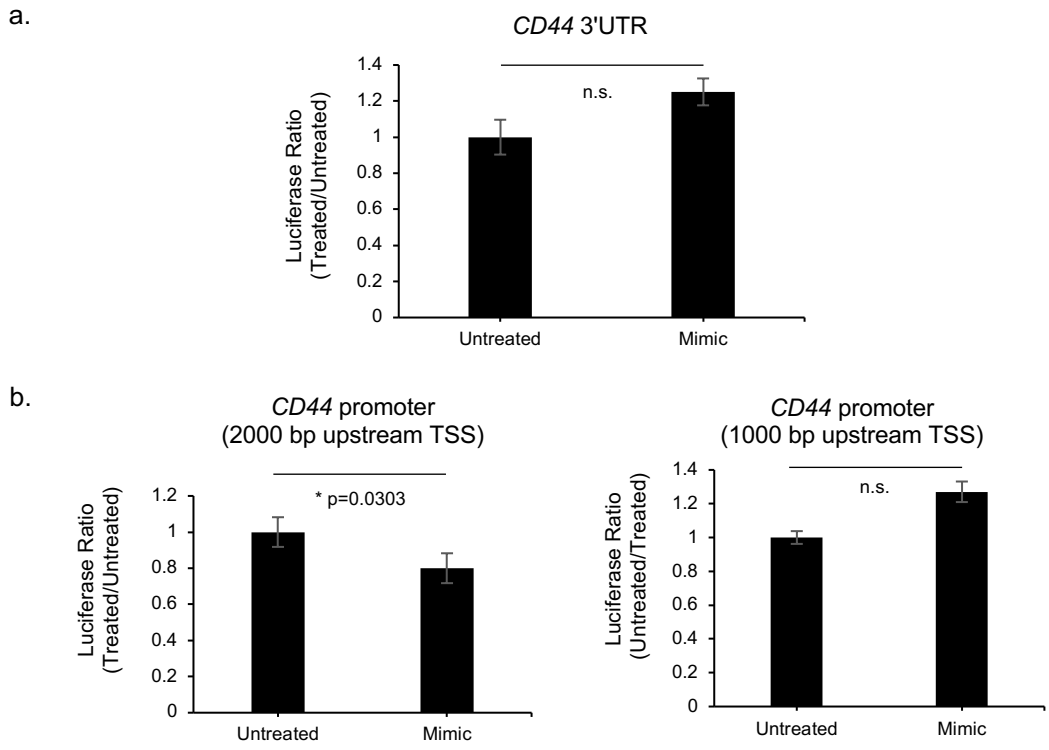

Figure 2.8 *CD44* transcription was suppressed by miR-96 through its promoter instead of 3'UTR

a. Relative luciferase activity of *Firefly* luciferase *Luc2* constructs containing 3'UTR of *CD44* mRNA after treatment with miR-96 mimic. HEK293T cells were co-transfected with *Firefly* and *Renilla* luciferase plasmids. Levels of *Firefly* and *Renilla* luciferase were measured. *Firefly* luciferase expression was normalized to *Renilla* luciferase level. **b.** The promoter region of CD44 spanning 2000 (*left*) or 1000 base pairs (*right*) upstream of the transcription start site (TSS) was cloned into the luciferase *Luc2* plasmid. Relative luciferase activity was measured as described previously. Error bars represent means of three independent experiments ± S.D. (N=3) (**$p < 0.0$, *$p < 0.05$, and n.s- not significant (*t*-test, two-tailed)).

Intrigued by this result, I speculated that the promoter region of *CD44* was targeted indirectly by miR-96, leading to its downregulation. To verify this, I cloned the *CD44* promoter region, 2000 base pairs upstream of the transcription start site (2000 bp upstream of TSS) or 1000 bp upstream of TSS into the pGL4.10 luciferase reporter vector and performed luciferase activity assay in the presence of miR-96. Upon co-transfection with miR-96 mimic, I observed a profound reduction in luciferase activity in *CD44* 2000 bp upstream of TSS promoter vector, but not in *CD44* 1000 bp upstream of TSS promoter vector (*Figure 2.8b*), implying that the promoter region between 1000 and 2000 bp upstream of TSS of *CD44* harbors binding sites for transcriptional factors influenced by miR-96 that control *CD44* expression.

2.4 Discussion

2.4.1 Differential expression of miR-96 contributes to heterogeneity of breast cancer cells

First of all, miR-96 is generally upregulated with varying level across different subtypes of breast cancer cells as reported by others who found that miR-96-5p is overexpressed in MCF7, MDA-MB231, ZR-75-1, SKBR3, and MDA-MB468 (Lin et al., 2010; Song et al., 2016;

Shi et al., 2017). However, it is interesting to find that the non-coding RNA, miR-96 is differentially expressed in distinct population of cells within a cancer cell line or tumor. Since breast CSCs only occupy a small portion of a tumor, their differential genetic makeup is often trumped by non-CSCs that make up the tumor bulk. Hence, the overall genetic or epigenetic profiles of tumor do not offer a full representation of the tumor phenotype. In the present study, the result of downregulation of miR-96 in breast CSCs carrying high CD44 expression and low CD24 levels complemented the findings reported by another group that demonstrated downregulation of miRNA clusters including miR-200 and miR-183 in breast CSCs (Shimono et al., 2009). This showcases the diversity of genetic and epigenetic landscape of cancer cells which contributes to tumor heterogeneity and its relevance to challenges for clinical oncology. There has been conflicting data about the role of miR-96, however, it is clear that miR-96's action varies among distinct subpopulation of cells. Hence, by keeping the importance of tumor heterogeneity in mind, I would like to propose that instead of dichotomizing a miRNA to either an oncogenic or tumor suppressive miRNA, it would be more appropriate that the role and function of a miRNA are examined in the context of cellular composition and phenotype.

2.4.2 miR-96 is capable of transforming breast CSCs' cell fate by altering their mRNA and protein expression

Following the observation of differential expression of miR-96 in CSCs versus non-CSCs, I showed that it was possible to modulate tumor plasticity by overexpressing a miRNA capable of altering the expression of CSCs' marker. It is important to note that the reduction of CSC population after forced expression of miR-96 was largely caused by the suppression of CD44. In MCF7, this is accompanied by an increase of CD24 expression. MCF7 is an estrogen receptor α (ERα) positive cell line whereby most of the cells are negative for CD24. A re-expression of CD24 could be a result of a downregulation of repressor for CD24 by miR-96

since one miRNA can have multiple targets. One of the mechanisms worth to be investigated is the ERα pathway that has been shown to mediate repression of CD24 in breast cancer cells (Kaipparettu et al., 2008). Meanwhile, *KLF4* mRNA that encodes a well-known transcription factor important for stem cell function and somatic reprogramming, was also found to be simultaneously downregulated in miR-96-overexpressed MCF7 cells (*Figure 2.9*). In fact, *KLF4* was found to be modulated by miR-96 and miR-183 which inhibited induction of EMT in p21-deficient colorectal cancer cells (Li et al., 2014b). This simultaneous repression of *KLF4* and *CD44* may present as an added advantage of miR-96 for tumor suppression in breast cancers that also commonly overexpress KLF4 from early to late stage tumors (Foster et al., 1999, 2000; Pandya et al., 2004).

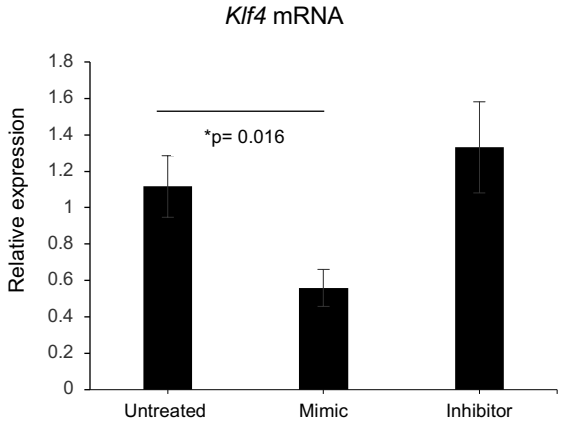

Figure 2.9 *KLF4* mRNA expression in miR-96 mimic or inhibitor-treated MCF7
The mRNA expression of MCF7 was analyzed by quantitative RT-PCR after treatment with miR-96 mimic or inhibitor for 72 h. Results are presented relative to *GAPDH* expression. Error bars represent means of three independent experiments ± S.D. (N=3).

Furthermore, it would be interesting to see how miR-96 influences the EMT program in breast cancer cells since CD44, EMT, and CSCs are closely related. To start with, it would be worthwhile looking into the changes within the EMT transcription factors, especially ZEB1 that had been shown to have a reciprocal regulation on a few commonly downregulated miRNAs, including miR-200 and miR-183 clusters in CSCs across different tumors (Burk et

al., 2008; Wellner et al., 2009; Li et al., 2014b). This would be followed by a thorough investigation into EMT-related functional phenotypes like cancer cell invasion and migration.

The alteration of CD44 and cellular behaviors discovered in this study implies that the plasticity that is exhibited by CSCs enables them to transition from a stem cell state to a non-stem cell state (Kreso and Dick, 2014). This transition of cellular phenotype from a dormant, capable of self-renewal and treatment-resistant CSC into a proliferative and differentiated state may sensitize tumors to chemotherapeutic agents, in particular cytotoxic drugs. On top of this, the reduction of CSC population may effectively prevent tumor relapse caused by CSCs' high tumorigenic potential as suggested by the *in vivo* xenotransplantation study showing a suppression of tumor growth by pre-treatment with a single miRNA. However, a more comprehensive *in vivo* study is required to analyze the phenotypic and functional changes, such as tumor invasion and metastasis with repeated doses of miR-96 mimic into the body or directly into the tumor. Nevertheless, this study highlights the concerted regulation of genes by a non-coding RNA in modulating cancer cell plasticity.

2.4.3 Possible mechanisms of CD44 downregulation by miR-96

Both the mRNA and protein level of CD44 had been significantly altered by overexpression of miR-96. Although it is proven that *CD44* mRNA is not a direct target of miR-96, it is clear that the transcription of *CD44* had been modulated via its promoter region. This is in contrast to the direct mechanism of action of other miRNAs on CD44 expression, for example, miR-143 or miR-34a which directly binds to the 3'UTR of *CD44*, leading to a reduction in breast (Yang et al., 2016) and prostate CSCs (Liu et al., 2011), respectively. To investigate this further, I performed luciferase reporter assay to nail down the promoter region that is affected by miR-96, which lies between 1000 and 2000 base pairs upstream of the transcription start site of *CD44*. When I searched the nucleotide sequence of this particular

region for potential binding by transcription factors using JASPAR database (Sandelin, 2004), among the predicted transcription factors, Forkhead box O3 (FOXO3), a transcription factor of the FOXO protein family stood out as the most probable transcriptional activator that may interact with *CD44* mRNA through one of the three consensus binding sites (*Table 3 & Figure 2.10*). As a matter of fact, FOXO3 had been proven as a direct target of miR-96 in human breast cancer cells (Lin et al., 2010b). Other studies in pancreatic cancer cells had also discovered that FOXO3 is essential for the expression of CD44, and knockdown of FOXO3 led to reduced pancreatic CSCs, supporting the relationship between FOXO3 and CD44 (Kumazoe et al., 2017a, 2017b). A rescue experiment to re-express FOXO3 protein in cells treated with miR-96 mimic would offer an explanation to the regulation of CD44 by FOXO3. This can be further confirmed by creating mutation on the predicted miR-96 binding site of *FOXO3* gene using mutagenesis assay and assess the effect on *CD44* transcription when cells are transfected with mutated *FOXO3* plasmids and miR-96 mimic.

Table 3 Predicted FOXO3 transcription factor binding sites within the promoter region of CD44 (1000 to 2000 base pairs upstream of TSS) identified by JASPAR

Matrix ID	Name	Score	Relative score[a]	Sequence ID	Start[b]	End[b]	Strand	Predicted sequence
MA0157.2	FOXO3	13.9794	0.988952870708	CD44	128	135	-	GTAAACAT
MA0157.2	FOXO3	7.25641	0.853368072115	CD44	256	263	+	ATAAACAG
MA0157.2	FOXO3	5.03513	0.808570692417	CD44	216	223	-	ATCAACAT

[a] The relative score is provided by JASPAR according to the similarity of motif sequence.

[b] The start and end binding sites correspond to the mRNA sequence 2000 base pairs upstream of TSS of *CD44* from 5'→3'.

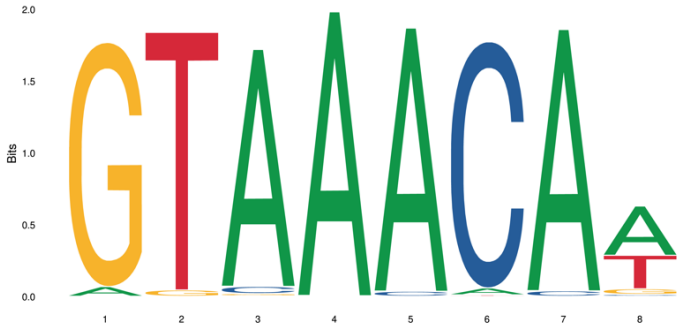

Figure 2.10 Top match FOXO3 (MA0157.2) binding motif in logo format for *CD44* promoter

While performing analysis using miRNA targets' prediction tool, TargetScan, one of the top putative targets of miR-96, heparin-binding epidermal growth factors (HB-EGF) appears to be an interesting molecule, given its close relationship with CD44. As mentioned in the introduction, heparan sulfate-modified CD44, in particular, CD44v3 isoform harbors unique motif that binds HB-EGF on the cell surface (Bennett et al., 1995; Greenfield et al., 1999). In breast tumor cells, CD44v3-heparan sulfate was found to contain additional growth factor binding site (Kalish et al., 1999b), and its expression is associated with breast CSCs (Olsson et al., 2011b). The finding that *CD44v3* mRNA expression was also altered in miR-96 mimic-treated cells hinted that there might be another mechanism possibly driven by HB-EGF downregulation in modulating CD44 expression in breast CSCs. To delve into this hypothesis, a series of experiments were carried out and will be presented in the next chapter.

In this study, I have also investigated a triple-negative breast cancer (TNBC) cell line, MDA-MB468, in which nearly all cells express CD44. They showed partial reduction of CD44 expression after treatment with miR-96 mimic (*Figure 2.4b*). The partial suppression of CD44 expression in these cells might be due to additional regulation of CD44 imposed on these

$CD44^{high}$ cells. Of note, there is a difference in epigenetic regulation of CD44 in TNBC vs non-TNBC, in which hypomethylation of CD44 has been observed in TNBC tumor samples (Kagara et al., 2012).

As I was analyzing the *in vivo* data, I found that even though miR-96 mimic-treated cells had suppressed tumor growth, the *CD44* expression of these tumors did not show obvious differences between the untreated and miR-96 mimic-treated groups (*Figure 2.11*). I speculate that this happened due to two reasons: (1) since CD44 is a cell adhesion molecule, the presence of extracellular matrix proteins within an *in vivo* environment might have contributed to the retention or re-expression of CD44 during tumor growth, and (2) the cancer cells were pre-treated with miR-96 mimic before xenografted into nude mice, so it is likely that a continuous supply or a greater dose of miR-96 is needed to cause a sustained suppression of CD44. Nevertheless, an initial reduction in CSCs caused by a pre-treatment with miR-96 mimic had effectively suppressed tumor growth in the breast cancer cells.

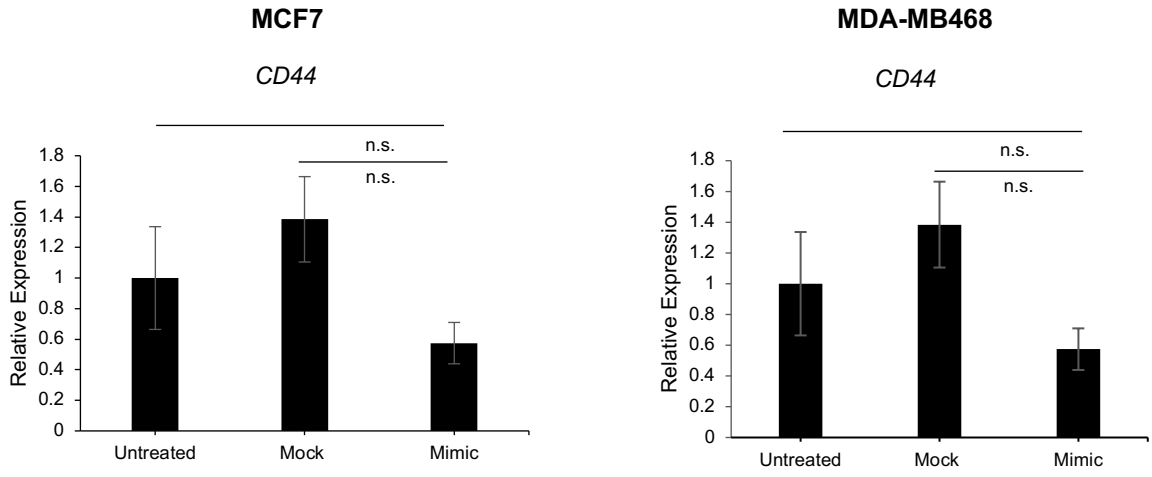

Figure 2.11 *CD44* mRNA levels in xenografted tumors

The mRNA expression of *CD44* in excised tumors from untreated, mock-treated, miR-96 mimic-treated MCF7 (*left*), and MDA-MB468 (*right*) samples was measured using quantitative RT-PCR analysis. Results are presented relative to *GAPDH* expression.

Other than the shortfall in the animal experimental setup, another major limitation of the current study is the lack of strong evidence in proving the link between CD44 and miR-96 in governing the function of breast CSCs. The lack of effectiveness of miR-96 inhibitor in suppressing miR-96 expression signals the limitation of performing such experiments using transient transfection with miR-96 mimic or inhibitor. In order to circumvent this issue and to strengthen the hypothesis, a stable transfection using lentiviral vectors with miRNA precursor or anti-miRNA sequence inserted into the expression construct, which had been proven effective even in an *in vivo* setting, should be conducted (Mishima et al., 2016).

Chapter 3

Heparin-binding Epidermal Growth Factors (HB-EGF) mediates the control of CD44 and cell proliferation in breast cancer

3.1 Introduction

3.1.1 HB-EGF regulates tissue homeostasis through EGF receptor and CD44

Heparin-binding epidermal growth factor (HB-EGF) is a mitogenic factor that belongs to the EGF family. As the name suggests, it contains both an EGF-like domain and a unique 21-residue N-terminal heparin-binding domain that facilitate binding to the EGF receptor and interact with heparin and heparan sulfate on cell surface, respectively (Higashiyama et al., 1991, 1993; Besner et al., 1992; Thompson et al., 1994). It was first identified as a secreted protein from conditioned medium of cultured human macrophages and monocytes (Besner et al., 1990; Higashiyama et al., 1991). Before being secreted into the extracellular space, HB-EGF is expressed as a transmembrane protein in a precursor form called pro-HB-EGF (Higashiyama et al., 1992). The membrane-anchored pro-HB-EGF needs to be cleaved by proteases such as disintegrin and metalloproteinase (ADAM) and matrix metalloproteinase (MMP), a process termed ectodomain shedding, to yield soluble, transmembrane and carboxy-terminal domains of HB-EGF (Raab et al., 1994; Goishi et al., 1995; Suzuki et al., 1997; Izumi et al., 1998).

The mature, soluble form of HB-EGF functions in an autocrine or paracrine manner by acting as a potent mitogen for fibroblasts, smooth muscle cells, and keratinocytes (Higashiyama et al., 1991; Marikovsky et al., 1993). It can bind EGF receptors, ErbB1, and ErbB4, to trigger receptor dimerization and tyrosine phosphorylation of receptor kinase domain (Higashiyama et al., 1991; Riese et al., 1996; Elenius et al., 1997), which consequently results in activation of mitogenic signaling cascades such as MAPK, PI3K/Akt, protein kinase C, and stress-activated protein kinase (Yarden and Sliwkowski, 2001). The result of this binding leads to cellular proliferation, migration, cell adhesion, and differentiation. Following ectodomain shedding, the cytoplasmic tail of pro-HB-EGF is also cleaved to form a carboxyl terminal fragment of HB-EGF termed HB-EGF-C, which also interacts with other intracellular molecules to exert biological effects (Nanba et al., 2003; Kinugasa et al., 2007). Meanwhile,

the membrane-bound pro-HB-EGF remains biological active and can interact in a juxtacrine manner with other membrane molecule like CD9 (Higashiyama et al., 1995; Sakuma et al., 1997) or transactivate EGFR on adjacent neighboring cells to potentiate cell adhesion and survival (Miyoshi et al., 1997; Prenzel et al., 1999; Dong et al., 2005). One unique property of the membrane-bound HB-EGF is that it possesses the ability to bind diphtheria toxin (Naglich et al., 1992; Mitamura et al., 1995; Louie et al., 1997).

HB-EGF is widely expressed in various tissues within the body, including skeletal muscle, lung, brain, heart, and skin (Abraham et al., 1993). It plays important normal physiological roles, for example blastocyst implantation (Das et al., 1994), proper heart organogenesis (Iwamoto et al., 2003), and skin wound healing (Marikovsky et al., 1993; Shirakata et al., 2005). Together with other EGF family member proteins, HB-EGF is also expressed in the mammary gland interacting with ErbB receptors throughout the entire stages of development, including pregnancy and lactation (Schroeder and Lee, 1998). For instance, the expression of ErbB4 receptor and its function in directing downstream signaling is crucial for mammary ductal morphogenesis, differentiation, and lactation (Jones et al., 1999; Long et al., 2003; Tidcombe et al., 2003). In postpartum mammary glands, pro-HB-EGF had been found to colocalize and assemble with heparan sulfate-modified CD44, namely CD44v3, and MMP-7 on the luminal epithelium, whereby upon proteolytic cleavage, activates its receptor, ErbB4 (Yu et al., 2002). Without CD44, the mammary glands failed to develop enlarged lobuloalveolar tissues with MMP-7, and heparan sulfate proteoglycan redistributed to the basal instead of the luminal side of epithelium, leading to a lack of production of mature HB-EGF, reduced ErbB4 activation, and subsequent cell death (Yu et al., 2002). This study underscores the importance of heparan sulfate-modified CD44, CD44v3 isoform, in regulating the presentation of pro-HB-EGF (Bennett et al., 1995), and its subsequent proteolytic cleavage by

MMP-7 (Prenzel et al., 1999) to ensure normal mammary gland development and tissue homeostasis.

3.1.2 HB-EGF pathway mediates transcriptional regulation of genes closely related to cancer

Despite activating mitogenic signaling pathways, HB-EGF had also been reported to function as a transcription factor in various tissues. It is therefore not uncommon to find HB-EGF overexpressed in cancers. First of all, HB-EGF serves as a transcriptional target of p53, which in turn initiates a feedback loop to counteract growth suppression. Under stress condition, p53 activation induces the upregulation of HB-EGF that subsequently triggers sustained activation of MAP kinases, Ras and Raf to protect cells from stress-induced apoptosis (Lee et al., 2000; Fang et al., 2001). The researchers continued to demonstrate that upon activation of p53 by oxidative or genotoxic stress in various normal and cancerous cell lines, the upregulation of HB-EGF drove MAPK-mediated induction of an enzyme, cyclooxygenase 2 (COX-2), which is responsible for prostaglandin synthesis in response to extracellular stimuli, to protect cells against apoptosis (Han et al., 2002). In prostate cancer cells, it had been shown that mutant p53 induced an early response transcription factor, Egr-1, which enhanced transcription and secretion of EGFR ligands including HB-EGF via the activation of MAPK pathway, presenting an autocrine feedback loop for sustained cell proliferation (Sauer et al., 2010).

Hypoxia is a common feature of highly malignant tumors in which the lack of oxygen triggers a transcriptional program via hypoxia-inducible factor (HIF-1) and vascular endothelial growth factor (VEGF) to induce new blood vessel formation or angiogenesis. In epidermal keratinocytes, hypoxia was found to induce enhanced expression of HB-EGF, followed by activation of MAPK and PI3K/Akt pathways, which increased VEGF production

to cause mitogenesis and chemotaxis (Nakai et al., 2009). Similarly, in bladder and breast cancer, overexpression of HB-EGF in tumor-bearing mice resulted in an increase of VEGF and tumor angiogenesis (Ongusaha et al., 2004; Yotsumoto et al., 2013). In highly malignant glioblastoma cells, hypoxia was able to induce secretion of microvesicle-coupled tissue factors to activate HB-EGF in endothelial cells (Svensson et al., 2011).

The cytoplasmic tail of pro-HB-EGF also undergoes cleavage by protease during ectodomain shedding of soluble HB-EGF to produce HB-EGF-C. HB-EGF-C is known to interact with gene promoter to regulate transcriptional activities. Subsequent to cleavage, HB-EGF-C is capable of translocating from plasma membrane into the nucleus to cause nuclear exclusion of a transcriptional repressor, promyelocytic leukemia zinc finger (PLZF) (Nanba et al., 2003). PLZF is known to repress *Cyclin A* transcription and causes inhibition of entry into S phase of cell cycle (Yeyati et al., 1999). As a result of nuclear export of PLZF upon entry of HB-EGF-C into the nucleus, *Cyclin A* transcription is disinhibited, leading to cell cycle progression and cellular proliferation (Nanba et al., 2003). Under similar mechanism, the nuclear translocation of HB-EGF had also shown to reverse the transcriptional repression of *Cyclin D2* gene by another PLZF-related transcriptional repressor, B-cell lymphoma 6 (BCL6) (Dhordain et al., 2000; Kinugasa et al., 2007). On top of this, HB-EGF-C can complex with a pro-survival chaperone protein, Bcl-2-associated anthanogene 1 (BAG-1), which acts synergistically with HB-EGF-C to inhibit apoptosis in cells (Lin et al., 2001; Hung et al., 2014). These studies highlighted the role of HB-EGF in transcriptional control of cell growth-related genes which explains why HB-EGF is often upregulated in human cancers. A simplified illustration is presented below to summarize the molecular interactions and mechanisms of HB-EGF (*Figure 3.1*).

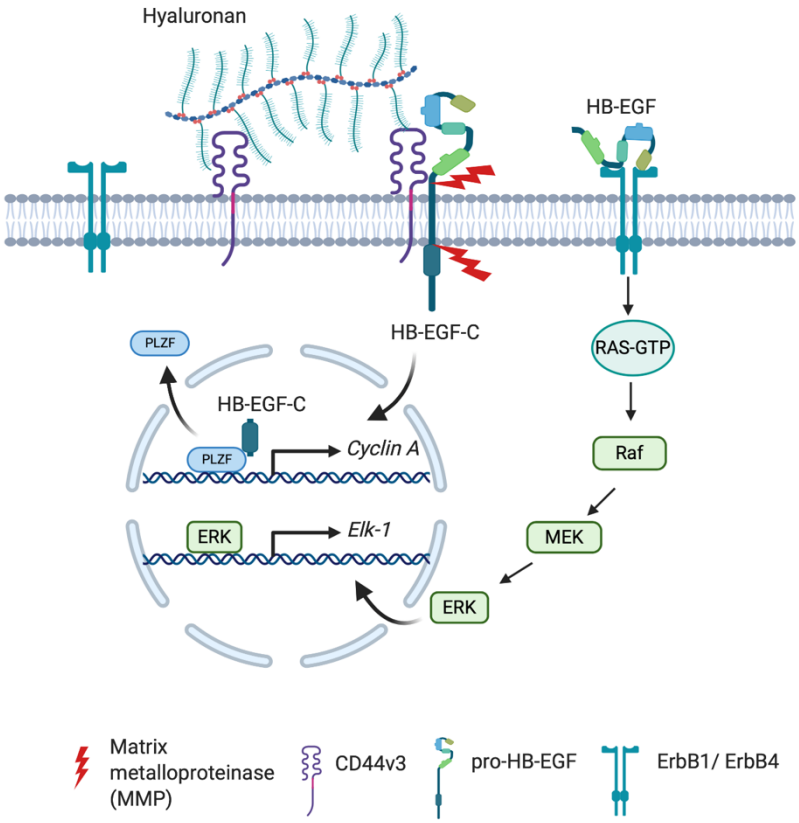

Figure 3.1 Illustration depicting the molecular interactions of HB-EGF

The precursor form, pro-HB-EGF, interacts with the CD44 variant isoform, CD44v3, on the cell membrane of luminal epithelium and activates matrix metalloproteinase, MMP7, to cleave pro-HB-EGF into secreted HB-EGF and HB-EGF-C, from the extracellular and cytoplasmic tail, respectively. Secreted, mature HB-EGF interacts with EGF receptors, ErbB1 or ErbB4, to activate downstream signaling, for instance MAPK which eventually leads to nuclear translocation of effector molecule, ERK to transcriptionally activate genes related to cell proliferation and survival. On the other hand, HB-EGF-C enters the nucleus to displace transcriptional repressor such as PLZF or BCL6, triggering transcription of genes related to cell cycle progression. (*Created with BioRender.com*)

3.1.3 Alteration of HB-EGF expression can lead to tumor attenuation

HB-EGF overexpression had been documented in human breast cancers (Ito et al., 2001). HB-EGF is found to be frequently co-expressed with other EGF ligands in breast cancer, and its expression correlates positively with histopathological grade (Révillion et al., 2008).

Zhou and colleagues reported that secreted HB-EGF from HB-EGF-overexpressing breast cancer cells acted in an autocrine fashion to induce EGFR activation and MMPs expression, resulting in increased tumor invasion through invadopodium formation, tumor cell intravasation into blood vessels, and lung metastases in mouse xenografts (Zhou et al., 2014). The enhanced intravasation of HB-EGF-expressing cells can also be attributed to the induction of integrin expression levels by HB-EGF that triggers selectin-mediated adhesion of cancer cells to the endothelial walls (Narita et al., 1996).

Due to the finding that diphtheria toxin is able to bind to pro-HB-EGF (Naglich et al., 1992), a non-toxic mutant diphtheria toxin, CRM197, was found to inhibit the mitogenic effects of HB-EGF on human cells (Mitamura et al., 1995). Studies using CRM197 had reported effective tumor growth inhibition by blocking MAPK and PI3K/Akt activation in aggressive TNBC and treatment-resistant breast cancer cells (Yotsumoto et al., 2010). Intravenous administration of CRM197 in immunocompromised mice grafted with human TNBC cells also showed effective reduction in tumor volume (Nam et al., 2016), which initiated an ongoing clinical trial in advanced TNBC patients.

Other than using CRM197 or neutralizing antibodies, there is also a possibility of altering HB-EGF expression using miRNAs. There is an increasing body of evidence showing physiological regulation of HB-EGF by a variety of microRNAs in cells or tissues, for example mast cells (Molnár et al., 2012), bone cells (Yu et al., 2013; Yang et al., 2014), skin (Li et al., 2015), and trophoblast cells (Jain et al., 2016). In treatment-resistant head and neck squamous cell carcinoma cells, addition of miR-212 mimic was found to inhibit HB-EGF and thus, induce sensitivity to EGFR inhibitor therapy (Hatakeyama et al., 2010). Inspired by a study demonstrating the ability of miR-96 to target HB-EGF in osteoblast and bone marrow-derived mesenchymal stem cells, which promotes osteogenic differentiation (Yang et al., 2014b), I hypothesized that miR-96 may also suppress breast CSCs' activity and cellular proliferation

through HB-EGF downregulation. To address this hypothesis, I have performed knockdown experiments using small interfering RNAs (siRNAs) against HB-EGF and compared the effects to cells treated with miR-96 mimic.

3.2 Materials and Methods

Transfection

To knockdown HB-EGF, small interfering RNAs targeting HB-EGF (siHB-EGF) (Invitrogen) were first diluted to a final concentration of 16 nM in 250 μL OPTI-MEM. This mixture was then added with 5 μL Lipofectamine® RNAiMax reagent in 250 μL OPTI-MEM and incubated for 10 min at RT. A scrambled siRNA (sense strand: UUCUCCGAACGUGUCACGUTT; antisense strand: ACGUGACACGUUCGGAGAATT) was used as a negative control (siCTRL).

DNA or plasmid constructs and luciferase assays

For luciferase reporter assays, the full-length 3'UTR of *HB-EGF* were amplified from human genomic DNA and cloned upstream of *Firefly* luciferase vector, *Luc2* (Promega). The primer sequences used for *HB-EGF* 3'UTR cloning were presented in *Table 2* (Chapter 2.2). Transfection and luciferase assay were conducted using HEK 293T cells and Promega Dual-Luciferase® Reporter Assay's (Promega) as described in Chapter 2.2. Relative luciferase activities were calculated as ratios of *Firefly* to *Renilla* luciferase index.

Determination of miRNA and mRNA expression levels

Total RNA was extracted using ISOGEN-II (Nippon Gene, Japan) reagent. For mRNA quantification, cDNA was synthesized from 1 μg of total RNA with Prime Script™ RT reagent (TAKARA, Japan). The quantification of miRNA and mRNA transcripts were performed using

quantitative RT-PCR as described in Chapter 2.2. *GAPDH* expression level was used for mRNA normalization while *U6 snRNA* was used for miRNA normalization. Primers employed in quantitative RT-PCR are listed in *Table 4* below.

Table 4 List of primers used for quantitative RT-PCR

Gene	Forward primer	Reverse primer
KLF4	GCGGCTTCGTGGCCGAGCTC	CGTACTCGCTGCCAGGGGCG
HB-EGF	GGTGGTGCTGAAGCTCTTTC	GCTGGTCCGTGGATACAGTG
CD44	CGGACACCATGGACAAGTTT	GAAAGCCTTGCAGAGGTCAG
CD44v3	GCACTTCAGGAGGTTACATC	CTGAGGTGTCTGTCTCTTTC
GAPDH	GAAGGTGAAGGTCGGAGTCA	TTGATGGCAACAATATCCACTT

Staining and flow cytometry analysis

Cells were detached by trypsinization and centrifuged after treatment. Cell pellets were resuspended in PBS with 2% FBS containing anti-human FITC-conjugated CD44 (clone BJ18) antibodies (Biolegend®) at a concentration of 1:1000. Anti-human IgG antibodies were used to determine the positive subsets of cells from background staining. Cells were incubated on ice in the dark for 30 min. Cells were washed 3 times with PBS before being analyzed by flow cytometry. 1 μg/mL 7-AAD was used as a viability dye (Sigma). Analysis was performed using a FACSAria™ III cell sorter system (BD Biosciences, San Jose, CA, USA).

Sphere formation assay

Both control and siHB-EGF-treated cells were harvested, and single cells (100 cells/well) were plated on 24-well ultra-low attachment tissue culture plates (Corning) in serum-free culture medium containing 10 ng/mL EGF, 10 ng/mL bFGF, and B27 up to 14 days. Tumorspheres

were measured and imaged using a Nikon Eclipse TS100 inverted microscope (Nikon Instruments, Tokyo, Japan) with a 4x objective lens. The number of tumorspheres over 50 μm was counted.

Cell proliferation assay

After transfection for 72 h, the untreated and siHB-EGF-treated cells were harvested by trypsinization after the removal of cell culture medium. The number of cells in each well was quantified using hematocytometer. The average cell numbers were calculated from at least 3 wells for each group.

Cell cycle analysis

Cells were fixed in 70% pre-chilled (-20°C) ethanol overnight. After centrifugation, cells were stained with 10 μg/mL propidium iodide (Sigma) in PBS containing 2% FBS and RNase A for 30 min at RT. Analysis was conducted on a BD FACSCalibur flow cytometer (BD Biosciences, San Jose, CA, USA) and data were analyzed with FlowJo™ Version 10 (Becton, Dickinson and Company, 2019).

Western blot analysis

Cells were lysed in lysis buffer (50 mM Tris-HCl [pH 7.5], 150 mM NaCl, 1 mM EDTA, 1% NP-40, complete protease inhibitor cocktail (Roche)) and incubated on ice for 20 min before protein lysates were collected by centrifugation. Protein concentrations were measured using the Pierce® BCA protein assay (Thermo Scientific). Lysates were resolved by SDS-PAGE and transferred to PVDF membranes before blocking with 5% skim milk in TBS-T solution for 1 hour at RT. Membranes were incubated with anti-Retinoblastoma (RB) (BD Pharmigen, clone G3-245, cat# 554136), anti-Cyclin A (Santa Cruz, clone E72.1, cat# sc53232), and anti-

GAPDH (Cell Signaling Technology, clone 14C10, cat# #2118L) at 4°C overnight. This was followed by secondary incubation with antibodies conjugated to horseradish peroxidase (GE Healthcare). Protein bands were detected with Western Lightning Plus-ECL, Enhanced Chemiluminescence Substrate (PerkinElmer, Waltham, MA, USA).

Statistics

Results are presented as means ± SD for at least three repeated individual experiments for each group. Statistically significant differences between mean values were determined using two-tailed Student's *t*-test (***$p < 0.001$, **$p < 0.01$ and *$p < 0.05$), unless otherwise specified.

3.3 Results

3.3.1 miR-96 regulates HB-EGF transcription by binding to its 3'untranslated region (UTR)

HB-EGF mRNA appeared to be a likely target of miR-96 according to TargetScan's prediction where its 3'-UTR harbors a binding site complementary to the seed sequence of miR-96 (*Figure 3.2a*). As mentioned earlier, HB-EGF, which is usually overexpressed in breast cancer, is strongly associated with CD44 (Yu et al., 2002). This prompted me to postulate that CD44 suppression might be a consequence of HB-EGF downregulation by miR-96. To validate this hypothesis, I first performed quantitative RT-PCR using MCF7 cell lysates to quantify the *HB-EGF* mRNA transcript level upon transfection with miR-96 mimics. Indeed, similar to *CD44* and *CD44v3, HB-EGF* mRNA expression was also significantly suppressed (*Figure 3.2b*). Next, I assessed the ability of miR-96 to regulate the 3'UTR of *HB-EGF* mRNA using a luciferase reporter assay as described earlier. The 3'UTR of *HB-EGF* mRNA, containing the predicted target sequence, was cloned into a pGL4.10 luciferase vector. Addition of miR-96

effectively suppressed the luciferase activity of the pGL4.10-HB-EGF 3'UTR vector by approximately four-fifth (*Figure 3.2c*). This finding verified that *HB-EGF* is a bona fide target of miR-96 via 3'UTR binding that induces mRNA degradation.

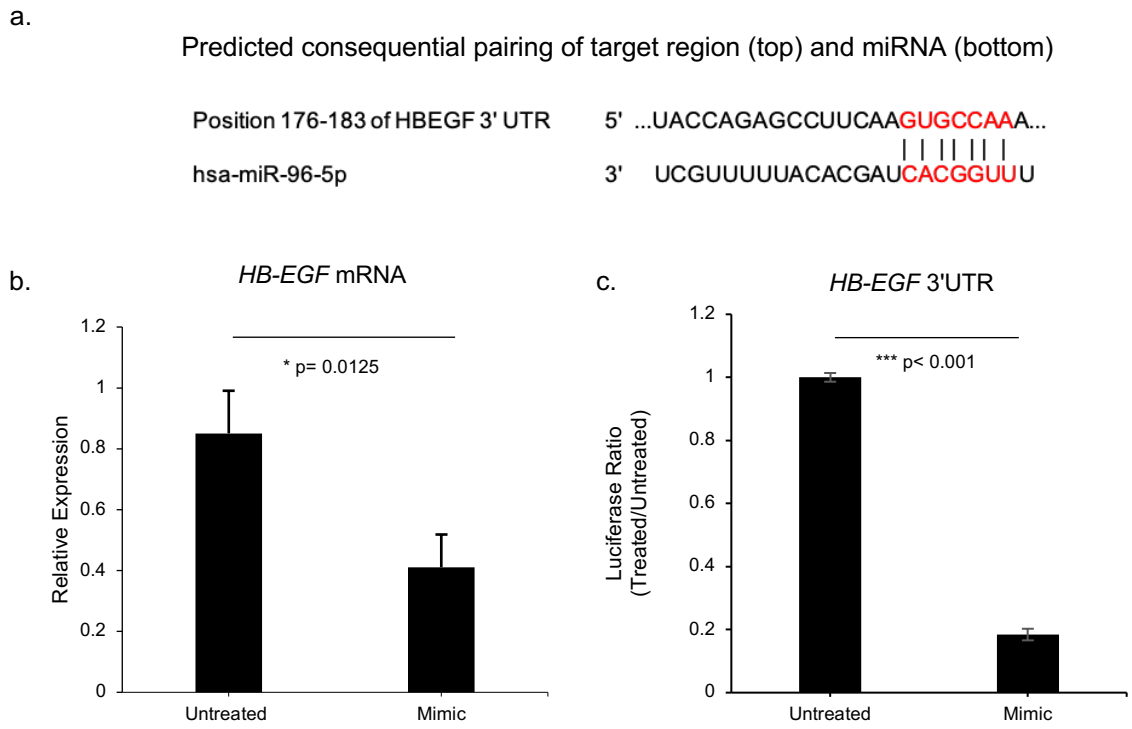

Figure 3.2 miR-96 represses *HB-EGF* transcription by binding to its 3'UTR

a. The 3'UTR of *HB-EGF* is predicted to harbor a binding site (marked in *red*) for miR-96 according to the prediction tool TargetScan (release 7.1, MIT). **b.** Quantitative RT-PCR of *HB-EGF* mRNA expression in miR-96 mimic-treated MCF7 cells. Results are presented relative to *GAPDH* expression. **c.** Relative luciferase activity of luciferase constructs containing 3'UTR of *HB-EGF* mRNA after treatment with miR-96 mimic in HEK293T cells. Experiments were performed as described in Chapter 2. Error bars represent means of three independent experiments ± S.D. (N=3).

3.3.2 Downregulating HB-EGF expression led to CD44 suppression

Both CD44 and HB-EGF were simultaneously repressed by miR-96, but by seemingly different mechanisms, the former by promoter activity suppression while the latter by direct binding to 3'UTR causing mRNA inactivation. How miR-96 represses *CD44* transcript and led

to downregulation of CSCs remain unresolved. To interrogate if HB-EGF regulates the transcription of *CD44*, I knocked down the HB-EGF level with small interfering RNAs (siHB-EGF) in both studied cell lines (*Figure 3.3*) and analyzed the expression of CD44. A siRNA targeting HB-EGF downregulated both *CD44* and *CD44v3* mRNA effectively in MCF7 and MDA-MB468 cells (*Figure 3.3*), as analyzed by quantitative RT-PCR.

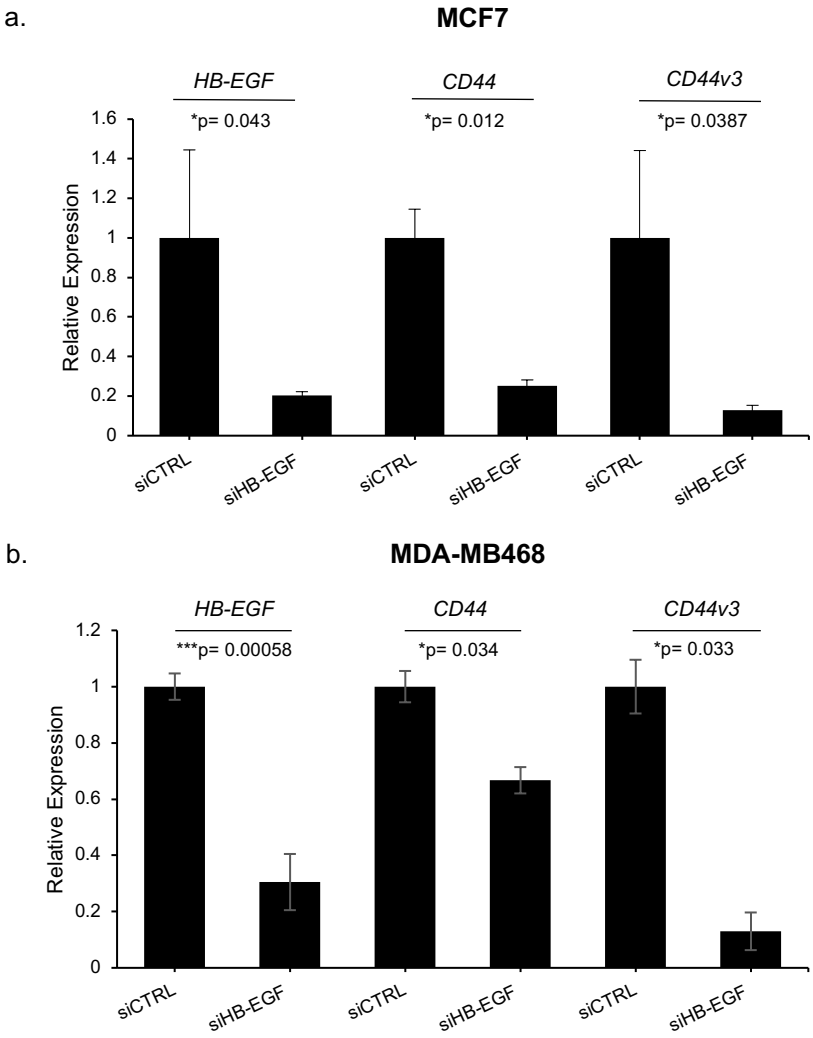

Figure 3.3 Expression of *HB-EGF*, *CD44*, and *CD44v3* mRNA transcripts after HB-EGF knockdown

Quantitative RT-PCR analysis of **a.** MCF7 and **b.** MDA-MB468 cells after treatment with siHB-EGF for 72 h for the expression of *HB-EGF* to confirm successful knockdown, *CD44* and *CD44v3*. Results are presented relative to *GAPDH* expression. Error bars represent means of three independent experiments ± S.D. (N=3) (***$p < 0.001$, *$p < 0.05$ (*t*-test, two-tailed)).

When I analyzed the protein expression of CD44 by flow cytometry, albeit less pronounced than the effects caused by miR-96 overexpression, siHB-EGF also repressed their expression on the cell surface in both MCF7 and MDA-MB468 (*Figure 3.4*). Both the mRNA and protein expressions were simultaneously repressed by loss of HB-EGF, implying that CD44 expression is controlled by HB-EGF.

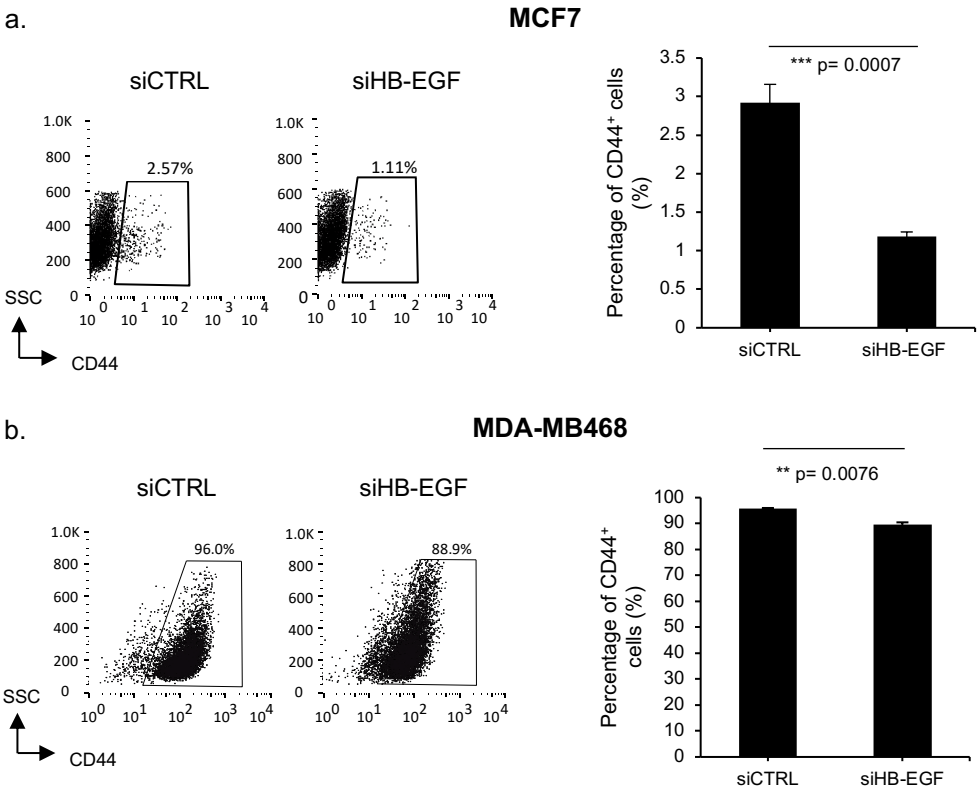

Figure 3.4 HB-EGF knockdown also suppressed CD44 protein expression on cell surface
Surface staining of CD44 on **a.** MCF7 and **b.** MDA-MB468 cells analyzed by flow cytometry after knockdown of HB-EGF (siHB-EGF) *vs* scrambled siRNA (siCTRL). Representative dot plots of cells with and without HB-EGF knockdown are presented with $CD44^+$ population marked in the box (*left*). Average percentage of $CD44^+$ cells in each group, as determined by FlowJo software in triplicate was calculated (*right*). Error bars represent means of three independent experiments ± S.D. (N=3) (***$p < 0.001$, **$p < 0.01$ (*t*-test, two-tailed)).

In order to analyze the functional effect of CD44 suppression as a result of HB-EGF knockdown, sphere formation assay was performed. In line with the results obtained from miR-

96 mimic transfection, HB-EGF knockdown in breast cancer cells also led to attenuation of tumorsphere formation *in vitro* (*Figure 3.5*). In MDA-MB468, none of the single cells effectively formed tumorspheres after HB-EGF knockdown.

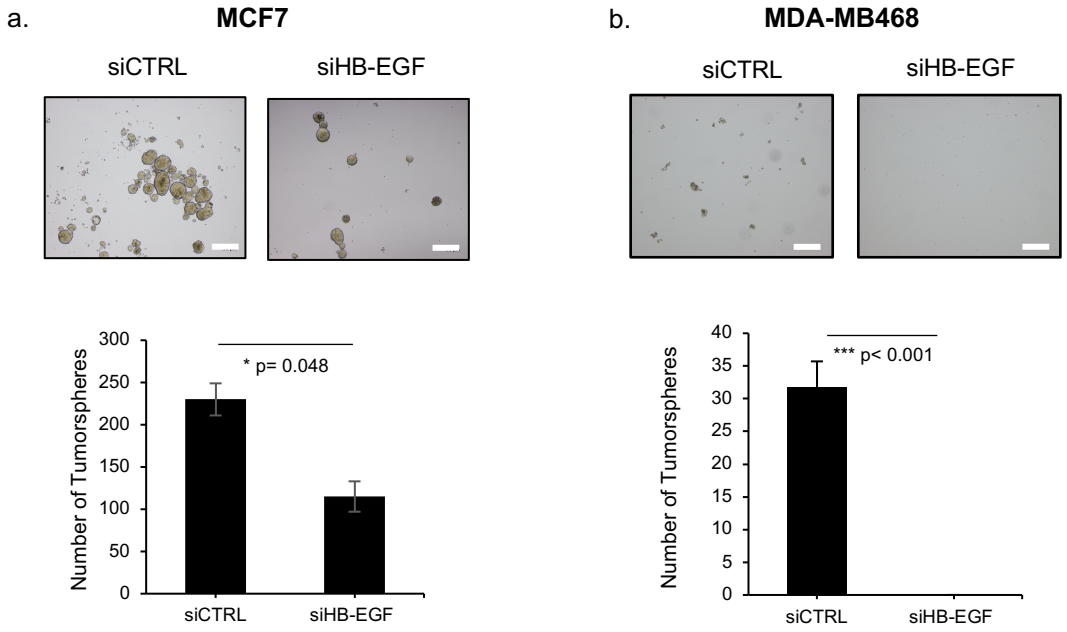

Figure 3.5 Knockdown of HB-EGF reduced sphere forming ability of breast cancer cells
Representative images of siCTRL or siHB-EGF-treated **a.** MCF7 and **b.** MDA-MB468 tumorspheres (*upper panels*) cultured in serum-free, low-attachment condition for 14 days. Average number of tumorspheres (> 50 μm) was calculated from triplicate wells and presented as bar charts for each group (*lower panels*). Scale bar represents 100 μm. Error bars represent means of three independent experiments ± S.D. (N=3) (***$p < 0.001$, **$p < 0.01$, and *$p < 0.05$ (*t*-test, two-tailed)).

3.3.3 miR-96 overexpression reduced cell proliferation and induced cell cycle arrest as in HB-EGF suppression

When carrying out the experiments, I noted a profound decrease in cell proliferation after both cell lines were treated with miR-96 mimic or siHB-EGF (*Figure 3.6*). However, the reduction in cell proliferation was not accompanied with an increase of cell death as ruled out

by cell viability staining of 7-AAD during flow cytometry analysis. Instead, both the miR-96 mimic and siHB-EGF-treated cells appeared to grow at a much slower rate than the controls.

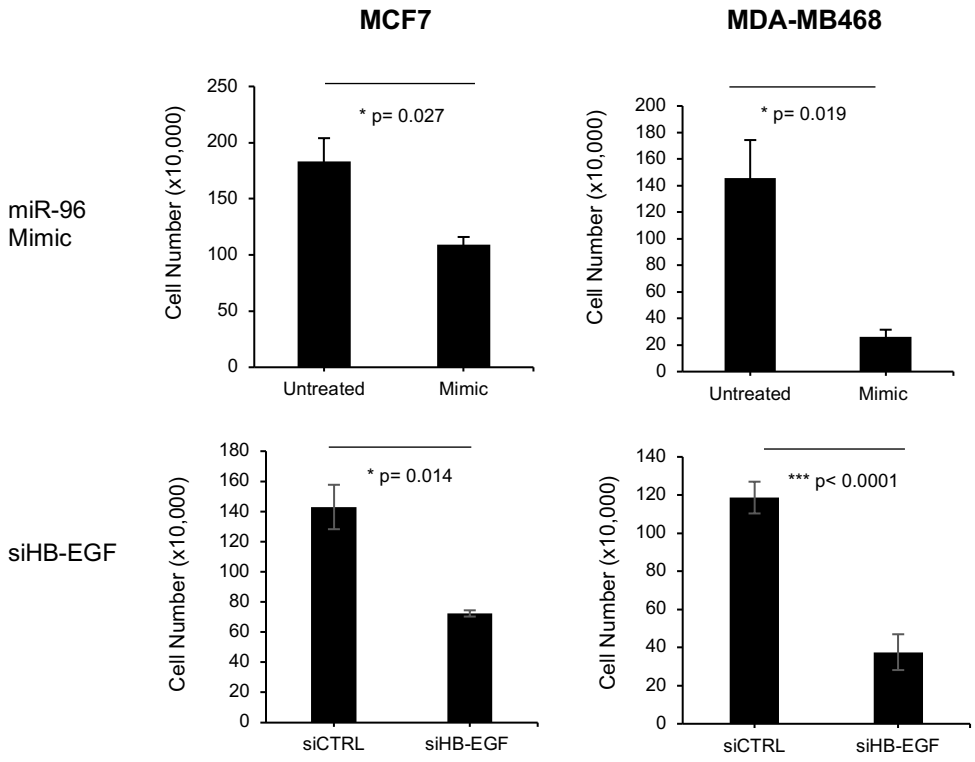

Figure 3.6 Cell numbers after treatment with miR-96 mimic or siHB-EGF for 72 h
After 72 h transfection with miR-96 mimic (*upper panels*) and *HB-EGF* siRNA (*lower panel*), MCF7 (*left*) and MDA-MB468 cells (*right*) were trypsinized and quantified using hematocytometer and the average cell number was calculated. Error bars represent means of three independent experiments ± S.D. (N=3) (***$p < 0.001$, *$p < 0.05$ (*t*-test, two-tailed)).

In fact, the mechanism of cell proliferation control by HB-EGF-C in cancer is well established as discussed in the introduction section of this chapter. In particular, HB-EGF-C accumulation in the nucleus results in nuclear exclusion of the transcriptional repressor, PLZF, enabling Cyclin A to be actively transcribed (Yeyati et al., 1999). To this end, I conducted cell cycle analysis after transfections were performed. As expected, overexpression of miR-96 in MCF7 cells caused cell cycle arrest at the G_1 to S-phase transition, where there was a significant reduction of cells entering S phase accompanied by an increase of cells in G_1 phase (*Figure*

3.7a). Similar phenomenon was observed in siHB-EGF-treated MCF7 cells (*Figure 3.7b*). This finding was supported by Western blots showing suppression of Cyclin A protein expression in cells overexpressing miR-96 (*Figure 3.7c*), whereby it is required from the beginning of S phase for DNA replication in mammalian cells (Girard et al., 1991; Pagano et al., 1992). Increased levels of the unphosphorylated form of retinoblastoma protein (RB) (*Figure 3.7c*) in cells treated with miR-96 mimic, further reaffirmed the hypothesis that cell cycle arrest serves as the main reason for reduced cell proliferation.

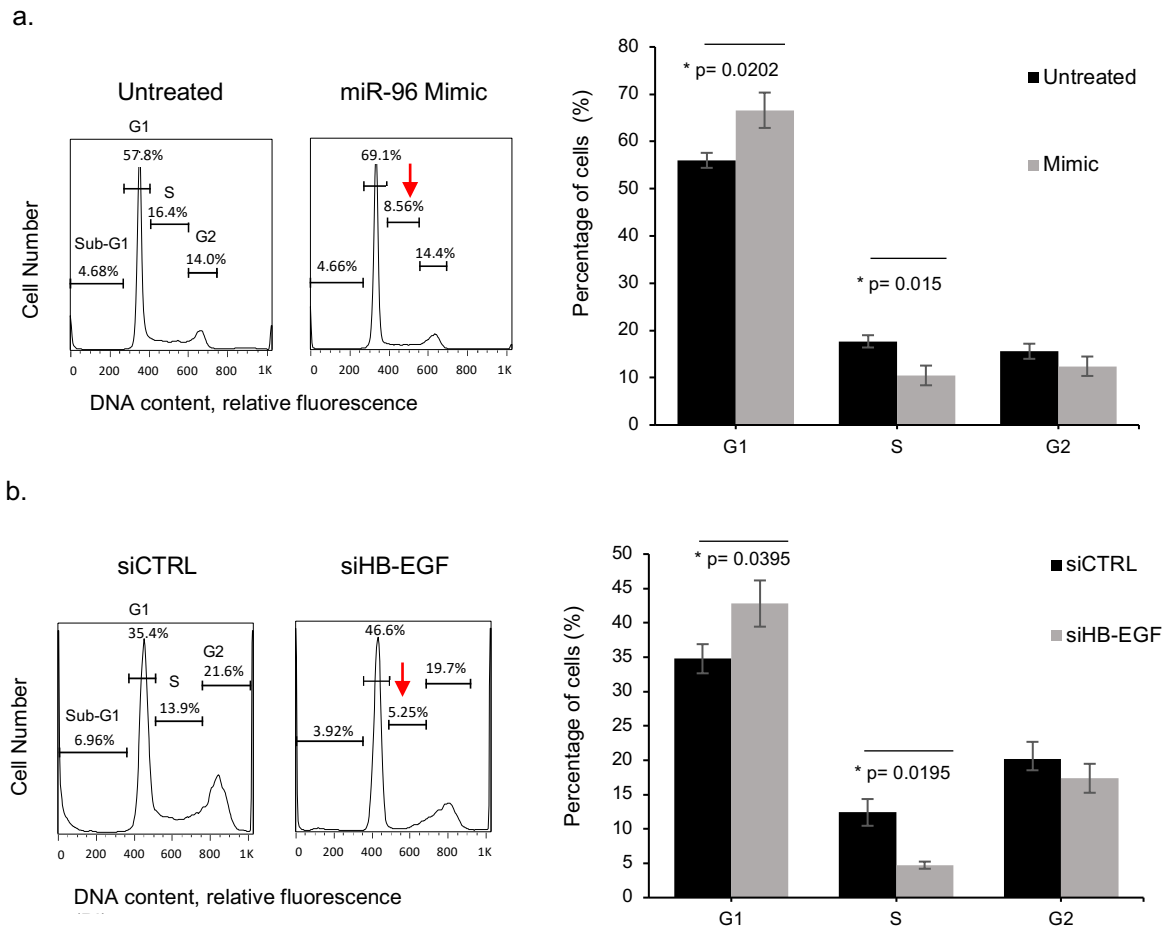

c.

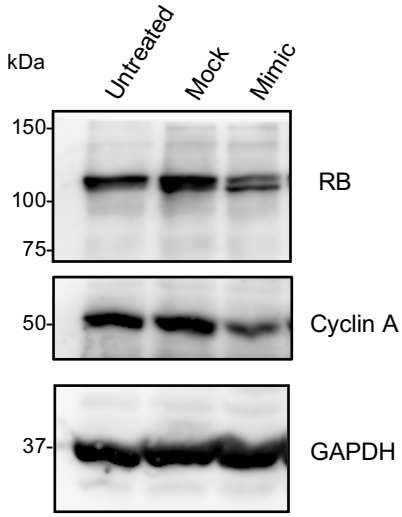

Figure 3.7 miR-96 mimic and HB-EGF knockdown caused cell cycle arrest

Histogram plots of flow cytometry analysis of **a.** miR-96 mimic *vs* untreated and **b.** siHB-EGF- *vs* siCTRL-treated MCF7 cells. Percentage of cells in S-phase for treated samples is marked with red arrows. Average percentage of cells in each cell cycle phase as determined by DNA content using Propidium Iodide staining fluorescence was quantified and compared between the treated cells *vs* control. Error bars represent means of three independent experiments ± S.D. (N=3). **c.** Immunoblot analysis of Cyclin A and RB in MCF7 lysates. GAPDH serves as a loading control.

3.4 Discussion

3.4.1 miR-96 targets HB-EGF, an oncogene in breast cancer cells

The downregulation of *HB-EGF* mRNA was confirmed to be a consequent of mRNA degradation caused by direct binding of miR-96 to the 3'UTR of *HB-EGF*. This finding validated the target gene prediction by TargetScan which determined a perfect match between the seed sequence of miR-96 and position 176-183 of HB-EGF 3'UTR. Furthermore, this also verified a previous study that reported suppression of HB-EGF by miR-96 in osteoblasts and confirmed the predicted target site.

Due to the fact that HB-EGF is an oncogene, targeting HB-EGF may have additional benefits. As such, suppression of HB-EGF will negatively affect cancer cell proliferation,

motility, and invasion by inhibiting its downstream signaling pathways including MAPK and PI3K/Akt. On top of that, HB-EGF-C which acts as a transcriptional regulator may also impact cellular growth by disinhibiting the transcription of cell cycle genes by displacing transcriptional repressor from their promoters. To this end, I have conducted cell cycle analysis on HB-EGF knockdown and miR-96 mimic-treated breast cancer cells and found that there is a significant increase of cells arresting in G_1-phase of the cell cycle together with a reduction in cells entering S phase in both groups. The arrest in G_1-S phase transition in miR-96 mimic-treated cells was consistent with the finding of decrease of Cyclin A protein, an important molecule present at the onset of S phase to regulate DNA replication and throughout the G_2-phase to play a role in activation of mitosis (Girard et al., 1991; Pagano et al., 1992). In this study, the downregulation of Cyclin A exerted a stronger effect on entry into S-phase and hence, resulted in an accumulation of cells cycling in G_1 phase. Taken together with the result of decreased phosphorylated form of RB protein which is critical for releasing E2F transcription factors to allow the expression of genes necessary for S-phase progression (Weinberg, 1995), the reduction of cell growth in the miR-96 mimic-treated cells can be attributed to cell cycle arrest at G_1-S phase caused by loss of HB-EGF. To investigate whether or not this is a result of sustained binding of transcriptional repressor PLZF on Cyclin A promoter, a chromatin immunoprecipitation using anti-PLZF antibody and DNA sequencing of the bound chromatin should be carried out in the future. The results obtained thus far had demonstrated an anti-proliferative effect of targeting HB-EGF in breast cancer cells.

3.4.2 HB-EGF also regulates CD44 in breast CSCs

Because of the close interaction between HB-EGF and CD44 on cell surface that regulates HB-EGF activities, I was interested to see if targeting HB-EGF has any effect in the CD44 expression as well. As expected, the mRNA transcripts of *CD44* and *CD44v3* were

simultaneously decreased upon knockdown of HB-EGF in both $CD44^{low}$ (MCF7) and $CD44^{high}$ (MDA-MB468) breast cancer cell lines. This is also followed by a significant suppression in the CD44 expression on the cell surface as revealed by flow cytometry results. The loss of CD44 expression, a well-known cell adhesion molecule and CSC marker, was accompanied by a reduction of tumorsphere formation *in vitro*, possibly due to an impaired self-renewal ability of cancer cells. A further *in vivo* animal xenotransplantation experiment looking into tumor growth, intravasation, and metastasis may confirm the above findings and complement previous studies that had reported the advantages of targeting HB-EGF in controlling tumor growth and metastasis.

The results of the effect of knocking down HB-EGF on CD44 mirror the findings obtained from overexpressing miR-96 in the breast cancer cells. Since, miR-96 targets *HB-EGF* directly through complementary binding on 3'UTR of the gene but not CD44, the mechanism behind control of CD44 by HB-EGF remains elusive. One possible mechanism is via the transcriptional repression exerted by either PLZF or BCL6. To examine this possibility, I searched the promoter sequence of *CD44* for potential binding motifs by the transcriptional repressors using JASPAR database and discovered that in between nucleotide sequence 1000 and 2000 bp upstream of TSS of *CD44*, there is a consensus DNA binding site for BCL6, 5'-TTCCTAGAA-3' (*Table 5 & Figure 3.8*). This prediction is supported by a study conducted in B lymphocytes which showed that *CD44* is one of the target genes of BCL6 during B cell activation and differentiation and its dysregulation also contributes to lymphomagenesis (Shaffer et al., 2000). To confirm this, chromatin immunoprecipitation using anti-BCL6 antibody should be carried out to determine increased binding of BCL6 on *CD44* promoters in HB-EGF knockdown and miR-96 mimic-treated cells. Once again, this study highlights the diverse mechanisms employed by HB-EGF in regulating gene transcription and expression via

intermediate molecules and therefore, demonstrating additional benefit of targeting HB-EGF in breast cancer.

Table 5 Predicted BCL6 transcriptional repressor binding site within the promoter region of CD44 identified by JASPAR

Matrix ID	Name	Score	Relative score [a]	Sequence ID	Start [b]	End [b]	Strand	Predicted sequence
MA0463.2	BCL6	8.52116	0.805883709044	CD44	581	596	+	CCCTTCTCTAGGAATG

[a] The relative score is provided by JASPAR according to the similarity of motif sequence.

[b] The start and end binding sites correspond to the mRNA sequence 2000 bp upstream of TSS of *CD44* from 5'→3'.

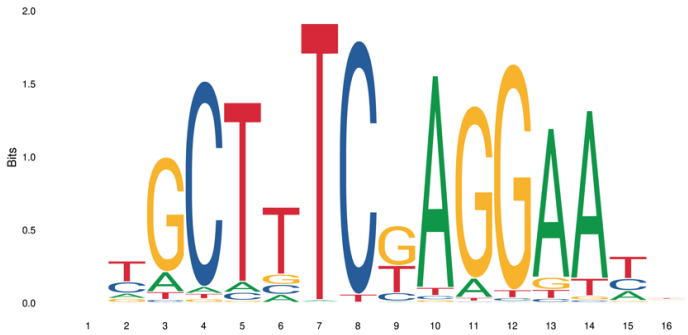

Figure 3.8 Predicted BCL6 (MA0463.2) binding motif sequence logo for *CD44* promoter from JASPAR

3.4.3 miR-96 has combinatorial effects by targeting oncogenes

The current study had demonstrated the heterogenous effects of miR-96 mimic on breast cancer cells. First of all, the downregulation of CD44 led to attenuation of breast CSC population and hence, slowed tumor formation. Secondly, repression of oncogenes by miR-96 resulted in growth suppression. Suppression of CSC marker, CD44 by miR-96 is shown to be directed by two possible transcriptional control mechanisms: (1) downregulation of FOXO3 which serves as an activator for *CD44* transcription and (2) sustained binding of a

transcriptional repressor, BCL6 on *CD44* regulatory region caused by a downregulation of HB-EGF. This study had mainly focused on the transcriptional regulation of CD44, however in future studies, it would be interesting to investigate the disrupted protein interaction between CD44 and HB-EGF on the cell membrane as a result of miR-96 overexpression, and how this influences the proteolytic action of MMP, ErbB4 binding as well as the activation of downstream EGF signaling.

HB-EGF, an oncogene which has been found upregulated in breast cancer cells seems to be the central mediator of miR-96. On the one hand, it controls the expression of CD44 that plays a crucial role in stem cell regulation. On the other hand, its indirect role of acting as a transcription factor in cell cycle progression also contributed significantly to the process of tumorigenesis. In this study, I reiterated the mechanism of HB-EGF in controlling cell cycle transition from G_1 to S-phase, via transcriptional repression of a cell cycle gene, Cyclin A. Another possible mechanism that was not explored in the current study was the effect on EGF and PI3K/Akt signals due to direct downregulation of HB-EGF. If the mitogenic signaling pathways were also proven to be suppressed, this would add another layer of negative control of cellular proliferation by miR-96 via HB-EGF. Overall, the results had revealed the multifaceted effects of a single miRNA in targeting a highly pleiotropic gene and demonstrated enhanced benefits of using miR-96 mimic in controlling tumor growth.

To supplement these *in vitro* findings, comprehensive *in vivo* experiments examining the mechanistic controls of HB-EGF as well as functional effects of targeting HB-EGF should be performed. Because of the heterogeneous expression of HB-EGF in various cell types including macrophages (Higashiyama et al., 1991), particular attention should be paid on the relevance of transcription factors' regulation by HB-EGF in an immune-intact *in vivo* environment. It has been shown that tumor-associated macrophages highly express and secrete

HB-EGF into the tumor microenvironment which induces tumor cell chemotaxis in patients with invasive breast cancer patients (Vlaicu et al., 2013).

In conclusion, this thesis had thus far examined and demonstrated the diverse and concerted transcriptional controls driven by a non-coding RNA, miR-96 in modulating breast cancer cells' fate and plasticity via two different target genes, *FOXO3* and *HB-EGF* which led to an overall tumor growth suppression. HB-EGF plays a dual role in regulating cancer stem cell fate as well as in controlling cell proliferation, which serves as a great candidate for anti-cancer therapy. Although the experiments had not been done extensive enough to comprehensively analyze the regulatory controls and functional effects of miR-96 including taking into consideration other target genes, the findings presented can still serve as foundational insights for further in-depth studies into the advantages of miR-96 or anti-HB-EGF in breast cancer therapy. However, it is important to note that it is still early to suggest the promising use of miR-96 as an add-on anti-tumor drug in clinical practice. Careful design of the drug delivery system for miR-96 which includes the use of drug carrier such as nanoparticles that are compatible with sustainable delivery, functionalization with a specific target of breast tumor tissues as well as the possible routes of administration should be considered. On top of this, it is also important to take note of the potential side effects or off-targets while considering the systemic use of miR-96 since miR-96 is expressed in sensory tissues, and that miR-96 also targets other genes or proteins which are widely expressed by other tissues, for instance physiological expression of HB-EGF by immune cells.

Chapter 4

Bioinspired self-assembling peptides alter pancreatic cancer cell fate by modifying its tumor microenvironment

4.1 Introduction

4.1.1 Desmoplastic reaction of pancreatic cancer influences metastatic behaviors

The desmoplastic TME that is manifested by an abundance of extracellular matrix components surrounding the tumor has been widely studied and regarded as a malignant property of PDAC. One of the most recognized roles of TME is its ability to drive metastasis, a common clinical presentation in PDAC patients and a major cause of cancer-related death. This is exemplified by the finding that desmoplasia in primary and metastatic tumors of PDAC are negatively correlated with patient survival (Whatcott et al., 2015b). One of the mechanisms exploited by desmoplasia in promoting metastasis is by creating a hypoxic microenvironment. In contrast to normal pancreas, pancreatic tumor is surrounded by low density of vasculatures in its fibrotic stroma which leads to hypoxia and increased expression of hypoxia-inducible factors (HIFs) in PDAC (Couvelard et al., 2005; Miyake et al., 2008; Erkan et al., 2009). This is further exacerbated by the fact that hypoxia induced secretion of extracellular matrix proteins including collagen and fibronectin into the TME (Erkan et al., 2009), fueling a vicious hypoxia-fibrosis cycle. It is now well established that hypoxia triggers downstream signaling pathways in PDAC via HIFs that result in pancreatic tumor progression and metastasis (Diaz and Yuen, 2014; Miller et al., 2015; Zhao et al., 2015; Zhou et al., 2018). For example, the upregulation of HIF-3α transcriptionally activates actin-regulatory network genes, including Rho-associated coiled-coil containing protein kinase 1 (*ROCK1*) and *RhoC*, stimulating F-actin polymerization which promotes cancer invasion and migration (Zhou et al., 2018).

Next, the heterogenous signaling present in the tumor stroma also contributed to the metastatic behaviors of PDAC. TGF-β, Sonic Hedgehog (Shh), hepatocyte growth factors (HGF), prostaglandins, chemokines, and cytokines like interleukins are among the myriad of soluble factors that can be found in the PDAC's tumor stroma (Zhang et al., 2019b). Upregulation of secreted factors by myofibroblasts like HGF and insulin-like growth factor-1

(IGF-1) can cooperate and mediate downstream signaling in PDAC, activating invasion and metastatic programs (Rucki et al., 2017). While some of the these signaling molecules interact with PDAC cells in a paracrine manner to induce metastasis, other soluble factors like interleukins and chemokines had been instrumental in inducing an immunosuppressive microenvironment by modulating immune cell infiltration and immune functions which exacerbate the malignant behaviors of PDAC (Liu et al., 2019).

ECM stiffness caused by deposition of matrix proteins is increasingly recognized as a driver of tumor cell migration and invasion. At specific stiffness as measured by atomic force microscopy (AFM), focal adhesion-rich invadopodia is formed and invadopodia-associated ECM degradation is activated, initiating cell invasion (Alexander et al., 2008). In sensing a stiff ECM, cancer cells may respond by activating biochemical pathways to increase collagen crosslinking, focal adhesions, followed by an enhanced PI3K and integrin signaling pathways which drive invasion (Levental et al., 2009). Very often, the process of mechanical activation of biochemical pathways termed mechanotransduction causes stimulation of cell cycle progression, EMT, and cell motility (Broders-Bondon et al., 2018). In PDAC, early study had reported that the synthesis of type I collagen by myofibroblasts increased survival and malignant potential of PDAC cells (Armstrong et al., 2004). Recent studies reinforced the notion of ECM rigidity in inducing malignant and metastatic behaviors of PDAC cells. For example, Rice and colleagues demonstrated that increased ECM rigidity during tumor progression is associated with EMT activation that underlies cancer aggressiveness and resistance to chemotherapeutic drug, paclitaxel (Rice et al., 2017). Similarly, the stiffness of pancreatic cancer cells has been found to be positively correlated with their invasiveness (Nguyen et al., 2016). Taken together, the complexity of TME contributes to the aggressiveness of PDAC via a variety of mechanisms. Clinically, this translates to a substantial barrier for effective PDAC treatment, leading to a dismal prognosis.

4.1.2 Laminin-integrin interaction plays important roles in physiological and pathological cellular functions

Laminins are made up of a family of large (ranging approximately 400 to 800 kDa) heterotrimeric multidomain proteins composed of α, β, γ chains (Aumailley et al., 2005). Together with type IV collagen, they constitute the bulk of basement membrane proteins by forming insoluble networks to provide a structural rigidity to the basal side of epithelium and endothelium. Because of their abundance and importance in maintaining basement membrane integrity, laminins are involved in processes regulating cell adhesion, differentiation, motility, survival, and are critical for both development and tissue homeostasis. To exert their cellular function, laminins bind to membrane receptors like integrins, the most common binding partners, to induce intracellular signaling pathways. The specific structural domains of α1, α2, α5, and γ2 chains of laminins are able to bind to several integrin isoforms including α1β1, α2β1, α3β1, and αVβ3 (Colognato-Pyke et al., 1995; Colognato et al., 1997; Decline and Rousselle, 2001; Nielsen and Yamada, 2001; Sasaki and Timpl, 2001).

Integrins are ubiquitously expressed as cell surface membrane receptors. They are heterodimeric proteins that possess bidirectional signaling abilities to mediate intracellular to extracellular signals (inside-out) and extracellular to intracellular signals (outside-in) (Harburger and Calderwood, 2009). On the extracellular side, the receptor domains of integrins bind ECM proteins which then relay the biochemical signals intracellularly via its cytoplasmic tail linkage with the cytoskeletal network to induce cellular responses. Once outside-in signaling is triggered, a series of biochemical signals, which include among others, focal adhesion kinase (FAK), Src-family kinase, integrin-linked kinase (ILK), and Rho GTPase are activated (Harburger and Calderwood, 2009). On the flip side, the extracellular domains of integrins are capable of undergoing conformational changes to influence ligand binding in response to intracellular signal molecules interacting with the their cytoplasmic domains

(Calderwood, 2004). The complex bidirectional signaling networks resulting from the binding between laminins and integrin receptors are essential for important cellular processes, and hence their dysregulation which follows by a disruption in ECM also promotes activities like cancer cell migration and tumor invasion during metastasis (Hamidi and Ivaska, 2018).

During the invasion process, the configuration of basement membrane is significantly altered in malignant tumors due to proteolytic degradation and penetration of tumor cells (Barsky et al., 1983). The same happens to the expression pattern and composition of laminins. Among all the laminin chains, laminin α5 has been found to be expressed universally in all epithelial tumors, and its expression pattern is disrupted in the invasive fronts in multiple malignant tumors (Määttä et al., 2001). Laminin α1, however, is sparingly distributed in thyroid, ovary, and breast carcinomas (Määttä et al., 2001). In PDAC, more invasive, less differentiated subtype of tumors were found to synthesize more laminin in an *in vitro* setting; their basement membrane is often less structured than their less invasive, more differentiated counterparts (Haberern-Blood et al., 1987). In particular, laminin-332 or formerly termed laminin-5, made up of α3, β3 and γ2 chains, is haphazardly deposited in the basement membrane and adhered by PDAC to drive migration (Tani et al., 1997). The overexpression of β3 chain of laminin-332 has been recently reported to associate with less differentiated, advanced phenotype, and poor survival (Chen et al., 2015).

On the other hand, integrin signaling has been found to be one the 12 core signaling pathways that have been uncovered to be genetically altered in most PDAC with representative integrin and laminin genes such as *ITGA4, ITGA9, ITGA11, LAMA1, LAMA4, LAMA5, FN1, ILK* (Jones et al., 2008). Genome-wide DNA methylation analysis of untreated resected PDACs also found that *ITGA2* locus is often hypomethylated causing high gene expression that is negatively correlated with survival rate (Nones et al., 2014). Integrin β1 expression was found in a several PDAC cell lines, and their expressions with the heterodimer partners, α2,

α5 and α6, are correlated with increased cellular adhesion to collagen, fibronectin, and laminin, respectively, that drives invasion (Arao et al., 2000). Through interacting with type I collagen, integrin α2β1 is implicated to mediate malignant properties including cellular proliferation and migration in multiple PDAC cell lines (Grzesiak and Bouvet, 2006). The interaction between integrin and collagen is further complicated by the fact that specific genotype of PDAC, for instance, loss of TGF-β signaling in a KRAS-driven PDAC mouse model, dictates the phenotype of fibrillar collagen deposited in TME and hence, altering the tissue tension and tumor progression (Laklai et al., 2016). Other than binding to collagen, another study reported that in a particular PDAC cell line, MIA PaCa2, which lacks collagen-binding integrins, α6β1 and α3β1 mediate the cellular adhesion and migration on laminin by enhanced secretion of chemokine, CXCR4 and IL-8 that further exacerbate the malignant phenotype (Grzesiak et al., 2007). In contrast, Walsh *et. al.* showed in an *in vitro* setting that knocking down the expression of *ITGB1*, *ITGA5* and *ITGA6* in a sub-clone of PDAC cell line, MIA PaCa2, rendered the cells less anchorage-dependent and more invasive through extracellular matrix (Walsh et al., 2009). It is therefore important to note that because of the intricate relationship between ECM proteins and integrins, manipulating their expression may have a profound effect on cellular behaviors and functions.

4.1.3 The potential of bioinspired self-assembling peptides in cancer therapy

The discovery of unique self-assembling property of short peptides derived from native proteins had expanded the field of peptide engineering for various applications including biomedical purposes. Early studies demonstrating the self-assembly property of biologically-inspired short peptides include chemically synthesized peptide of *Escherichia coli* fimbriae which self-assembled to mediate attachment of bacteria to eukaryotic cells (Abraham and Beachey, 1987), aggregation of amyloid peptides resembling Alzheimer's amyloid plaques

(Burdick et al., 1992), hydrophobic α-helical peptides aggregate to form voltage-gated ion channel in the lipid bilayer membrane (Yukio and Kimura, 1992), and an alternating hydrophobic and hydrophilic peptide sequence of a yeast protein that adopted a β-sheet structure aggregated under specific circumstances (Zhang et al., 1993). These studies had provided a selection of building blocks for self-assembled peptide structures containing different amino acids, peptide chains or motifs. Among them, the simplest building block is diphenylalanine peptide (L-Phe-L-Phe; FF), two aromatic amino acids that are found in Alzheimer's β-amyloid peptide. It has been shown by multiple studies that the dipeptides self-assemble into supramolecular hydrogels of distinct ordered structures such as nanotubes or nanofibers, depending on the configuration (Reches and Gazit, 2003; Mahler et al., 2006; Yang et al., 2006). Under mild conditions or specific modifications, the dipeptide assembles into a rigid hydrogel structure based on π-π stacking interactions between the aromatic rings (Mahler et al., 2006; Smith et al., 2008). This design was later enhanced by adding an extra phenylalanine to produce a triphenylalanine peptide (L-Phe-L-Phe-L-Phe; FFF) that adopts a conformation with phenyl rings orienting outward to form intermolecular π-π stacking interactions (Tamamis et al., 2009; Han et al., 2010;). The triphenylalanine peptides can self-assemble into larger β-sheet-like supramolecular structures including nanospheres, nanorods and diverse shapes resembling helical-ribbons, needle-like, and leaf-like nanostructures (Guo et al., 2014; Mayans et al., 2017).

These self-assembling peptides offer several advantages including ease for biological functionalization, biocompatibility with lack of immune or inflammatory responses, and biodegradability. Because of these properties, they have been actively explored for potential biomedical applications for tissue engineering, disease modeling and cancer therapy. For example, functionalizing the self-assembling blocks with peptide sequence or motifs of ECM protein may produce synthetic hydrogel scaffolds for study of cell-matrix interactions or tissue

regeneration. For cancer therapy, self-assembling dipeptides can be used for direct targeting of cancer cells or delivery of drugs. For instance, paclitaxel-conjugated self-assembling hydrogel with a cleavable site by esterase was synthesized and shown to induce nanofiber formation intracellularly upon enzymatic cleavage which led to cell death (Yang et al., 2007). Using triphenylalanine self-assembling block together with diglutamate, Mao and colleagues conjugated two drugs, dexamethasone and paclitaxel via disulfide linkage to produce a co-delivery hydrogel to target cancer cells (Mao et al., 2012). Self-assembling block functionalized with integrin binding sequence, a tripeptide RGD, derived from fibronectin, and conjugated with curcumin, a hydrophobic polyphenol by disulfide linkage to form a hydrogelator, had been demonstrated to target integrins overexpressed on tumor cells, whereby upon RGD cleavage, the release of curcumin also exerted cytotoxic effect on tumor cells (Yang et al., 2014a). These studies offer initial insights into the potential of self-assembling peptides in cancer therapy at a preclinical level.

In this study, inspired by the laminin-integrin interaction within the TME, a self-assembling peptide combining a triphenylalanine sequence and a short laminin peptide was used to examine the functional as well as molecular effects on pancreatic cancer cells that overexpress specific integrins. This study aims to preliminary assess the potential of such peptide on altering the cell fate of PDAC cells *in vitro* before more advanced experiments on evaluating its potential clinical application are conducted.

4.2 Materials and Methods

Cell lines

Human pancreatic adenocarcinoma cell lines, PANC-1 (TKG0606) and MIA PaCa-2 (ATCC® CRL-1420™) were obtained from RIKEN BioResource Research Center (BRC) Cell Bank, Japan and American Type Culture Collection (ATCC, USA), respectively, prior to the start of the experiment. PANC-1-GFP cells were created by Dr. Shirai of Cell Signal Unit, OIST Graduate University by transfecting GFP plasmid into PANC-1 cells obtained from RIKEN BRC Cell Bank. PANC-1 and PANC-1-GFP were maintained in RPMI1640 medium (GIBCO®) supplemented with 10% fetal bovine serum (FBS) and 1% penicillin/streptomycin while MIA PaCa-2 was maintained in high glucose DMEM medium (GIBCO®) supplemented with 10% fetal bovine serum, 2.5% horse serum and 1% penicillin/streptomycin at 37°C and a humidified atmosphere of 5% CO_2.

Peptide synthesis

The peptides were designed by the Bioinspired Soft Matter Unit and were synthesized and purchased from GL Biochem (Shanghai) Ltd. China and provided in a powder form with a purity of 99%. Amino acid sequence analysis was performed by mass spectrometry.

Transmission electron microscopy (TEM) imaging

10 μl of peptide solution was added and allowed to stand for 30 s at room temperature on a glow-discharged, thin carbon film-coated copper grid (400 mesh). The grid was washed with deionized water once before staining with 1.0% (w/v) uranyl acetate solution for 30 s. After washing with deionized water twice, the grid was air-dried. Images were taken under high vacuum condition using transmission electron microscope JEM-1230R (JEOL, Japan).

Ultraviolet-visible (UV-vis) spectroscopy

Peptide solution was added into a cuvette with a path length of 1 cm. The UV-vis spectra were collected using a NanoDrop 2000c spectrophotometer (Thermo Scientific, USA) with a range of detection set between 250 and 700 nm and the spectral resolution set at 1.0 nm.

Cell viability assay

PANC-1 cells ($5x10^3$/well) and MIA PaCa-2 cells ($7x10^3$/well) were plated in 96-well plates in triplicates and were allowed to grow overnight. Cells were then treated with the peptides at desired concentrations and durations. At the end of incubation, 10 µl of 3-(4,5-dimethylthiazol-2-yl)-2, 5-diphenyltetrazolium bromide (MTT) solution was added into each well and incubated for 4 h at 37°C in dark. Next, 100 µl of 10% (w/v) sodium dodecyl sulfate (SDS) solution was added to solubilize the purple formazan. Absorbance was measured using a microplate reader at the wavelength of 570 nm. The cell viability values for all samples were expressed as a percentage relative to the untreated (control) condition set at 100%.

Wound healing assay

PANC-1 ($3x10^4$/well) and MIA PaCa-2 cells ($4x10^4$/well) were seeded into each well of a 96-well ImageLock culture plate (Essen BioScience, USA) with culture media containing 10% FBS. After achieving near 100% confluency, cells were starved using culture medium containing 2% FBS for 4 h. Next, homogenous scratch wounds of 700-800 µm in width were made on each well using WoundMaker™ (Essen BioScience, USA). After washing twice with PBS to remove detached cells, cells were treated with varying concentration of peptide solution diluted in culture medium containing 2% FBS. Cells were imaged every 6-hour using 10% objective lens of IncuCyte® S3 Live Cell Analysis Systems (Essen BioScience, USA). To measure the cell migration rate, a confluence mash based on images taken at time point 0 h was

defined by IncuCyte® software analysis tool and the percentage of wound confluence at each time point was quantified. Cells were seeded in triplicates for each treatment condition.

Western blot analysis

Cells were lysed in lysis buffer (50 mM Tris-HCl [pH 7.5], 150 mM NaCl, 1 mM EDTA, 1% NP-40, complete protease inhibitor cocktail (Roche)) and incubated on ice for 20 min before protein lysates were collected by centrifugation. Protein concentrations were measured using the Pierce® BCA protein assay (Thermo Scientific). Lysates were resolved by SDS-PAGE and transferred to PVDF membranes before blocking with *Blocking One* blocking buffer (Nacalai Tesque) for 1 hour at RT. Membranes were incubated with anti-ROCK1 (Abcam, clone EP786Y, cat# ab45171) and anti-GAPDH (Abcam, clone 6C5, cat# ab8245) at 4°C overnight. This was followed by secondary incubation with antibodies conjugated to horseradish peroxidase (GE Healthcare). Protein bands were detected with Western Lightning Plus-ECL, Enhanced Chemiluminescence Substrate (PerkinElmer, Waltham, MA, USA).

Transwell® invasion assay

24 well culture plate with transwell permeable supports with 8 μm pores (Corning, MA, USA) was used to assess the invasion ability of cells. The upper surface of the transwell inserts were coated with 100 μl Matrigel matrix diluted in 0.01M Tris (pH 8.0), 0.7% NaCl buffer to a final protein concentration of 250 μg/mL at 37°C for 2 h. Cells were trypsinized, centrifuged and resuspended in culture medium containing 2% FBS and respective concentration of peptide solution. $3x10^3$/mL cell suspension was seeded into the transwell insert (300 μl/well) while the bottom chamber was filled with 500 μl of culture medium containing 10% FBS. After 48 hours of incubation at 37°C, the culture medium was removed, and a cotton swab moistened with medium was used to remove non-invading cells in the apical side of transwell inserts. Cells

that had invaded to the basal side were fixed in 100% methanol for 10 min and stained with crystal violet solution for 15 min. The membrane was washed with deionized water till excess crystal violet solution was removed. After the membrane was air-dried, cells were imaged using an inverted microscope. Invaded cells were counted using automated counting plugin in ImageJ analysis software. Cells were seeded in triplicates for each treatment condition.

Scanning electron microscopy imaging

Both untreated and treated cells were cultured on a 3.5 cm glass bottom dish. After incubation for desired treatment time, culture medium was removed, and cells were washed with PBS three times before fixation was performed using 2.5% glutaraldehyde in 0.1 M cacodylate buffer for 2 h at room temperature. After rinsing for three times with 0.1 M cacodylate buffer, the samples were post-fixed with 1% osmium tetraoxide in 0.1 M cacodylate buffer for 30 min at room temperature. They were then washed three times with deionized water for 5 min, followed by gradual dehydration using a graded series of ethanol (70, 80, 90 and 95%, 3 min each) and lastly, 100% ethanol twice for 3 min each. The samples were rinsed with *t*-butanol, three times for 3 min each and freeze-dried overnight. After coating with platinum, the samples were imaged using a Quanta 250 FEG scanning electron microscope (FEI, USA) at an accelerated voltage of 5kV.

RNA extraction and next generation sequencing

Total RNA of untreated and treated PANC-1 cells for three time points (6, 12 and 36 h) were extracted using 1 mL TRIzol® reagent for each 10 cm tissue culture plate following manufacturer's instruction. RNA purity was evaluated by spectrophotometry using NanoPhotometer® (INPLEN, CA, USA) and concentration was measured using Qubit® 3.0 Fluorometer (Life Technologies, CA, USA) and 2100 RNA Nano 6000 Assay Kit (Agilent

Technologies, CA, USA). mRNA library preparation was carried out using TruSeq Stranded mRNA Library Prep Kit (Illumina, CA, USA) with polyA-Oligo(dT)-based purification method, followed by fragmentation into short fragments. Double-stranded cDNA was synthesized, end-repaired, ligated to Illumina adapters and PCR amplified. The cDNA library sequencing was performed by Annoroad Genome Technology Corporation (Beijing, China) using NovaSeq 6000 System (Illumina) with three biological replicates for each condition.

RNA sequencing data analysis

Paired-end reads were mapped to the *Homo sapiens* reference genome GRCh38.87 from Ensembl. Measurement of transcript abundance for each replicate was performed using Fragments per Kilobase per Million Mapped Fragments (FPKM) method. For differential expression analysis, DESeq2 was carried out by comparing the FPKM values of treated samples to the controls and $\log_2$ fold change ≥ 1 and adjusted p value < 0.05 were used as cut-off. Significantly upregulated and downregulated genes were subjected to Gene Ontology (GO) enrichment analysis using Database for Annotation, Visualization and Integrated Discovery (DAVID) v6.8 bioinformatics tools (https://david.ncifcrf.gov) (Huang et al., 2009a, 2009b).

Extracellular Acidification Rate assays

The extracellular acidification rate (ECAR) was measured using the Seahorse XF^e 96 Extracellular Flux Analyzer (Seahorse Bioscience). Cells were prepared according to Seahorse XF Glycolysis Stress Test Kit's (Agilent Technologies) instruction. Briefly, $8x10^3$ cells were seeded into a Seahorse XF 96 cell culture microplate and allow to grow overnight before treatment for different time points was initiated. At the end of the treatment, medium was removed, and cells were washed twice with PBS, followed by incubation with Seahorse XF Base Medium in a 37°C non-CO_2 incubator for 45 min prior to the assay. To measure ECAR,

glucose, oligomycin (an oxidative phosphorylation inhibitor), and 2-DG (glycolytic hexokinase inhibitor) were sequentially injected into each well at the indicated time points. Data were analyzed by Seahorse XF-96 Wave software and ECAR is reported as mpH/min.

Metabolic assays

To measure level of ATP, lactate and lactate dehydrogenase activity, CellTiter-Glo® 2.0 Assay (Promega, WI, USA), Lactate Colorimetric Assay Kit II (BioVision) and Lactate Dehydrogenase Activity Colorimetric Assay Kit (BioVision) were used, according to the manufacturer's protocols.

For ATP concentration analysis, PANC-1 cells ($8x10^4$/well) were seeded into a 96-well tissue culture plate and allowed to grow overnight before adding the peptide compound for 6, 12, 24 and 36 h. Once treatment incubation was completed, 100 µl of CellTiter-Glo® 2.0 Reagent was added into each well. To induce cell lysis, the contents were mixed for 2 minutes on an orbital shaker before incubating at room temperature for 10 minutes. The mixture was then transferred to a dark 96-well plate and luminescence was recorded on a luminometer. The measured values of treated samples were normalized to controls.

For lactate and lactate dehydrogenase concentration measurement, PANC-1 cells ($2.5x10^5$/well) were seeded on a 6-well tissue culture plate and treated with peptide compound for the desired duration. After treatment, cells from each condition were trypsinized and centrifuged. $2x10^5$ cells were collected and homogenized by 100 µl of lactate or lactate dehydrogenase assay buffer. Cell lysates were then centrifuged at $1.2x10^4$ rpm for 15 min and the supernatant was assessed by adding reaction mixture prepared from the Lactate Colorimetric Assay Kit II (BioVision) and Lactate Dehydrogenase Activity Colorimetric Assay Kit (BioVision),

respectively. After incubating at 37°C for 30 min in dark, the absorbance was measured at 450 nm in a microplate reader. Values were normalized to the control samples.

Animal xenotransplantation experiment

Animal experiments were performed in accordance with protocol approved by the Animal Experiment Review Committee of the institute. First, $1.5x10^6$ PANC-1 cells were harvested and resuspended in 100 µl Matrigel®. They were then xenografted subcutaneously into the flanks of 6-week old, female BALB/c nu/nu nude mice. Once the tumors were detected, control and treated mice, 3 for each group, were injected with 70 µl vehicle (deionized water containing 5% DMSO) or peptide compound (50 mg/kg dissolved in deionized water containing 5% DMSO) peritumorally, every 3 days up to a maximum of 5 doses. The tumor growth was monitored by total radiant efficiency ([p/s]/ [µW/cm^2]) prior to each treatment injection using IVIS® Spectrum *In Vivo* Imaging System (PerkinElmer, USA). Twenty-five days after xenografting, the tumors were dissected. Tumor size and mass were measured using calipers and a precision balance, respectively. Tumor volume (mm^3) was calculated using the formula: $(xy)^{(\frac{3}{2})} \times \frac{\pi}{6}$.

Statistics

Results are presented as means ± SEM for at least three repeated individual experiments for each group. Statistically significant differences between mean values were determined using two-tailed Student's *t*-test (***$p < 0.001$, **$p < 0.01$, and *$p < 0.05$), unless otherwise specified.

4.3 Results

4.3.1 Design and characterization of laminin-derived self-assembling (LDSA) peptides

The peptide compound, FFFIKLLI, is designed by conjugating the IKLLI sequence that is derived from the α1 chain of laminin-1, with three phenylalanine amino acids (FFF) that promote self-assembly. For simplicity, the peptide is referred to as laminin-derived self-assembling peptide (LDSA) from this point onwards. The peptide sequence and chemical structure are illustrated in *Figure 4.1a*. IKLLI-containing peptide had been shown in a previous study to possess the ability to interact with cells and alter biological activities through its heparin-binding and by binding to integrin α3β1 (Tashiro et al., 1999). By conjugating the peptide with triphenylalanine peptide, self-assembly was enabled through the intermolecular π-π stacking between the aromatic side chains and the hydrogen-bonding interactions between the charged termini (Tamamis et al., 2009; Guo et al., 2014). Due to high hydrophobicity of the peptide, I first dissolved the peptide powder in a small amount of DMSO, followed by diluting it to the desired concentration using deionized water. When the peptide solution was subjected to TEM imaging, the peptide assumed an organized nanofiber structures of tubular morphologies with a width of approximately 50 nm (*Figure 4.1b*). UV-vis spectroscopy results confirmed the presence of high phenylalanine content in the peptide solution whereby a concentration-dependent, characteristic absorption peak around 250- 260 nm was observed (*Figure 4.1c*).

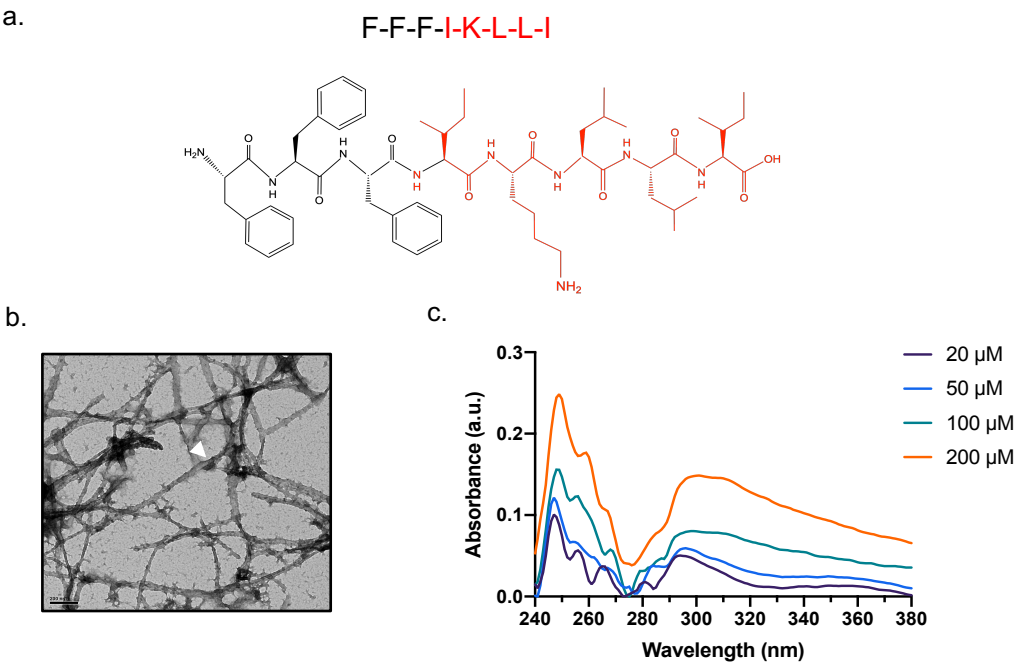

Figure 4.1 Chemical structure and characteristics of LDSA peptide

a. The chemical structure of the peptide is illustrated with the self-assembling block, triphenylalanine (FFF) marked in black and the laminin-derived peptide (IKLLI) marked in red. **b.** Representative TEM image of nanofibers formed by 200 μM LDSA peptides dissolved in deionized water containing 1.0% (v/v) DMSO. The width of the nanofiber is measured between the white lines and arrows. Scale bar represents 200 nm. **c.** UV-vis absorption of the peptide dissolved in deionized water and DMSO to various concentration.

4.3.2 LDSA peptides suppressed pancreatic cancer cell migration and invasion *in vitro*

To assess the biological effects of the peptides, I had used two common pancreatic adenocarcinoma cell lines, PANC-1 and MIA PaCa-2, for *in vitro* experiments. First of all, I tested the viability of cells upon treatment with varying concentrations of the peptide solution diluted in culture medium for 24, 36 and 72 h using MTT assay. Interestingly, the LDSA peptide fiber did not have an apparent influence of cell proliferation or cell growth, even at concentration as high as 200 μM (*Figure 4.2*).

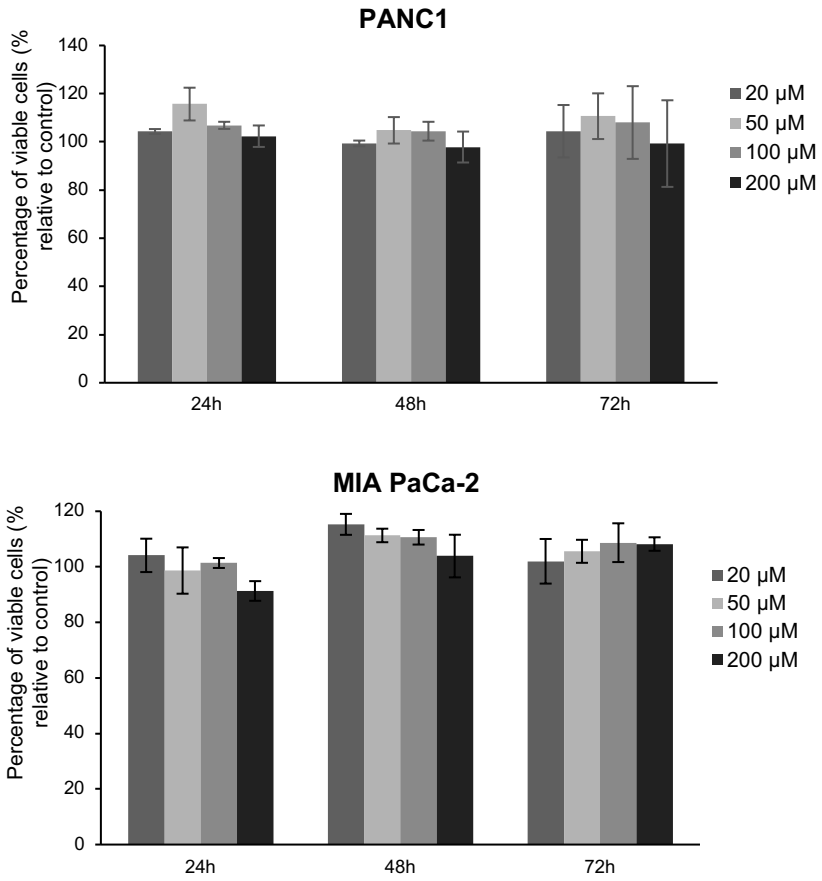

Figure 4.2 MTT viability assay of LDSA peptide treated PDAC cell lines

The viability of PDAC cell lines, PANC-1 (*upper panel*) and MIA PaCa-2 (*lower panel*) was evaluated using MTT after treatment with LDSA peptide solution dissolved in culture medium to concentrations of 20, 50, 100 and 200 µM for 24, 48 and 72 h. Results are presented in percentage relative to the control (untreated) samples. Data represents the mean ± standard error of mean (SEM).

Next, to study the effect of LDSA peptides on cell movement, I performed wound healing assays by tracking the collective movement of pancreatic cancer cells towards the scratched wound using live cell imaging. Both cell lines responded with a dose-dependent migration inhibitory effect by the LDSA peptides (*Figure 4.3 a, b & c*). Especially for PANC-1, the inhibition effect was especially great at concentration of 200 µM where cell movement was slowed by 50% (*Figure 4.3a & b*).

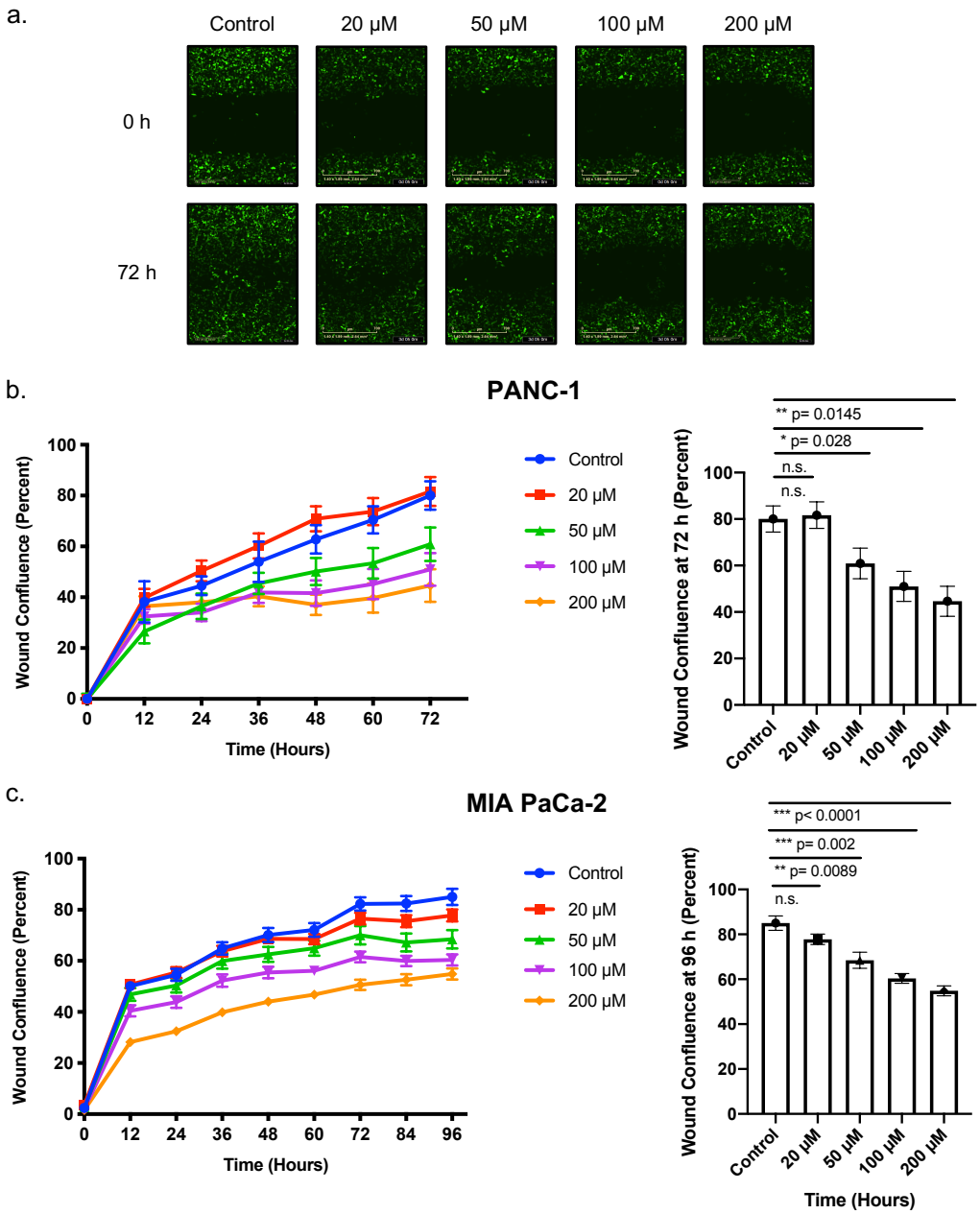

Figure 4.3 Migration assay of PDAC cells upon treatment with LDSA peptides

a. Representative images of GFP-labelled PANC-1 untreated or treated with LDSA peptides at increasing concentration at initial (0 h) and end of migration assay (72 h) tracked by Incucyte® S3 Live Cell Analysis Systems. The percentage of wound confluence, areas occupied by GFP-labelled **b.** PANC-1, and **c.** MIA PaCa-2 at each time point was quantified and presented in the line graphs (*left*). The wound confluence at endpoints 72 h (PANC-1) and 96 h (MIA PaCa-2) was further quantified and analyzed for statistical significance as shown in the bar graphs

(*right*). Data represents the mean ± standard error of mean (SEM) of three independent experiments.

To further reinforce the observation that LDSA peptides inhibited cell movement, LDSA peptide treated PANC-1 cells were subjected to protein extraction and Western blotting for ROCK1, an actomyosin regulatory protein that has been found to be prominently expressed in pancreatic adenocarcinoma to promote invasive growth (Kaneko et al., 2002; Rath et al., 2017). In line with the wound healing assay data, ROCK1 expression was decreased in treated cells in a concentration-dependent fashion (*Figure 4.4a*). Lastly, in order to confirm that the inhibitory effect on migration was caused by the self-assembly of peptides induced by triphenylalanine (FFF), I have also included a control sample that was treated with IKLLI peptide only. The result demonstrated that IKLLI by itself did not exert any inhibition in the collective cell movement across the scratched wound (*Figure 4.4b*), and hence, the triphenylalanine sequence is pivotal in inducing self-assembly of the peptide in order to exert a significant effect on cells' biological functions.

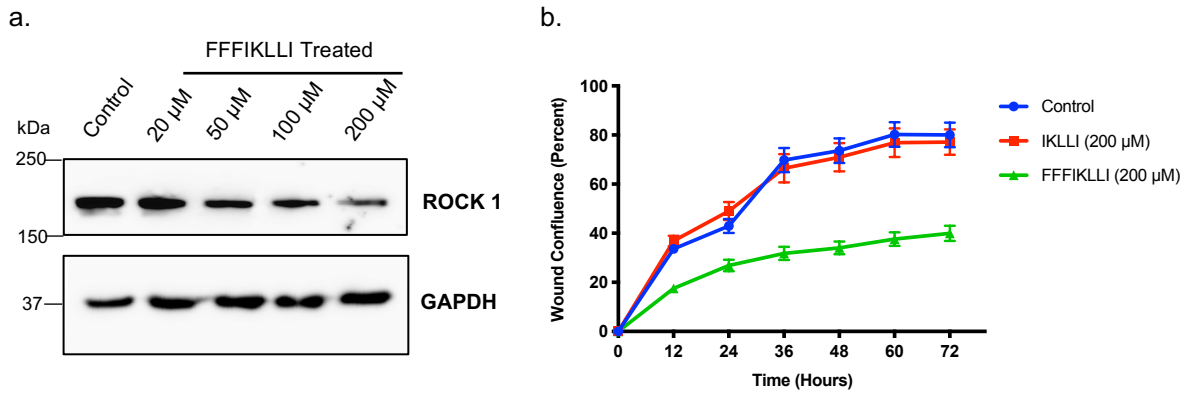

Figure 4.4 Confirmation of migration inhibition by LDSA peptides

a. PANC-1 that were treated with LDSA peptides for 48 h were lysed and proteins were extracted for Western blot using anti-ROCK1 antibodies. GAPDH was used as a loading control. **b.** Migration assay measuring percentage of wound confluence by control, IKLLI and FFFIKLLI-treated GFP-labelled PANC-1 tracked for 72 h. Data represents the mean ± standard error of mean (SEM) of three independent experiments.

Since wound healing assay was carried out in 2D, to investigate the response of cells in a 3D configuration, a transwell® invasion assay was performed. Cells were seeded on a transwell insert coated with Matrigel® for 48 h, and cells that had invaded the Matrigel® to the bottom side of the insert were stained and quantified. The results showed that the invasive ability of both cell lines was greatly inhibited (*Figure 4.5*). For PANC-1, the inhibition effect was pronounced and followed a concentration-dependent manner with almost no cells invaded at a concentration of 200 μM. On the other hand, though LDSA peptides successfully inhibited the invasion of cells over Matrigel in MIA PaCa-2, the effect was not as great as PANC-1 cells. The discrepancy in the inhibitory effect of both cells lines may be accounted by the difference in their integrin expression on the cell membrane as reported by a previous study which discovered that PANC-1 cells express higher level of most integrin subunits than MIA PaCa-2 (Grzesiak and Bouvet, 2006).

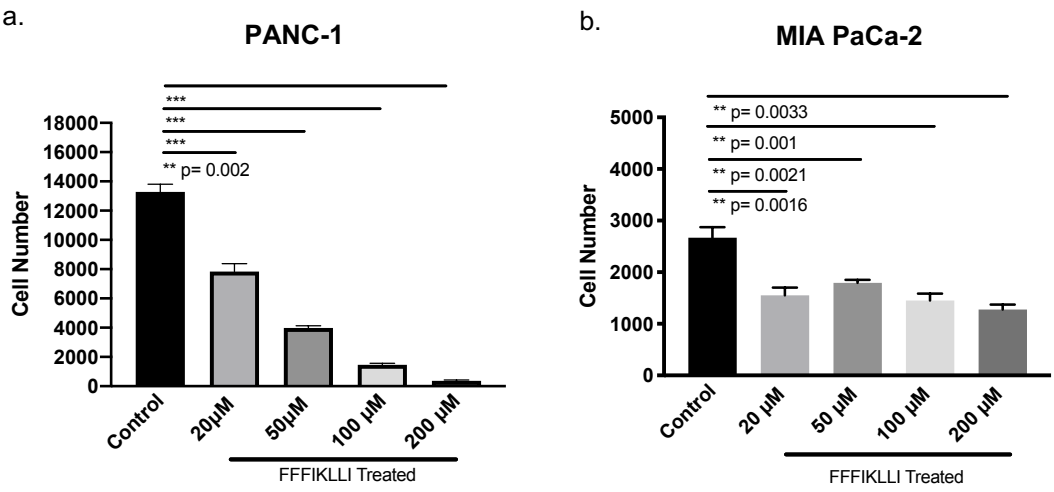

Figure 4.5 Invasion ability of PDAC cells after treatment with LDSA peptides

The three-dimensional invasion abilities of **a.** PANC-1 and **b.** MIA PaCa-2 were evaluated using Matrigel®-coated transwell inserts. Cells that had successfully invaded over the Matrigel® to the bottom side of the inserts were stained and quantified. Data represents the mean ± standard error of mean (SEM) of three independent experiments.

4.3.3 LDSA peptides bound cell surface and altered cell shape

To elucidate how the LDSA peptide affects migration and invasion of pancreatic cancer cells, I used scanning electron microscopy to image cells after treatment with the LDSA peptides. Since 200 μM exerted the greatest inhibition on both cellular migration and inhibition without compromising the cell viability, this concentration had been chosen to evaluate the cell morphology after treatment for 6, 12, 24 and 36 h. Upon treatment, the LDSA peptide started to self-assemble to form an organized nanofibrous meshwork on the apical cell surface as early as 6 h (*Figure 4.6*). With time, the nanofibers grew to cover a larger area of the cell membrane and at 36 h, the entire PANC-1 cells were covered by an aggregate of nanofibrous meshwork. It is interesting to note that the nanofibrous meshwork also extended to cover the lamellipodia of the cells and cell edges (*Figure 4.6, white arrow*), signifying that the LDSA peptide has a high specificity to cell surface membrane. Apart from this, the treated PANC-1 cells presented with a more elongated, fibroblast-like morphology as compared to the control cells that assume a cuboidal, epithelial-like morphology.

In contrast, the nanofibers that formed on MIA PaCa-2 cell membrane altered the initially fibroblast-like cells to become more rounded and epithelial-like. The nanofibrous meshwork also did not show a uniform aggregate on the MIA PaCa-2 cells, even at extended incubation period of 36 h. This difference in the binding of LDSA peptide fibers in these two PDAC cell lines may be a result of differential expression of integrin on each cell surface as discussed earlier, and it goes parallel with the results generated from wound healing and invasion assays. As in wound healing assay, an IKLLI-treated only sample was included to support the fact that triphenylalanine is essential in the formation of peptide self-assembly on cell surface.

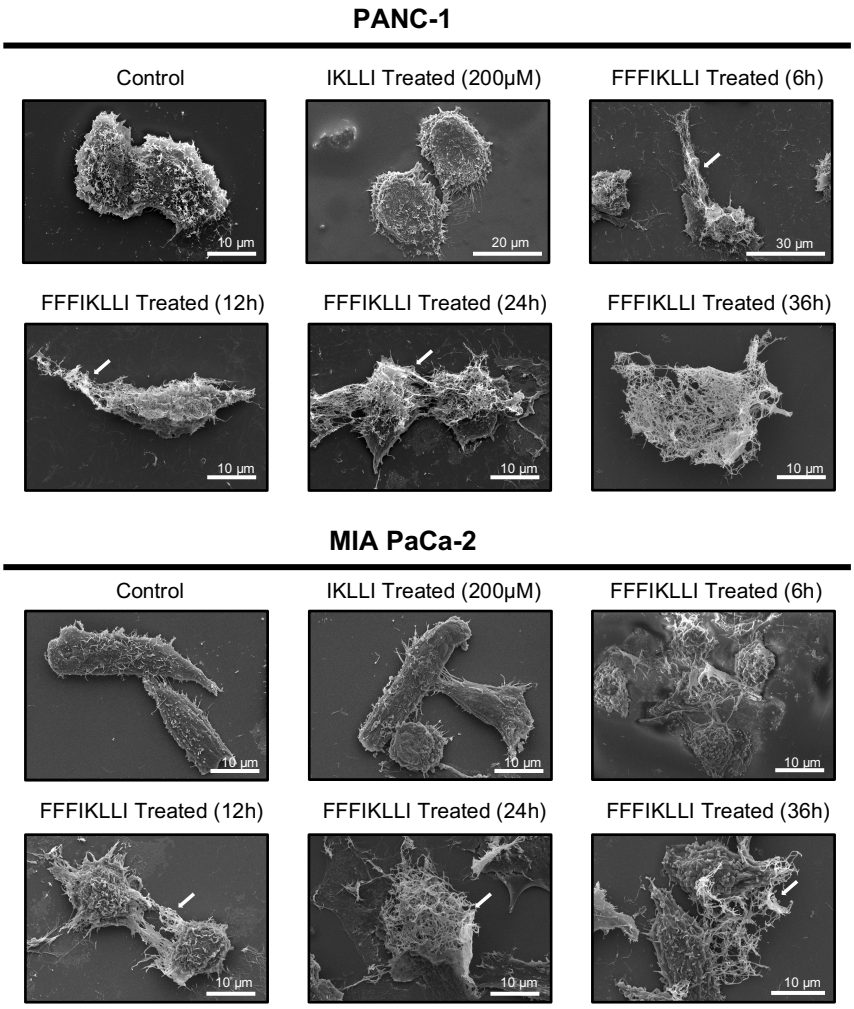

Figure 4.6 Scanning electron micrographs showing binding of LDSA peptide fibers to the cell membrane

FFFIKLLI peptides formed nanofibrous network on the apical membrane of PANC-1 and MIA PaCa-2 after treatment for time periods of 6, 12, 24 and 36 h, but not on control or IKLLI-treated cells. The nanofibers also extended to cell edges and lamellipodia (*white arrow*).

4.3.4 LDSA peptides changed the global transcriptome of pancreatic cancer cells

Following the above findings, I next investigated the molecular changes in the LDSA-treated cells that had brought about the phenotypic alterations. To do this, I isolated RNAs from untreated (control) and 6, 12 and 36 h LDSA peptide-treated PANC-1 cells and subjected them to RNA sequencing to determine their gene expression profiles.

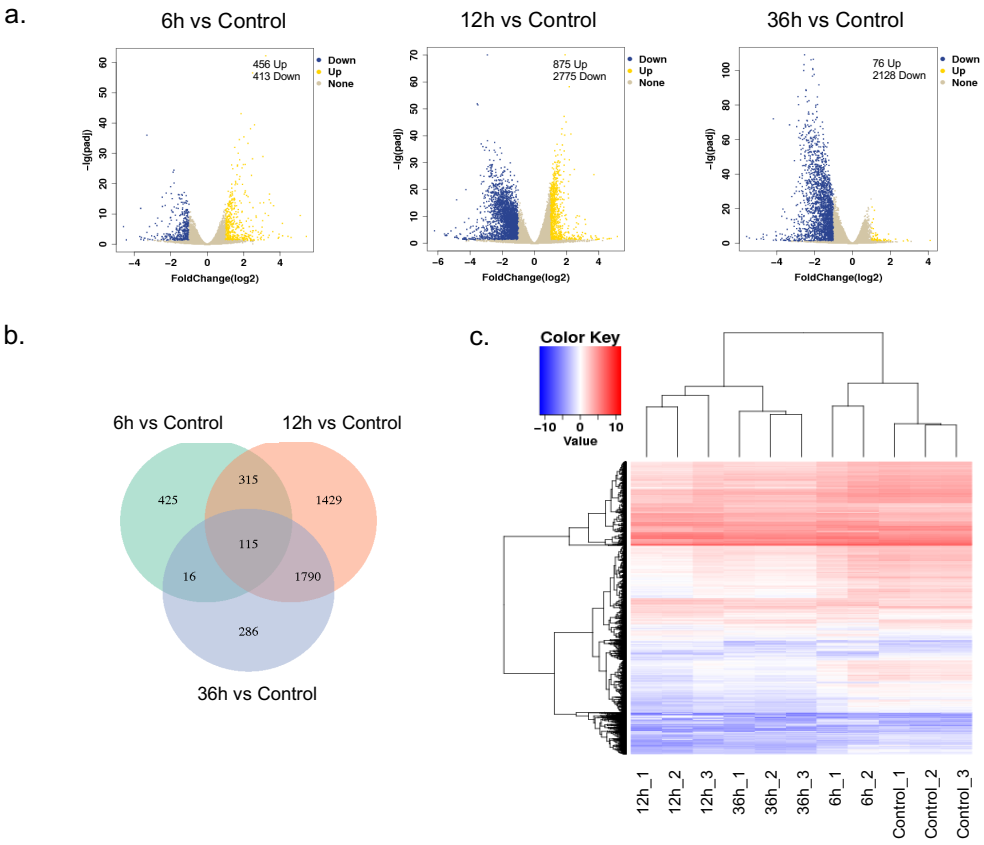

Figure 4.7 Differentially expressed genes in LDSA peptide-treated PANC-1 cells by RNA sequencing

a. Volcano plots showing differentially expressed genes at 6, 12, and 36 h post-treatment. Yellow and blue dots indicate significantly upregulated and downregulated genes (fold change >2, p< 0.05), respectively. **b.** Venn diagram summarizing the overlap between differentially expressed genes at 6, 12 and 36 h time points. The number of genes that are shared by two time points is indicated by the overlap between the two circles. **c.** Heatmap of hierarchical clustering indicating differentially expressed genes (*rows*) between all samples including controls.

In comparison to control cells, there was an approximately equal number of genes that were upregulated (456 genes) or downregulated (413 genes) at 6 h after treatment (*Figure 4.7a*). However, a significant increase of upregulated (875 genes) and downregulated genes (2775 genes) was observed at 12 h (*Figure 4.7a*). Lastly, at 36 h, there was strikingly more

downregulated genes (2128 genes) than the upregulated ones (76 genes) (*Figure 4.7a*). The differentially expressed genes showed a high degree of overlap between 12 h and 36 h treated samples and very little overlap between 6 h and 36 h treated samples, as depicted in the Venn diagram (*Figure 4.7b*). Similarly, hierarchical clustering analysis of the differentially expressed genes revealed that 12 h and 36 h treated samples formed a cluster while the control and 6 h treated samples clustered closely to each other (*Figure 4.7c*).

Gene Ontology (GO) analysis is useful in dissecting the biological processes and molecular functions of a vast number of differentially expressed genes in order to create a better understanding of the molecular changes in the treated samples. To do this, a list of significantly upregulated or downregulated genes for each time point was uploaded to DAVID bioinformatics tool (Huang et al., 2009b). In terms of biological processes, the upregulated genes found at 6 h treated samples are related mostly to inflammatory and immune responses including NF-kappaB signaling as well as extracellular matrix organization and actin cytoskeleton regulation whereas the downregulated genes are highly related to signal transduction and cell division (*Figure 4.8a*). As for the molecular functions, the upregulated genes are involved in poly(A) RNA, receptor, heparin, integrin, and heparin binding while the downregulated genes are involved in DNA, actin, syntaxin, and calcium-dependent phospholipid binding (*Figure 4.8a*).

In contrast, an entirely different landscape of biological processes and molecular functions was represented by the differentially expressed genes for 12 h or 36 h treated samples. Genes that were upregulated after 12 h of treatment play function in oxidation-reduction process, protein transport, rRNA processing, response to lipopolysaccharides, tumor necrosis factor (TNF) signaling, and extracellular matrix organization while downregulated genes play important and diverse biological functions like DNA transcription, cell division, protein phosphorylation, ubiquitination, and DNA repairs (*Figure 4.8b*). At the first glance, most of

the upregulated and downregulated genes are molecularly related to protein binding. Meanwhile, metal ion, DNA, and ATP binding were also significantly represented in the downregulated gene sets. Since there were a low number of upregulated genes in 36 h treated samples and the gene sets required for each functional analysis was less than 5, they are excluded from the GO analysis. The biological processes and molecular functions that are represented by the downregulated genes of 36 h-treated samples are quite similar to those of 12 h-treated samples, with DNA replication and protein binding appeared as the top represented biological process and molecular function, respectively (*Figure 4.8c*).

Collectively, these results showed that treatment with LDSA peptides induced a dynamic change in the PANC-1 cells at a molecular level. Based on this data, I speculate that upon treatment, the cells initially responded by upregulating a transient inflammatory and immune response as well as extracellular matrix reorganization due to the binding of the peptide nanofibers on the cell membrane which was also shown by an increase in molecules that are receptor, heparin or integrin related. However, at 12 h and 36 h after treatment, the molecular dynamics changed vastly and the downregulated genes are mainly involved in important cellular processes that are highly ATP-dependent like, DNA transcription, DNA replication, cell division, protein functions, and signal transduction.

a.

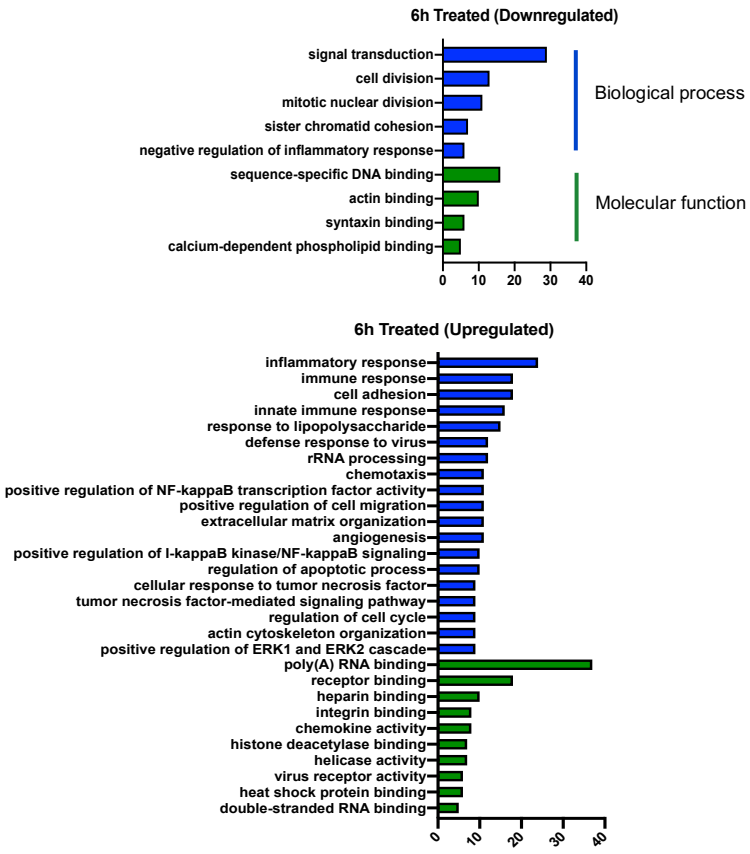
6h Treated (Downregulated)
signal transduction
cell division
mitotic nuclear division
sister chromatid cohesion
negative regulation of inflammatory response
sequence-specific DNA binding
actin binding
syntaxin binding
calcium-dependent phospholipid binding
Biological process
Molecular function
0 10 20 30 40
6h Treated (Upregulated)
inflammatory response
immune response
cell adhesion
innate immune response
response to lipopolysaccharide
defense response to virus
rRNA processing
chemotaxis
positive regulation of NF-kappaB transcription factor activity
positive regulation of cell migration
extracellular matrix organization
angiogenesis
positive regulation of I-kappaB kinase/NF-kappaB signaling
regulation of apoptotic process
cellular response to tumor necrosis factor
tumor necrosis factor-mediated signaling pathway
regulation of cell cycle
actin cytoskeleton organization
positive regulation of ERK1 and ERK2 cascade
poly(A) RNA binding
receptor binding
heparin binding
integrin binding
chemokine activity
histone deacetylase binding
helicase activity
virus receptor activity
heat shock protein binding
double-stranded RNA binding
0 10 20 30 40

b.

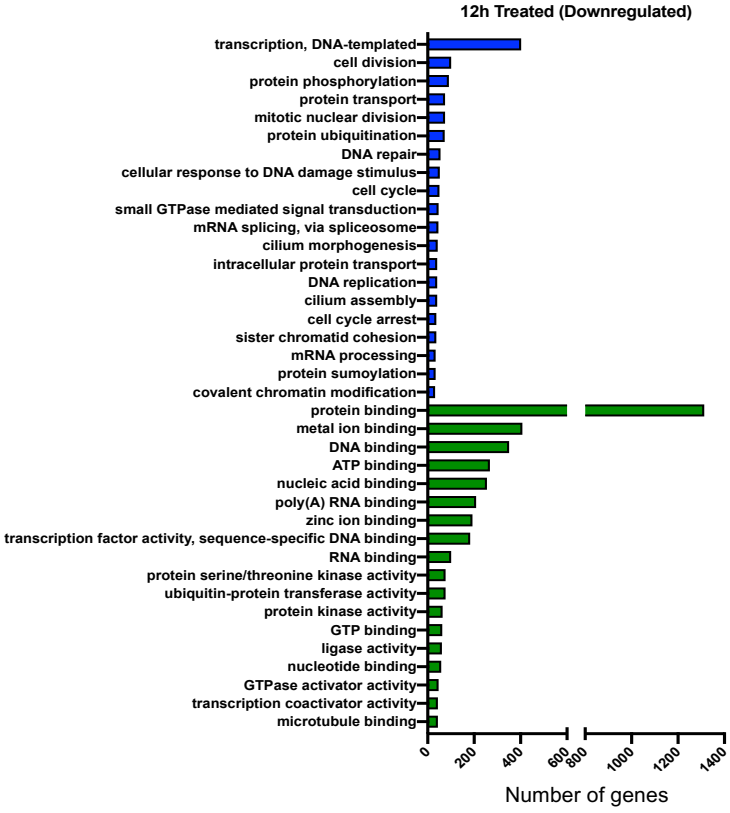
12h Treated (Downregulated)
transcription, DNA-templated
cell division
protein phosphorylation
protein transport
mitotic nuclear division
protein ubiquitination
DNA repair
cellular response to DNA damage stimulus
cell cycle
small GTPase mediated signal transduction
mRNA splicing, via spliceosome
cilium morphogenesis
intracellular protein transport
DNA replication
cilium assembly
cell cycle arrest
sister chromatid cohesion
mRNA processing
protein sumoylation
covalent chromatin modification
protein binding
metal ion binding
DNA binding
ATP binding
nucleic acid binding
poly(A) RNA binding
zinc ion binding
transcription factor activity, sequence-specific DNA binding
RNA binding
protein serine/threonine kinase activity
ubiquitin-protein transferase activity
protein kinase activity
GTP binding
ligase activity
nucleotide binding
GTPase activator activity
transcription coactivator activity
microtubule binding
0 200 400 600 800 1000 1200 1400
Number of genes

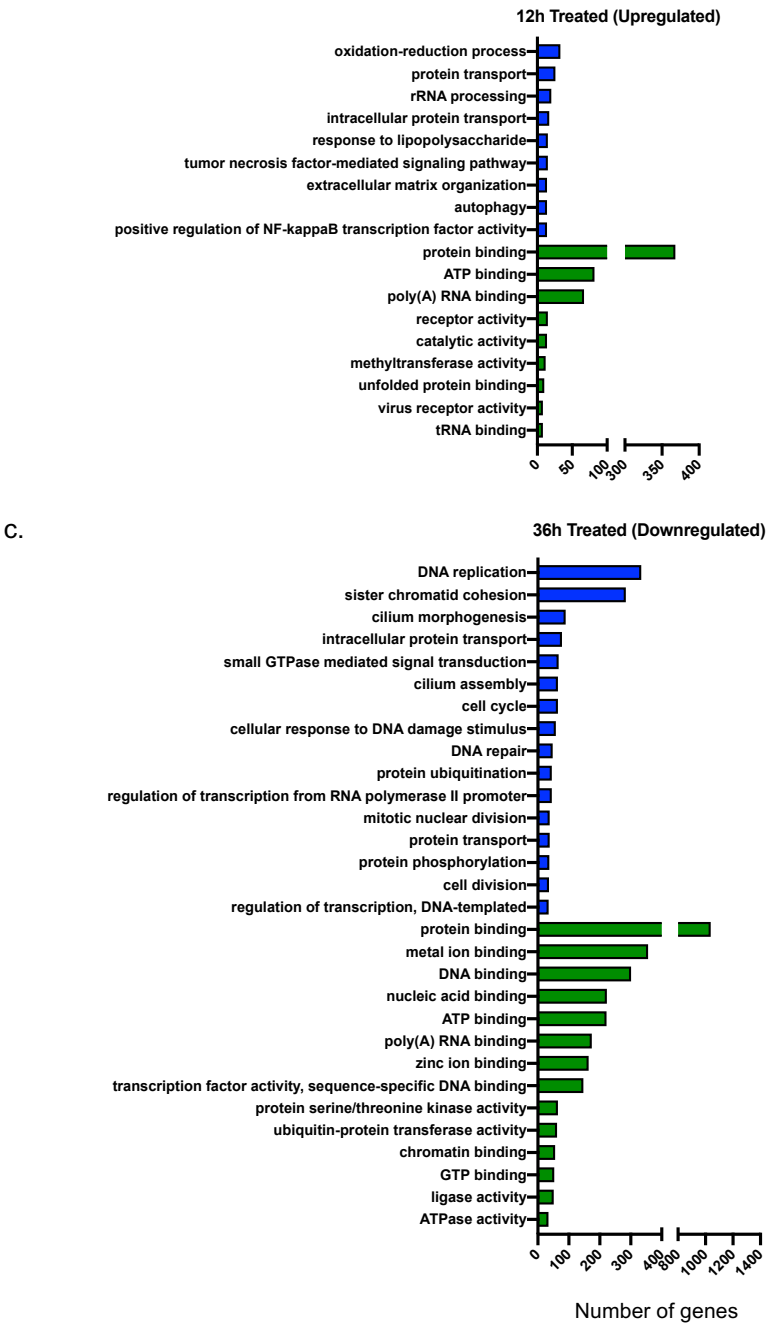

Figure 4.8 Gene Ontology enrichment analysis of differentially expressed genes

DAVID functional Gene Ontology analysis of significantly downregulated and upregulated genes at **a.** 6 h **b.** 12 h and **c.** 36 h post-treatment with LDSA peptides. Biological processes are highlighted with *blue* bars while molecular functions are highlighted with *green* bars. *x*-axis represents the number of genes within each category.

4.3.5 LDSA peptides altered the metabolic activities of cancer cells

Adenosine 5'-triphosphate (ATP) is the molecular currency of intracellular energy transfer that is essential for multiple cellular processes. To evaluate if the LDSA peptides affect the ATP production within the treated cells, I first conducted a metabolic assay to measure the ATP level within cells using luminescence method. The ATP concentration initially increased 6 h after treatment, and gradually decreased from 12 h up to 36 h where there was a significant drop in the ATP level compared to basal level (*Figure 4.9a*). Since cancer cells primarily utilize aerobic glycolysis instead of oxidative phosphorylation for energy production and produce lactate from pyruvate in the presence of oxygen, a phenomenon termed 'Warburg effect' (Warburg et al., 1927; Warburg, 1956), it is reasonable to postulate that a decrease of cellular ATP concentration in the treated cancer cells is associated with a drop in lactate production. To confirm such phenomenon, I conducted metabolic assays to quantify the cellular lactate concentration and lactate dehydrogenase (LDH) enzyme levels using colorimetric analysis. Similar to ATP production level, both cellular lactate and lactate dehydrogenase concentrations were elevated initially at 6 h and followed by a decline from 12, 24 h to a significant drop at 36 h (*Figure 4.9b & c*).

The above findings revealed that there was an impairment in glycolysis in cells treated with LDSA peptides, I followed up the experiment by running a glycolytic stress test. As expected, though all treated cells responded to the exogenous glucose as the control cells, when oligomycin, an ATP synthase complex V inhibitor, was added, the cellular response by extracellular acidification rate (ECAR) production was diminished, most significantly at 36 h (*Figure 4.9d*), suggesting a decrease in the capability of the cells to respond to an energetic demand, referred to as 'glycolytic reserve', of the treated cells (*Figure 4.9e*). These data suggest that an impairment of glycolysis causes a lack of ATP production, which in return

contributed to the reduction in ATP-dependent cellular processes and similarly, inhibits an energy-demanding tasks like cell migration and invasion.

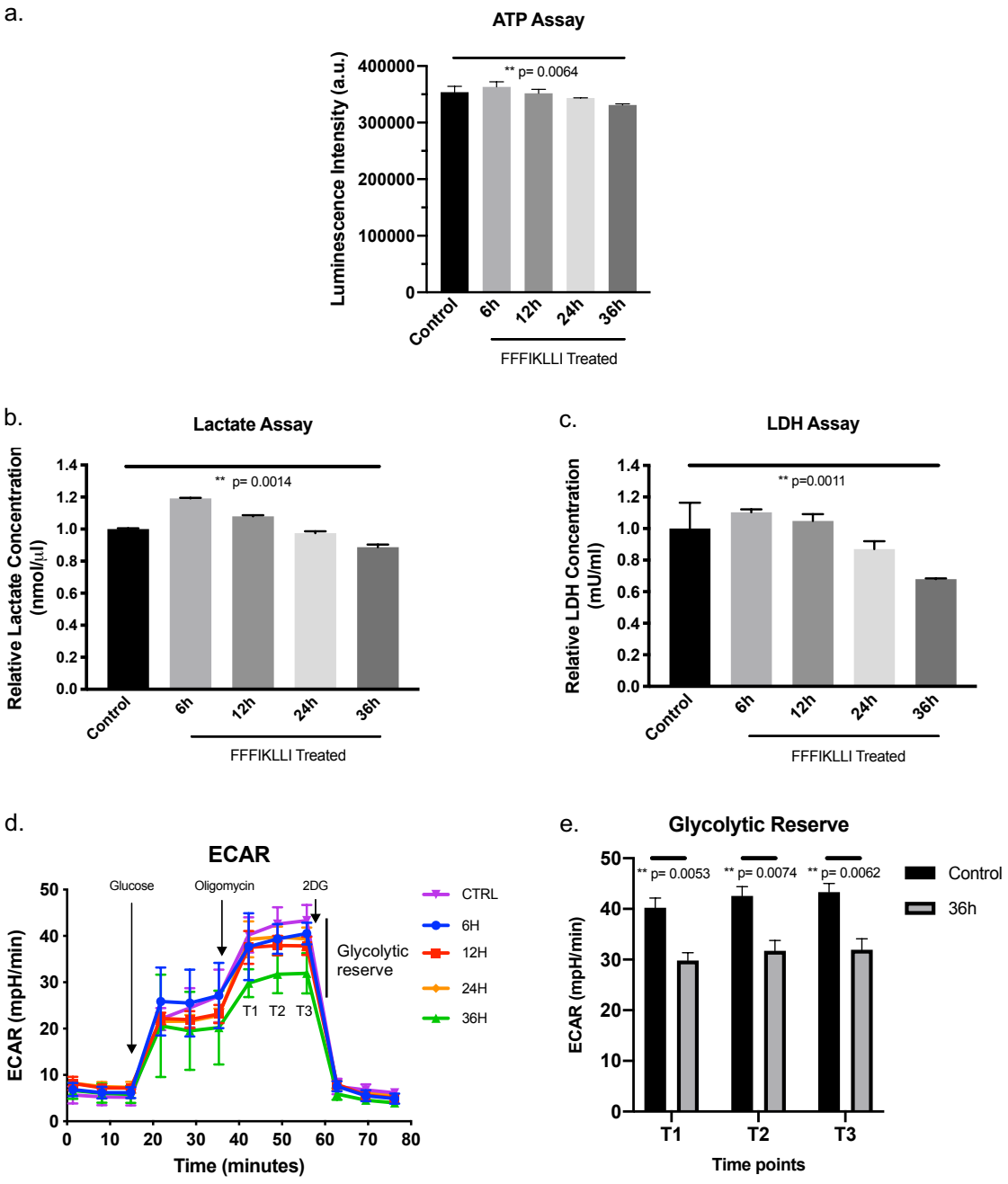

Figure 4.9 Metabolic assays of LDSA peptide-treated PANC-1 cells

a. CellTiter-Glo® 2.0 bioluminescence assay was used to measure the ATP level within the cells after treatment with FFFIKLLI (LDSA peptides) for 6, 12, 24 and 36 h. **b.** Calorimetric assay measuring lactate production by cells. Results are represented as lactate concentrations at each time points relative to the control. **c.** Calorimetric assay measuring the activity of lactate

dehydrogenase (LDH) in cells. Results are represented as LDH concentrations at each time point relative to the control. **d.** Extracellular acidification rate (ECAR) by control and treated cells at basal level and after sequential injections of indicated compounds: glucose (10 mM), oligomycin (1.0 μM), and 2-deoxy-D-glucose (2-DG) (50 mM). Glycolytic reserve which measures the maximum ability of a cell responding to an energetic demand is indicated by the slope after addition of oligomycin. **e.** Average value of glycolytic reserves of control and 36 h-treated cells were quantified and compared. T1, T2 and T3 correspond to time point measurements after addition of oligomycin indicated in *d*. Data represents the mean ± standard error of mean (SEM) of three independent experiments (**$p < 0.01$ (*t*-test, two-tailed)).

4.3.6 Animal xenotransplantation study revealed the effect of LDSA peptides on tumor growth *in vivo*

To supplement the *in vitro* findings, an animal xenotransplantation study was carried out by first, xenografting PANC-1-GFP cells subcutaneously into BALB/c nu/nu nude mice, followed by treating the formed tumors with LDSA peptides peritumorally every 3 days for up to 5 doses (*Figure 4.10a*). Live *in vivo* animal imaging was used to track the growth of PANC-1-GFP tumors by measuring the total radiant efficiency of GFP signals in the vehicle-treated (control) or LDSA peptide-treated group. Upon treatment with the first dose of LDSA peptide, the tumors started to grow slower than the control ones up until the end of the experiment (*Figure 4.10b & c*). The health of the mice for both groups remained healthy as monitored by body weight measurement every 3 days throughout the experimental period (*Figure 4.10d*). As expected, the treated tumors were much smaller than the control tumors, both in terms of volume and mass, as revealed by the measurements done after dissection (*Figure 4.10e, f & g*). These *in vivo* findings supplemented the potential of the LDSA peptides in suppressing tumor expansion, including possible invasion into the surrounding tissues.

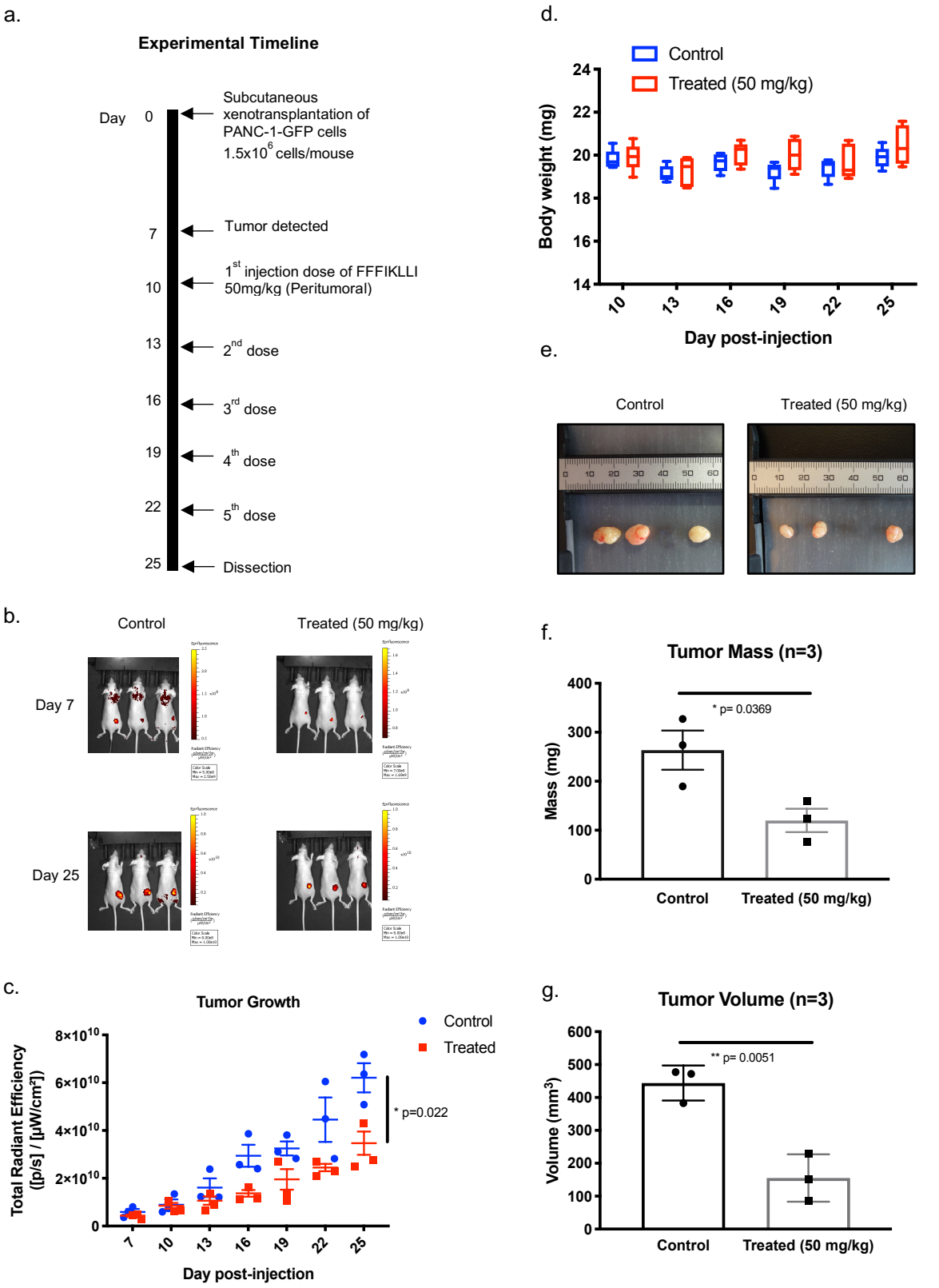

Figure 4.10 *In vivo* study of LDSA treatment on xenografted PANC-1 tumors in nude mice

a. Timeline summarizing the experimental setup and procedure during the entire duration of *in vivo* experiment. **b.** *In vivo* fluorescence images of PANC-1-GFP subcutaneous tumor-bearing mice at day 7 when tumors were detected and at day 25 before the dissection, treated with vehicle (*control*, deionized water containing 5% DMSO) or LDSA peptide compound (*treated*, 50 mg/kg dissolved in deionized water containing 5% DMSO). **c.** Fluorescence signals measured by IVIS Spectrum Imaging System at each time point are presented as total radiant efficiency. **d.** Body weight of the mice was measured using weighing balance before each injection of LDSA peptide to monitor the health status of the mice. **e.** Images of excised control and LDSA-treated tumors on day 25 post-transplantation. **f.** Tumor mass was measured, and the average of each experimental group is presented. **g.** Tumor volume (mm^3) was calculated based on the width (x) and length (y) of each tumor measured with calipers. Average tumor volume from three biological replicates were quantified. Data represents the mean ± standard error of mean (SEM), (**$p < 0.01$, *$p < 0.05$ (t-test, two-tailed)).

4.4 Discussion

4.4.1 Self-assembly peptide containing sequence of laminin helped guide binding to the cancer cell membrane

The LDSA peptide was designed and synthesized by combining a fragment of α1 chain of laminin-1 with a self-assembling block, triphenylalanine. Unfortunately, the peptide design did not take into consideration the expression of laminin or its associated integrin receptors in PDAC tumors, which led to the difficulty in demonstrating the binding of peptides to the integrin receptors. Confocal imaging studies investigating the expression and engagement of integrin receptors using immunofluorescence on LDSA peptide-bound cells had been inconclusive. This is hindered by the fact that the large-sized LDSA peptides also randomly captured immunofluorescence antibodies, possibly due to binding complementarity or size restriction.

The effects observed are likely caused by self-assembling of the peptides while the biologically relevant part of laminin sequence serves as a guide to anchor the peptides to the

cell membrane as shown in the scanning electron microscopic images. In normal pancreas, it has been reported that in contrast to laminin β1 and γ1 chains, α1-chain of laminin-1 was practically absent in the adult pancreatic parenchyma (Virtanen et al., 2000; Jiang et al., 2002). Furthermore, there is no direct evidence of interaction of laminin α1 and integrin in human PDAC specimen described in the literature so far, making the hypothesis of binding of the LDSA peptide to integrin receptors obsolete.

Moreover, the adhesiveness of the LDSA peptide to the cell membrane should be assessed in a greater detail. This is particularly important to show that the peptide has a strong affinity to the cellular membrane in order to exert its effects. Preliminary experiment had been carried out by coating the cell culture dishes with LDSA peptide or Matrigel (control), a basement membrane derived from the TME of a mouse sarcoma, called Engelbreth-Holm-Swarm (EHS) tumor (Kleinman et al., 1986; Danielson et al., 1992), where laminin is of abundance, before seeding the cancer cells. The adhesiveness of cells was next evaluated by measuring the number of cells remained after digesting with EDTA. However, the adhesiveness of cells to LDSA peptides was not superior to that of Matrigel, a natural ECM (*Figure 4.11*). This also implies that the LDSA peptides may be subjected to proteolysis by proteases such as matrix metalloproteinases that are present in the *in vivo* TME. This should be confirmed by administering the LDSA peptide *in vivo* to analyze its pharmacokinetics including bioavailability within the tissues, biodegradability, and half-life.

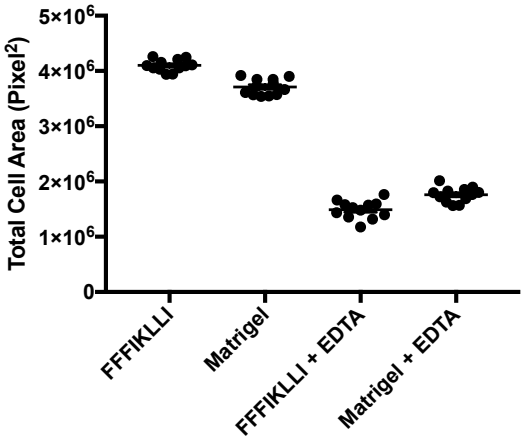

Figure 4.11 Cell adhesion and peptide digestibility assay of LDSA peptides *versus* Matrigel

Cells that adhered to tissue culture wells coated with either FFFIKLLI (LDSA peptide) or Matrigel® overnight were imaged and the average area occupied by adhered cells were quantified. Peptide digestibility assay was performed by treating adhered cells with EDTA. Cells that remain adhered to the FFFIKLLI peptide or Matrigel®-coated wells after digestion were imaged, and the average area occupied by cells were measured.

4.4.2 LDSA peptides physically restricted the cell motility in PDAC cells

The LDSA peptides not only suppressed cellular migration in a 2D setting, they also possess the ability to restrict PDAC cell invasion in a 3D setting. The cell migration machinery was affected by the binding of the self-assembled LDSA peptides on PDAC cell membrane. This result was supported by the suppression of ROCK1, a serine/threonine protein kinase downstream of small GTPase RhoA which functions as a inducer of actomyosin contractility and actin stress fiber formation (Kimura et al., 1996; Amano et al., 1997) through phosphorylation of substrates, including myosin light chain 2 (MLC), MLC phosphatase, and LIM domain kinase 1 and 2 (LIMK), to regulate cell migration and invasion (Ridley, 2001; Julian and Olson, 2014). In fact, ROCK1 had been shown to be upregulated in PDAC cell lines and tissue samples, and its downregulation by morpholino oligo antisense (Kaneko et al., 2002)

or small molecule inhibitors (Vennin et al., 2017; Whatcott et al., 2017; Rath et al., 2018) had been proven to be effective at blocking cell migration, tumor proliferation, invasion, metastasis, and activation of stromal fibroblast.

The mechanism underlying the suppression of ROCK1 in PANC-1 cells by the ITGA peptides remains to be elucidated. However, in view of the widespread binding of LDSA peptides on the cell membrane, it is likely that the physical tension exerted by the self-assembling nanofibers had also restricted the motility and contractility of the cells, leading to loss of molecules involved in stress fiber contraction. As a matter of fact, RhoA, the upstream molecule of ROCK1 is known to be involved in forming integrin-based cell-matrix contacts, called focal adhesions in response to mechanical stresses in the ECM (Nobes and Hall, 1995; Rottner et al., 1999; Ridley, 2001). To examine this hypothesis, a mechanical experiment using atomic force microscopy (AFM) should be performed to reveal the tensile force of the nanofibers exerted to the cells, followed by biochemical studies of mechanosensing proteins including focal adhesion molecules, cytoskeletal scaffolding proteins or downstream Rho GTPases.

4.4.3 Limitations of the *in vitro* study and proposal of better models to study LDSA peptide in PDAC

Though this study was conducted using two established human PDAC cell lines, they are not optimal to assess the development of effective anti-PDAC therapies preclinically for three reasons: (1) they do not represent a heterogenous nature of PDAC, (2) they have been selected for its growth advantage in a monolayer, and (3) a lack of proper tumor architecture and tumor microenvironment (Gillet et al., 2013).

As discussed earlier, PDAC is well characterized with an extensive desmoplasia consisting of dense ECM and fibroblasts within its tumor microenvironment (Xie and Xie,

2015; Neesse et al., 2019). To properly evaluate the effects of LDSA peptide that was designed and constructed based on the sequence of an extracellular matrix protein, it is therefore more appropriate to conduct the experiments using a pathologically relevant model, for instance *in vitro* 3D PDAC model. In fact, Matrigel is widely used in *in vitro* 3D tissue culture. It is made up of primarily laminin, type IV collagen, entactin, and heparan sulfate proteoglycan (perlecan) (Kleinman and Martin, 2005), that are also commonly found in a TME. In 2015, two studies simultaneously reported that Matrigel together with a cocktail of growth factors in culture medium had been successfully used to establish normal and cancerous murine and human 3D pancreas tissue *in vitro*, termed organoids, from pancreatic ductal cells or pluripotent stem cells (Boj et al., 2015; Huang et al., 2015). The cultured organoids largely recapitulate major biological functions and the *in vivo* tissue architecture. Since then, the established organoid culture techniques have been employed widely to become a common model for researches into pancreatic cancer biology as well as for novel therapeutic screening and evaluation. Such culture system allows us to test how LDSA peptide penetrates the Matrigel and interfere with the interaction between cultured ductal tissues and the surrounding matrix *in vitro* as well as to evaluate the biological responses such as migration and invasion.

Similarly, organoids consisting normal pancreatic, preneoplastic, and immune cells should also be included to study the response of heterogenous assortment of cells to the LDSA peptide during various stages of disease progression. The flexibility of organoid culture system has enabled the modulation of TME and cell-to-cell interaction to match different study aims and to answer research questions in a holistic manner. The finding of activation of inflammatory and innate immune response at 6 hours after treatment from the RNA sequencing data can be functionally validated and the immunogenic effect of LDSA peptide can be investigated using established organoid model which successfully incorporates tumor immune

microenvironment including tumor-associated macrophages and tumor-infiltrating T-lymphocytes (Neal et al., 2018; Tsai et al., 2018).

4.4.4 LDSA peptides restricted cancer cells' energy production leading to global shutdown of cellular functions

The metabolic activity of the PDAC cells treated with LDSA peptides had been altered in a dynamic fashion where energy production switched from increased glycolysis in the initial period of treatment, generating higher amount of ATP and lactate, to an overall reduction after a prolonged period of treatment. Correlating this results with the RNA sequencing data, it is plausible that the initial engagement of LDSA peptides with the cell surface membrane triggered an increase in demand for energy for cells to accommodate cellular activities like immune response and extracellular matrix protein production which led to an eventual exhaustion, as exemplified by the decrease in glycolysis, ATP production, and downregulation of ATP-related cellular activities at 36 h. On the other hand, a gradual increase of LDSA peptide binding to the cells and a formation of tight nanofibrous meshwork over time may also limit the access of macronutrients or oxygen present in the culture medium. Attempt to investigate the glucose uptake ability of treated cells was conducted, however, no conclusive results could be drawn from the findings. Meanwhile, according to the RNA sequencing data, there was no changes to the mammalian target of rapamycin (mTOR) signaling pathway which acts as the central regulator of cell metabolism for growth, proliferation, and survival (Laplante and Sabatini, 2009). Likewise, hypoxia signaling was also largely intact except for a significant decrease *HIF1A* transcripts at 12 h, followed by an increase at 36 h. However, this change has to be further confirmed using gene and protein expression studies.

Since metabolic reprogramming is common among human malignancies and it contributes to the evolution of cancer (Ward and Thompson, 2012; Faubert et al., 2020), it is

possible that the reduction of glycolytic capacity at later time points coincides with a metabolic switch where cells rely on mitochondrial oxidative phosphorylation for energy production. Nonetheless, it is interesting to find that there was a widespread downregulation of biological functions which are highly ATP-dependent in cells after 12 hours of treatment even though the cells remain viable after 72 hours as shown in the cell viability assay. To understand this phenomenon, further studies should also include looking into cellular senescence and dormancy to determine the ultimate cellular phenotype changes caused by the LDSA peptide.

4.4.5 Comprehensive *in vivo* analysis of the effect of LDSA peptides

The *in vivo* analysis in this study was performed using a subcutaneous model of tumor xenograft using an established human PDAC cell line. This approach possesses significant weaknesses that limit their ability to adequately evaluate the therapeutic responses in a preclinical setting. The two main reasons for its inferiority are: 1) lack of stromal infiltration and adequate TME to support tumor growth in subcutaneous transplantation, 2) the murine models of xenografts are immunocompromised hindering the assessment of therapeutic effect in the presence of immune cells.

Though the results presented suggested that there was an effect on tumor growth and possibly invasion by the peritumoral injection of LDSA peptide, a more comprehensive *in vivo* analysis using biologically relevant model is needed to ensure that the results are reliable and clinically relevant. Genetically-engineered PDAC mouse model bearing mutations in *Kras* and *Trp53* that targets the pancreas specifically using Cre-lox technology, named *LSL-*$Kras^{G12D/+}$*;LSL-*$Trp53^{R172H/+}$*;Pdx-1-Cre* (KPC) mouse model of PDAC, is by far the most reliable tool for preclinical drug studies for its close recapitulation to many clinical, histopathological, and immunocompetent features of PDAC (Hingorani et al., 2005; Lee et al., 2016). In addition, KPC mice encompass a full spectrum of PDAC development, with normal

pancreata at birth and developed precursor lesion, pancreatic intraepithelial neoplasia (PanIN), before accelerated into PDAC stage with metastases found in approximately 80% of the animals (Hingorani et al., 2003, 2005). Since LDSA peptide aims to suppress metastasis of pancreatic tumor, preferably at an early and less-aggressive stage, KPC mice should be used to investigate its effectiveness both at PanIN and PDAC stages.

Another murine model that is more clinically relevant is patient-derived tumor xenografts (PDX), where tumor tissues together with their surrounding stroma that were surgically removed from PDAC patients are transplanted into a mouse body for growth. In particular, an orthotopic approach (tumor tissues are transplanted directly into the organ where the tissue is originated from) instead of a subcutaneous approach should be conducted. Earlier studies had demonstrated that such approach yielded PDXs that retain morphological characteristics of the original human PDAC specimen and successfully recapitulated the metastatic activity of primary tumors (Fu et al., 1992; Loukopoulos et al., 2004). Furthermore, orthotopically transplanted PDAC cell lines also showed acquisition of malignant EMT traits such as loss of E-cadherin than subcutaneously transplanted PDAC cell lines, suggesting the importance of a proper TME in attaining malignant behaviors (Takahashi et al., 2018).

Even with the use of proper murine model for *in vivo* evaluation, the challenge of route of administration of LDSA peptides remains. LDSA peptide presents as hydrogel, and its viscosity hinders it from being administered via oral or intravenous route. Because of its low specificity, intraperitoneal use also poses significant difficulty for precise targeting. The only viable option is direct delivery into the peritumoral region using ultrasound-guided injection through the abdominal route, though feasible but not ideal in a clinical setting. I had attempted such approach for orthotopic tumor transplantation, however, because of the lack of expertise and support as well as the availability of proper equipment setup, this approach was eventually abandoned.

In addition, the need of repetitive dosing of LDSA peptides hints that the tumors may regrow in the absence of LDSA peptide. This is also evidenced by the continuous tumor growth in the treated group even after multiple injections and may be explained by the lack of specificity of the LDSA targets as well as the biodegradability of the peptides (*Figure 4.11*). In my opinion, given the known characteristic of self-assembling peptides in solution, the initial design conceptualization should have taken into consideration route of administration of the peptide *in vivo*.

To supplement the results obtained from *in vitro* experiments, below are the biological assays that need to be carried out. First, assessment of pharmacokinetics of the LDSA peptide in the peritumoral region with a special focus on its bioavailability, distribution among the normal and cancerous tissues, metabolism, and half-life. Second, tumor invasion into surrounding normal tissues assessed by *in vivo* imaging using fluorescently labeled tumor cells and histological evaluation of tumor samples and its basement membrane after dissection. Third, tumor metastasis into distant organs, both micro and macrometastases, can be studied by *in vivo* imaging and assessment of all tissue organs using histopathology with particular attention to common metastatic sites like liver, peritoneum, lungs, and lymph nodes. Fourth, functional analysis of indicators of cancer dissemination that are present in the bloodstream, for example circulating tumor cells (CTCs) and exosomes. Of note, CTCs and cancer-cell derived exosomes have been implicated in pancreatic cancer progression and metastasis (Kulemann et al., 2015; Melo et al., 2015; Qiu et al., 2018). For instance, PDAC-derived exosomes containing high level of migration inhibitory factor (MIF) induced pre-metastatic niche formation in the liver (Costa-Silva et al., 2015). In the same year, another published study showed that distinct integrin expression on tumor-derived exosomes from various cancer types including PDAC direct organ-specific metastasis by interacting with target organ ECM (Hoshino et al., 2015). Therefore, it would be interesting to analyze the distribution of PDAC-

specific, integrin-bearing exosomes in the bloodstream of mice that are treated with LDSA peptide in order to comprehensively evaluate its clinical efficacy.

4.4.6 The potential of using LDSA peptides in combination with conventional therapy to prevent metastasis and relapse in PDAC

Since LDSA peptides did not induce any cytotoxic effect on PDAC cells, its clinical application is very limited in oncology. However, it can be potentially useful as an add-on therapy to suppress metastasis with conventional cytotoxic chemotherapeutic drug like gemcitabine for metastatic PDAC. Once again, this would need to be evaluated in both *in vitro* and *in vivo* settings using appropriate experimental models. It is not uncommon that most preclinical studies and clinical trials are conducted in an adjuvant setting to evaluate the add-on value of novel therapeutics in clinical outcomes, which include overall response rate, progression-free survival, and overall survival. Such experiments are also needed to determine if the nanofibrous meshwork formed on the cells or tumor's surrounding impedes the delivery of cytotoxic drugs or renders the cells resistant to the cytotoxic effect of chemotherapy due to major alteration to the biological activities of the cancer cells.

In the present study, there is a lack of evidence showing the specificity of binding of LDSA peptide to the integrin receptors on the pancreatic cancer cells. Instead, the LDSA peptides had been shown to have widespread effects on the cellular phenotypes and functions that extend beyond targeting the integrin signaling pathway. This can be explained partially by the extensive, non-specific binding of the peptide nanofibers on the cellular membrane. This is merely a preliminary study to explore the preclinical effects of LDSA peptide, and since the potential clinical use of LDSA peptide remains largely elusive, it is important not to take the results of this part of the thesis literally.

Conclusion and Summary

Tumor heterogeneity and cellular plasticity continue to pose a great challenge for clinical cancer treatment. This property of cancer remains a topic of intensive research investigation. This thesis investigated cancer cell plasticity using biological agents, microRNAs and extracellular matrix-derived self-assembling peptides, in breast and pancreatic cancer cell, respectively.

First of all, in order to fulfill the primary aims of targeting cancer stem cells, I had discovered a microRNA, miR-96, which can transcriptionally regulate the CSC's surface marker CD44 in breast cancer cells. By overexpressing miR-96 which is often downregulated in breast CSCs using exogenous mimic, I demonstrated the effect of tumor growth inhibition and uncovered the molecular mechanism behind the suppression of CD44. This is summarized in the illustration below (*Figure 5.1*).

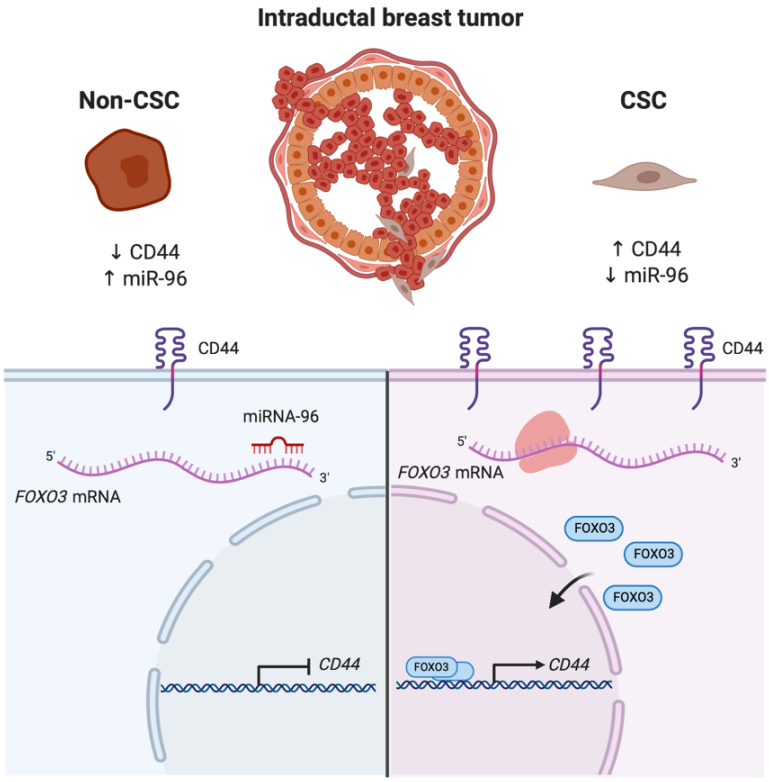

Figure 5.1 Illustration summarizing the transcriptional control of *CD44* by miR-96 in non-CSCs and CSCs (*Created with BioRender.com*)

Secondly, I investigated additional effect of miR-96 mimic in controlling cancer cell growth by targeting HB-EGF, a commonly upregulated oncogene in breast cancer which plays roles by using its extracellularly secreted molecule that binds EGF receptor to mediate intracellular signaling and an intracellular portion, HB-EGF-C that transcriptionally control expression of genes related to cell cycle and CSC's marker, CD44 through nuclear exclusion of transcriptional repressors. The transcriptional regulation of *Cyclin A* and *CD44* by HB-EGF-C and the effects of miR-96 mimic are summarized in a schematic illustration below (*Figure 5.2*).

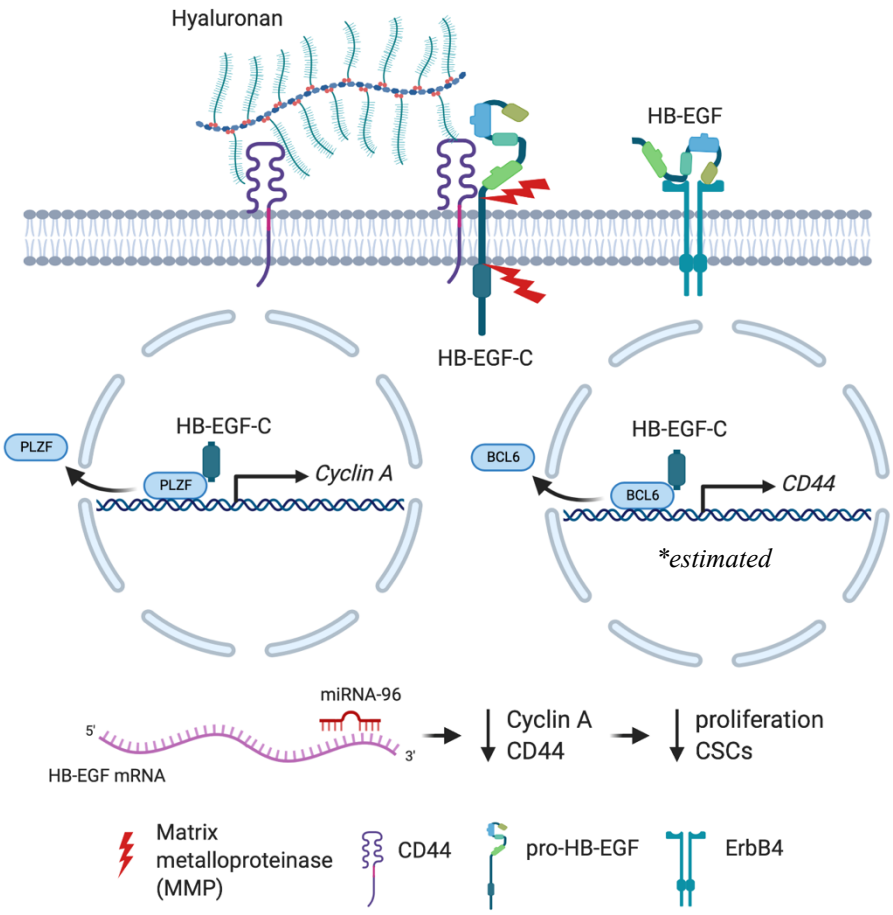

Figure 5.2 Schematic illustration showing the transcriptional control of *Cyclin A* and the estimated mechanism of control of *CD44* genes by HB-EGF-C as well as the molecular and functional effects of miR-96 mimic (*Created with BioRender.com*)

Lastly, I investigated the preliminary effects of a self-assembling biomaterial designed based on a peptide sequence derived from an extracellular matrix protein, laminin, on pancreatic cancer cells. The biomaterial self-assembled into a nanofibrous network on cellular membrane that expresses integrin and altered the cell fate including a myriad of cellular processes and metabolic activities. The extensive effects of the biomaterial are summarized in the illustration below (*Figure 5.3*).

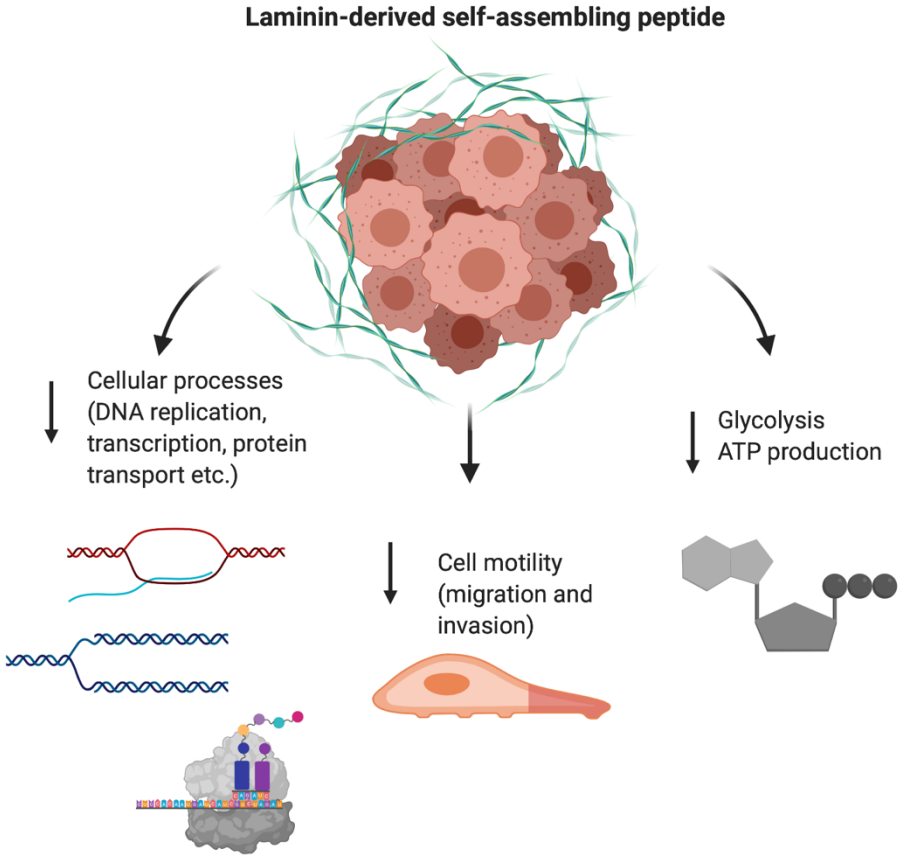

Figure 5.3 Illustration depicting the binding of laminin-derived self-assembling peptides to cell membrane and their effects on pancreatic cancer cells (*Created with BioRender.com*)

Although filled with limitations as discussed in each chapter, this thesis reaffirms the unique property of cancer cell plasticity which can be harnessed as a target to control the hallmarks of cancer including sustained growth and proliferation, tumor invasion, and metastasis using exogenous biological agents.

Bibliography

Abraham, S.N., and Beachey, E.H. (1987). Assembly of chemically synthesized peptide of Escherichia coli type 1 fimbriae into fimbria-like antigenic structures. J. Bacteriol. *169*, 2460–2465.

Abraham, J.A., Damm, D., Bajardi, A., Miller, J., Klagsbrun, M., and Ezekowitz, R.A.B. (1993). Heparin-Binding EGF-like Growth Factor: Characterization of Rat and Mouse cDNA Clones, Protein Domain Conservation across Species, and Transcript Expression in Tissues. Biochem. Biophys. Res. Commun. *190*, 125–133.

Agarwal, V., Bell, G.W., Nam, J.W., and Bartel, D.P. (2015). Predicting effective microRNA target sites in mammalian mRNAs. Elife *4*, e05005.

Aigner, S., Ruppert, M., Hubbe, M., Sammar, M., Sthoeger, Z., Butcher, E.C., Vestweber, D., and Altevogt, P. (1995). Heat stable antigen (mouse CD24) supports myeloid cell binding to endothelial and platelet P-selectin. Int. Immunol. *7*, 1557–1565.

Aigner, S., Sthoeger, Z.M., Fogel, M., Weber, E., Zarn, J., Ruppert, M., Zeller, Y., Vestweber, D., Stahel, R., Sammar, M., et al. (1997). CD24, a mucin-type glycoprotein, is a ligand for P-selectin on human tumor cells. Blood *89*, 3385–3395.

Al-Hajj, M., Wicha, M.S., Benito-Hernandez, A., Morrison, S.J., and Clarke, M.F. (2003). Prospective identification of tumorigenic breast cancer cells. Proc. Natl. Acad. Sci. *100*, 3983–3988.

Alexander, N.R., Branch, K.M., Parekh, A., Clark, E.S., Iwueke, I.C., Guelcher, S.A., and Weaver, A.M. (2008). Extracellular Matrix Rigidity Promotes Invadopodia Activity. Curr. Biol. *18*, 1295–1299.

Amano, M., Chihara, K., Kimura, K., Fukata, Y., Nakamura, N., Matsuura, Y., and Kaibuchi,

K. (1997). Formation of actin stress fibers and focal adhesions enhanced by Rho- kinase. Science *275*, 1308–1311.

Andea, A., Sarkar, F., and Adsay, V.N. (2003). Clinicopathological Correlates of Pancreatic Intraepithelial Neoplasia: A Comparative Analysis of 82 Cases With and 152 Cases Without Pancreatic Ductal Adenocarcinoma. Mod. Pathol. *16*, 996–1006.

de Antonellis, P., Medaglia, C., Cusanelli, E., Andolfo, I., Liguori, L., de Vita, G., Carotenuto, M., Bello, A., Formiggini, F., Galeone, A., et al. (2011). MiR-34a targeting of notch ligand delta-like 1 impairs CD15 +/CD133 + tumor-propagating cells and supports neural differentiation in medulloblastoma. PLoS One *6*, e24584.

Apte, M. V., Haber, P.S., Darby, S.J., Rodgers, S.C., McCaughan, G.W., Korsten, M.A., Pirola, R.C., and Wilson, J.S. (1999). Pancreatic stellate cells are activated by proinflammatory cytokines: Implications for pancreatic fibrogenesis. Gut *44*, 534–541.

Apte, M. V., Park, S., Phillips, P.A., Santucci, N., Goldstein, D., Kumar, R.K., Ramm, G.A., Buchler, M., Friess, H., McCarroll, J.A., et al. (2004). Desmoplastic reaction in pancreatic cancer: Role of pancreatic stellate cells. Pancreas *29*, 179–187.

Apte, M. V, Haber, P.S., Applegate, T.L., Norton, I.D., Mccaughan, G.W., Korsten, M.A., Pirola, R.C., and Wilson, J.S. (1998). Periacinar stellate shaped cells in rat pancreas: identification, isolation, and culture. Gut *43*, 128–133.

Arao, S., Masumoto, A., and Otsuki, M. (2000). β1 Integrins play an essential role in adhesion and invasion of pancreatic carcinoma cells. Pancreas *20*, 129–137.

Armstrong, T., Packham, G., Murphy, L.B., Bateman, A.C., Conti, J.A., Fine, D.R., Johnson, C.D., Benyon, R.C., and Iredale, J.P. (2004). Type I collagen promotes the malignant phenotype of pancreatic ductal adenocarcinoma. Clin. Cancer Res. *10*, 7427–7437.

Aruffo, A., Stamenkovic, I., Melnick, M., Underhill, C.B., and Seed, B. (1990). CD44 is the

principal cell surface receptor for hyaluronate. Cell *61*, 1303–1313.

Aßmann, V., Kern, H.F., and Elsässer, H.P. (1996). Differential Expression of the Hyaluronan Receptors CD44 and RHAMM in Human Pancreatic Cancer Cells. Clin. Cancer Res. *2*, 1607–1618.

Aumailley, M., Bruckner-Tuderman, L., Carter, W.G., Deutzmann, R., Edgar, D., Ekblom, P., Engel, J., Engvall, E., Hohenester, E., Jones, J.C.R., et al. (2005). A simplified laminin nomenclature. Matrix Biol. *24*, 326–332.

Bachem, M.G., Schneider, E., Groß, H., Weidenbach, H., Schmid, R.M., Menke, A., Siech, M., Beger, H., Grünert, A., and Adler, G. (1998). Identification, culture, and characterization of pancreatic stellate cells in rats and humans. Gastroenterology *115*, 421–432.

Bachem, M.G., Schünemann, M., Ramadani, M., Siech, M., Beger, H., Buck, A., Zhou, S., Schmid-Kotsas, A., and Adler, G. (2005). Pancreatic carcinoma cells induce fibrosis by stimulating proliferation and matrix synthesis of stellate cells. Gastroenterology *128*, 907–921.

Bailey, P., Chang, D.K., Nones, K., Johns, A.L., Patch, A.M., Gingras, M.C., Miller, D.K., Christ, A.N., Bruxner, T.J.C., Quinn, M.C., et al. (2016). Genomic analyses identify molecular subtypes of pancreatic cancer. Nature *531*, 47–52.

Balko, J.M., Giltnane, J.M., Wang, K., Schwarz, L.J., Young, C.D., Cook, R.S., Owens, P., Sanders, M.E., Kuba, M.G., Sánchez, V., et al. (2014). Molecular profiling of the residual disease of triple-negative breast cancers after neoadjuvant chemotherapy identifies actionable therapeutic targets. Cancer Discov. *4*, 232–245.

Barsky, S.H., Siegal, G.P., Jannotta, F., and Liotta, L.A. (1983). Loss of basement membrane components by invasive tumors but not by their benign counterparts. Lab. Investig. *49*, 140–147.

Basyuk, E., Suavet, F., Doglio, A., Bordonné, R., and Bertrand, E. (2003). Human let-7 stem-loop precursors harbor features of RNase III cleavage products. Nucleic Acids Res. *31*, 6593–6597.

Baumann, P., Cremers, N., Kroese, F., Orend, G., Chiquet-Ehrismann, R., Uede, T., Yagita, H., and Sleeman, J.P. (2005). CD24 expression causes the acquisition of multiple cellular properties associated with tumor growth and metastasis. Cancer Res. *65*, 10783–10793.

Bennett, K.L., Jackson, D.G., Simon, J.C., Tanczos, E., Peach, R., Modrell, B., Stamenkovic, I., Plowman, G., and Aruffo, A. (1995). CD44 isoforms containing exon V3 are responsible for the presentation of heparin-binding growth factor. J. Cell Biol. *128*, 687–698.

Besner, G., Higashiyama, S., and Klagsbrun, M. (1990). Isolation and characterization of a macrophage-derived heparin-binding growth factor. Cell Regul. *1*, 811–819.

Besner, G.E., Whelton, D., Crissman-Combs, M.A., Steffen, C.L., Kim, G.Y., and Brigstock, D.R. (1992). Interaction of heparin-binding EGF-like growth factor (HB-EGF) with the epidermal growth factor receptor: Modulation by heparin, heparinase, or synthetic heparin-binding HB-EGF fragments. Growth Factors *7*, 289–296.

Biankin, A. V., Waddell, N., Kassahn, K.S., Gingras, M.C., Muthuswamy, L.B., Johns, A.L., Miller, D.K., Wilson, P.J., Patch, A.M., Wu, J., et al. (2012). Pancreatic cancer genomes reveal aberrations in axon guidance pathway genes. Nature *491*, 399–405.

Bissell, M.J., and Hines, W.C. (2011). Why don’t we get more cancer? A proposed role of the microenvironment in restraining cancer progression. Nat. Med. *17*, 320–329.

Boj, S.F., Hwang, C. Il, Baker, L.A., Chio, I.I.C., Engle, D.D., Corbo, V., Jager, M., Ponz-Sarvise, M., Tiriac, H., Spector, M.S., et al. (2015). Organoid models of human and mouse ductal pancreatic cancer. Cell *160*, 324–338.

Bonetti, P., Climent, M., Panebianco, F., Tordonato, C., Santoro, A., Marzi, M.J., Pelicci,

P.G., Ventura, A., and Nicassio, F. (2019). Dual role for miR-34a in the control of early progenitor proliferation and commitment in the mammary gland and in breast cancer. Oncogene *38*, 360–374.

Borchert, G.M., Lanier, W., and Davidson, B.L. (2006). RNA polymerase III transcribes human microRNAs. Nat. Struct. Mol. Biol. *13*, 1097–1101.

Bourguignon, L., Singleton, P., Diedrich, F., and Zhu, H. (2003). Hyaluronan-mediated CD44 interaction with RhoGEF and Rho-kinase promotes Gab-1 phosphorylation and PI3 kinase signaling leading to cytokine (M-CSF) production &breast tumor progression. J. Biol. Chem. *278*, 29420–29434.

Bourguignon, L.Y.W., Gunja-Smith, Z., Iida, N., Zhu, H.B., Young, L.J.T., Muller, W.J., and Cardiff, R.D. (1998). CD44v3,8-10 is involved in cytoskeleton-mediated tumor cell migration and matrix metalloproteinase (MMP-9) association in metastatic breast cancer cells. J. Cell. Physiol. *176*, 206–215.

Bourguignon, L.Y.W., Zhu, H., Shao, L., Zhu, D., and Chen, Y.W. (1999). Rho-kinase (ROK) promotes CD44v3,8-10-ankyrin interaction and tumor cell migration in metastatic breast cancer cells. Cell Motil. Cytoskeleton *43*, 269–287.

Bourguignon, L.Y.W., Hongbo, Z., Shao, L., and Chen, Y.W. (2000). CD44 interaction with Tiam1 promotes Rac1 signaling and hyaluronic acid- mediated breast tumor cell migration. J. Biol. Chem. *275*, 1829–1838.

Broders-Bondon, F., Ho-Bouldoires, T.H.N., Fernandez-Sanchez, M.E., and Farge, E. (2018). Mechanotransduction in tumor progression: The dark side of the force. J. Cell Biol. *217*, 1571–1587.

Brown, R.L., Reinke, L.M., Damerow, M.S., Perez, D., Chodosh, L.A., Yang, J., and Cheng, C. (2011). CD44 splice isoform switching in human and mouse epithelium is essential for

epithelial-mesenchymal transition and breast cancer progression. J. Clin. Invest. *121*, 1064–1074.

Buck, M.B., Fritz, P., Dippon, J., Zugmaier, G., and Knabbe, C. (2004). Prognostic Significance of Transforming Growth Factor β Receptor II in Estrogen Receptor-Negative Breast Cancer Patients. Clin. Cancer Res. *10*, 491–498.

Burdick, D., Soreghan, B., Kwon, M., Kosmoski, J., Knauer, M., Henschen, A., Yates, J., Cotman, C., and Glabe, C. (1992). Assembly and aggregation properties of synthetic Alzheimer's A4/β amyloid peptide analogs. J. Biol. Chem. *267*, 546–554.

Burk, U., Schubert, J., Wellner, U., Schmalhofer, O., Vincan, E., Spaderna, S., and Brabletz, T. (2008). A reciprocal repression between ZEB1 and members of the miR-200 family promotes EMT and invasion in cancer cells. EMBO Rep. *9*, 582–589.

Calderwood, D.A. (2004). Integrin activation. J. Cell Sci. *117*, 657–666.

Calin, G.A., Sevignani, C., Dumitru, C.D., Hyslop, T., Noch, E., Yendamuri, S., Shimizu, M., Rattan, S., Bullrich, F., Negrini, M., et al. (2004). Human microRNA genes are frequently located at fragile sites and genomic regions involved in cancers. Proc. Natl. Acad. Sci. U. S. A.

Campbell, P.J., Yachida, S., Mudie, L.J., Stephens, P.J., Pleasance, E.D., Stebbings, L.A., Morsberger, L.A., Latimer, C., McLaren, S., Lin, M.L., et al. (2010). The patterns and dynamics of genomic instability in metastatic pancreatic cancer. Nature *467*, 1109–1113.

Chaffer, C.L., Brueckmann, I., Scheel, C., Kaestli, A.J., Wiggins, P.A., Rodrigues, L.O., Brooks, M., Reinhardt, F., Suc, Y., Polyak, K., et al. (2011). Normal and neoplastic nonstem cells can spontaneously convert to a stem-like state. Proc. Natl. Acad. Sci. U. S. A. *108*, 7950–7955.

Chaffer, C.L., Marjanovic, N.D., Lee, T., Bell, G., Kleer, C.G., Reinhardt, F., D'Alessio,

A.C., Young, R.A., and Weinberg, R.A. (2013). Poised chromatin at the ZEB1 promoter enables breast cancer cell plasticity and enhances tumorigenicity. Cell *154*, 61–74.

Chen, C., Zhao, S., Karnad, A., and Freeman, J.W. (2018). The biology and role of CD44 in cancer progression: Therapeutic implications. J. Hematol. Oncol. *11*, e64. https://doi.org/10.1186/s13045-018-0605-5.

Chen, J., Wang, W., Wei, J., Zhou, D., Zhao, X., Song, W., Sun, Q., Huang, P., and Zheng, S. (2015). Overexpression of β3 chains of laminin-332 is associated with clinicopathologic features and decreased survival in patients with pancreatic adenocarcinoma. Appl. Immunohistochem. Mol. Morphol. *23*, 516–521.

Cheng, X.B., Sato, N., Kohi, S., and Yamaguchi, K. (2013). Prognostic impact of hyaluronan and its regulators in pancreatic ductal adenocarcinoma. PLoS One *8*, e80765.

Cohen, S.J., Alpaugh, R.K., Palazzo, I., Meropol, N.J., Rogatko, A., Xu, Z., Hoffman, J.P., Weiner, L.M., and Cheng, J.D. (2008). Fibroblast activation protein and its relationship to clinical outcome in pancreatic adenocarcinoma. Pancreas *37*, 154–158.

Collisson, E.A., Sadanandam, A., Olson, P., Gibb, W.J., Truitt, M., Gu, S., Cooc, J., Weinkle, J., Kim, G.E., Jakkula, L., et al. (2011). Subtypes of pancreatic ductal adenocarcinoma and their differing responses to therapy. Nat. Med. *17*, 500–503.

Colognato-Pyke, H., O'Rear, J.J., Yamada, Y., Carbonetto, S., Cheng, Y.S., and Yurchenco, P.D. (1995). Mapping of network-forming, heparin-binding, and α1β1 integrin-recognition sites within the α-chain short arm of laminin-1. J. Biol. Chem. *270*, 9398–9406.

Colognato, H., MacCarrick, M., O'Rear, J.J., and Yurchenco, P.D. (1997). The laminin α2-chain short arm mediates cell adhesion through both the a1β1 and α2β1 integrins. J. Biol. Chem. *272*, 29330–29336.

Costa-Silva, B., Aiello, N.M., Ocean, A.J., Singh, S., Zhang, H., Thakur, B.K., Becker, A.,

Hoshino, A., Mark, M.T., Molina, H., et al. (2015). Pancreatic cancer exosomes initiate pre-metastatic niche formation in the liver. Nat. Cell Biol. *17*, 816–826.

Couvelard, A., O'Toole, D., Leek, R., Turley, H., Sauvanet, A., Degott, C., Ruszniewski, P., Belghiti, J., Harris, A.L., Gatter, K., et al. (2005). Expression of hypoxia-inducible factors is correlated with the presence of a fibrotic focus and angiogenesis in pancreatic ductal adenocarcinomas. Histopathology *46*, 668–676.

Creighton, C.J., Li, X., Landis, M., Dixon, J.M., Neumeister, V.M., Sjolund, A., Rimm, D.L., Wong, H., Rodriguez, A., Herschkowitz, J.I., et al. (2009). Residual breast cancers after conventional therapy display mesenchymal as well as tumor-initiating features. Proc. Natl. Acad. Sci. U. S. A. *106*, 13820–13825.

Dagogo-Jack, I., and Shaw, A.T. (2018). Tumour heterogeneity and resistance to cancer therapies. Nat. Rev. Clin. Oncol. *15*, 81–94.

Dall, P., Heider, K. -H, Sinn, H. -P, Skroch-Angel, P., Adolf, Gün., Kaufmann, M., Herrlich, P., and Ponta, H. (1995). Comparison of immunohistochemistry and RT-PCR for detection of CD44v-expression, a new prognostic factor in human breast cancer. Int. J. Cancer *60*, 471–477.

Danielson, K.G., Martinez-Hernandez, A., Hassell, J.R., and Iozzo, R. V. (1992). Establishment of a Cell Line from the EHS Tumor: Biosynthesis of Basement Membrane Constituents and Characterization of a Hybrid Proteoglycan Containing Heparan and Chondroitin Sulfate Chains. Matrix *12*, 22–35.

Das, S.K., Wang, X.N., Paria, B.C., Damm, D., Abraham, J.A., Klagsbrun, M., Andrews, G.K., and Dey, S.K. (1994). Heparin-binding EGF-like growth factor gene is induced in the mouse uterus temporally by the blastocyst solely at the site of its apposition: A possible ligand for interaction with blastocyst EGF-receptor in implantation. Development *120*, 1071–

1083.

Decline, F., and Rousselle, P. (2001). Keratinocyte migration requires α2β1 integrin-mediated interaction with the laminin 5 γ2 chain. J. Cell Sci. *114*, 811–823.

Dhordain, P., Albagli, O., Honore, N., Guidez, F., Lantoine, D., Schmid, M., De The, H., Zelent, A., and Koken, M.H.M. (2000). Colocalization and heteromerization between the two human oncogene POZ/zinc finger proteins, LAZ3 (BCL6) and PLZF. Oncogene *19*, 6240–6250.

Diaz, B., and Yuen, A. (2014). The impact of hypoxia in pancreatic cancer invasion and metastasis. Hypoxia *2*, 91–106.

Ding, L., Ellis, M.J., Li, S., Larson, D.E., Chen, K., Wallis, J.W., Harris, C.C., McLellan, M.D., Fulton, R.S., Fulton, L.L., et al. (2010). Genome remodelling in a basal-like breast cancer metastasis and xenograft. Nature *464*, 999–1005.

Doench, J.G., and Sharp, P.A. (2004). Specificity of microRNA target selection in translational repression. Genes Dev. *18*, 504–511.

Dong, J., Opresko, L.K., Chrisler, W., Orr, G., Quesenberry, R.D., Lauffenburger, D.A., and Wiley, H.S. (2005). The membrane-anchoring domain of epidermal growth factor receptor ligands dictates their ability to operate in juxtacrine mode. Mol. Biol. Cell *16*, 2984–2998.

Dvorak, H.F. (1986). Tumors: wounds that do not heal. Similarities between tumor stroma generation and wound healing. N. Engl. J. Med. *315*, 1650–1659.

Elenius, K., Paul, S., Allison, G., Sun, J., and Klagsbrun, M. (1997). Activation of HER4 by heparin-binding EGF-like growth factor stimulates chemotaxis but not proliferation. EMBO J. *16*, 1268–1278.

Erkan, M., Michalski, C.W., Rieder, S., Reiser-Erkan, C., Abiatari, I., Kolb, A., Giese, N.A.,

Esposito, I., Friess, H., and Kleeff, J. (2008). The Activated Stroma Index Is a Novel and Independent Prognostic Marker in Pancreatic Ductal Adenocarcinoma. Clin. Gastroenterol. Hepatol. *6*, 1155–1161.

Erkan, M., Reiser-Erkan, C., Michalski, C.W., Deucker, S., Sauliunaite, D., Streit, S., Esposito, I., Friess, H., and Kleeff, J. (2009). Cancer-stellate cell interactions perpetuate the hypoxia-fibrosis cycle in pancreatic ductal adenocarcinoma. Neoplasia *11*, 497–508.

Eulalio, A., Huntzinger, E., and Izaurralde, E. (2008). GW182 interaction with Argonaute is essential for miRNA-mediated translational repression and mRNA decay. Nat. Struct. Mol. Biol. *15*, 346–353.

Fabian, M.R., and Sonenberg, N. (2012). The mechanics of miRNA-mediated gene silencing: A look under the hood of miRISC. Nat. Struct. Mol. Biol. *19*, 586–593.

Fang, L., Li, G., Liu, G., Lee, S.W., and Aaronson, S.A. (2001). p53 induction of heparin-binding EGF-like growth factor counteracts p53 growth suppression through activation of MAPK and PI3K/Akt signaling cascades. EMBO J. *20*, 1931–1939.

Faubert, B., Solmonson, A., and DeBerardinis, R.J. (2020). Metabolic reprogramming and cancer progression. Science *368*, eaaw5473.

Feig, C., Gopinathan, A., Neesse, A., Chan, D.S., Cook, N., and Tuveson, D.A. (2012). The pancreas cancer microenvironment. Clin. Cancer Res. *18*, 4266–4276.

Filipowicz, W., Bhattacharyya, S.N., and Sonenberg, N. (2008). Mechanisms of post-transcriptional regulation by microRNAs: Are the answers in sight? Nat. Rev. Genet. *9*, 102–114.

Fogel, M., Friederichs, J., Zeller, Y., Husar, M., Smirnov, A., Roitman, L., Altevogt, P., and Sthoeger, Z.M. (1999). CD24 is a marker for human breast carcinoma. Cancer Lett. *143*, 87–94.

Fogerty, J., Stepanyan, R., Cianciolo, L.T., Tooke, B.P., and Perkins, B.D. (2019). Genomic non-redundancy of the mir-183/96/182 cluster and its requirement for hair cell maintenance. Sci. Rep. *9*, 10302. https://doi.org/10.1038/s41598-019-46593-y.

Foster, K.W., Ren, S., Louro, I.D., Lobo-Ruppert, S.M., McKie-Bell, P., Grizzle, W., Hayes, M.R., Broker, T.R., Chow, L.T., and Ruppert, J.M. (1999). Oncogene expression cloning by retroviral transduction of adenovirus E1A-immortalized rat kidney RK3E cells: Transformation of a host with epithelial features by c-MYC and the zinc finger protein GKLF. Cell Growth Differ. *10*, 423–434.

Foster, K.W., Frost, A.R., McKie-Bell, P., Lin, C.Y., Engler, J.A., Grizzle, W.E., and Ruppert, J.M. (2000). Increase of GKLF messenger RNA and protein expression during progression of breast cancer. Cancer Res. *60*, 6488–6495.

Fries, H., Elsässer, H.P., Mahlbacher, V., Kern, H.F., and Neumann, K. (1994). Localisation of hyaluronate (HA) in primary tumors and nude mouse xenografts of human pancreatic carcinomas using a biotinylated HA-binding protein. Virchows Arch. *424*, 7–12.

Fu, X., Guadagni, F., and Hoffman, R.M. (1992). A metastatic nude-mouse model of human pancreatic cancer constructed orthotopically with histologically intact patient specimens. Proc. Natl. Acad. Sci. U. S. A. *89*, 5645–5649.

Gao, R., Davis, A., McDonald, T.O., Sei, E., Shi, X., Wang, Y., Tsai, P.C., Casasent, A., Waters, J., Zhang, H., et al. (2016). Punctuated copy number evolution and clonal stasis in triple-negative breast cancer. Nat. Genet. *48*, 1119–1130.

Gao, X. hui, Zhang, Y. li, Zhang, Z. ye, Guo, S. shuang, Chen, X. bing, and Guo, Y. zhen (2020). MicroRNA-96-5p represses breast cancer proliferation and invasion through Wnt/β-catenin signaling via targeting CTNND1. Sci. Rep. *10*, 44. https://doi.org/10.1038/s41598-019-56571-z.

Gilam, A., Conde, J., Weissglas-Volkov, D., Oliva, N., Friedman, E., Artzi, N., and Shomron, N. (2016). Local microRNA delivery targets Palladin and prevents metastatic breast cancer. Nat. Commun. *7*.

Gillet, J.P., Varma, S., and Gottesman, M.M. (2013). The clinical relevance of cancer cell lines. J. Natl. Cancer Inst. *105*, 452–458.

Ginestier, C., Hur, M.H., Charafe-Jauffret, E., Monville, F., Dutcher, J., Brown, M., Jacquemier, J., Viens, P., Kleer, C.G., Liu, S., et al. (2007). ALDH1 Is a Marker of Normal and Malignant Human Mammary Stem Cells and a Predictor of Poor Clinical Outcome. Cell Stem Cell *1*, 555–567.

Girard, F., Strausfeld, U., Fernandez, A., and Lamb, N.J.C. (1991). Cyclin A is required for the onset of DNA replication in mammalian fibroblasts. Cell *67*, 1169–1179.

Giricz, O., Reynolds, P.A., Ramnauth, A., Liu, C., Wang, T., Stead, L., Childs, G., Rohan, T., Shapiro, N., Fineberg, S., et al. (2012). Hsa-miR-375 is differentially expressed during breast lobular neoplasia and promotes loss of mammary acinar polarity. J. Pathol. *226*, 108–119.

Godar, S., Ince, T.A., Bell, G.W., Feldser, D., Donaher, J.L., Bergh, J., Liu, A., Miu, K., Watnick, R.S., Reinhardt, F., et al. (2008). Growth-Inhibitory and Tumor- Suppressive Functions of p53 Depend on Its Repression of CD44 Expression. Cell *134*, 62–73.

Goishi, K., Higashiyama, S., Klagsbrun, M., Nakano, N., Umata, T., Ishikawa, M., Mekada, E., and Taniguchi, N. (1995). Phorbol ester induces the rapid processing of cell surface heparin-binding EGF-like growth factor: Conversion from juxtacrine to paracrine growth factor activity. Mol. Biol. Cell *6*, 967–980.

Gómez-Miragaya, J., Palafox, M., Paré, L., Yoldi, G., Ferrer, I., Vila, S., Galván, P., Pellegrini, P., Pérez-Montoyo, H., Igea, A., et al. (2017). Resistance to Taxanes in Triple-Negative Breast Cancer Associates with the Dynamics of a CD49f+ Tumor-Initiating

Population. Stem Cell Reports *8*, 1392–1407.

Greenfield, B., Wang, W.C., Marquardt, H., Piepkorn, M., Wolff, E.A., Aruffo, A., and Bennett, K.L. (1999). Characterization of the heparan sulfate and chondroitin sulfate assembly sites in CD44. J. Biol. Chem. *274*, 2511–2517.

Gregory, P.A., Bert, A.G., Paterson, E.L., Barry, S.C., Tsykin, A., Farshid, G., Vadas, M.A., Khew-Goodall, Y., and Goodall, G.J. (2008). The miR-200 family and miR-205 regulate epithelial to mesenchymal transition by targeting ZEB1 and SIP1. Nat. Cell Biol. *10*, 593–601.

Gregory, R.I., Yan, K.P., Amuthan, G., Chendrimada, T., Doratotaj, B., Cooch, N., and Shiekhattar, R. (2004). The Microprocessor complex mediates the genesis of microRNAs. Nature *432*, 235–240.

Grzesiak, J.J., and Bouvet, M. (2006). The α2β1 integrin mediates the malignant phenotype on type I collagen in pancreatic cancer cell lines. Br. J. Cancer *94*, 1311–1319.

Grzesiak, J.J., Smith, K.C., Burton, D.W., Deftos, L.J., and Bouvet, M. (2007). Integrin-mediated laminin-1 adhesion upregulates CXCR4 and IL-8 expression in pancreatic cancer cells. Surgery *141*, 804–814.

Günthert, U., Hofmann, M., Rudy, W., Reber, S., Zöller, M., Haußmann, I., Matzku, S., Wenzel, A., Ponta, H., and Herrlich, P. (1991). A new variant of glycoprotein CD44 confers metastatic potential to rat carcinoma cells. Cell *65*, 13–24.

Guo, C., Luo, Y., Zhou, R., and Wei, G. (2014). Triphenylalanine peptides self-assemble into nanospheres and nanorods that are different from the nanovesicles and nanotubes formed by diphenylalanine peptides. Nanoscale *6*, 2800–2811.

Guo, W., Keckesova, Z., Donaher, J.L., Shibue, T., Tischler, V., Reinhardt, F., Itzkovitz, S., Noske, A., Zürrer-Härdi, U., Bell, G., et al. (2012). Slug and Sox9 cooperatively determine

the mammary stem cell state. Cell *148*, 1015–1028.

Gupta, P.B., Fillmore, C.M., Jiang, G., Shapira, S.D., Tao, K., Kuperwasser, C., and Lander, E.S. (2011). Stochastic state transitions give rise to phenotypic equilibrium in populations of cancer cells. Cell *146*, 633–644.

Guttilla, I.K., and White, B.A. (2009). Coordinate regulation of FOXO1 by miR-27a, miR-96, and miR-182 in breast cancer cells. J. Biol. Chem. *284*, 23204–23216.

Ha, M., and Kim, V.N. (2014). Regulation of microRNA biogenesis. Nat. Rev. Mol. Cell Biol. *15*, 509–524.

Haber, P.S., Keogh, G.W., Apte, M. V, Moran, C.S., Stewart, N.L., Crawford, D.H., Pirola, R.C., McCaughan, G.W., Ramm, G.A., and Wilson, J.S. (1999). Activation of pancreatic stellate cells in human and experimental pancreatic fibrosis. Am. J. Pathol. *155*, 1087–1095.

Haberern-Blood, C., Liotta, L.A., Rao, C.N., and Kupchik, H.Z. (1987). Laminin expression by human pancreatic carcinoma cells in the nude mouse and in culture. J. Natl. Cancer Inst. *79*, 891–898.

Hamidi, H., and Ivaska, J. (2018). Every step of the way: integrins in cancer progression and metastasis. Nat. Rev. Cancer *18*, 533–548.

Hammond, S.M., Bernstein, E., Beach, D., and Hannon, G.J. (2000). An RNA-directed nuclease mediates post-transcriptional gene silencing in Drosophila cells. Nature *404*, 293–296.

Han, J., Lee, Y., Yeom, K.H., Kim, Y.K., Jin, H., and Kim, V.N. (2004). The Drosha-DGCR8 complex in primary microRNA processing. Genes Dev. *18*, 3016–3027.

Han, J., Lee, Y., Yeom, K.H., Nam, J.W., Heo, I., Rhee, J.K., Sohn, S.Y., Cho, Y., Zhang, B.T., and Kim, V.N. (2006). Molecular Basis for the Recognition of Primary microRNAs by

the Drosha-DGCR8 Complex. Cell *125*, 887–901.

Han, J.A., Kim, J. Il, Ongusaha, P.P., Hwang, D.H., Ballou, L.R., Mahale, A., Aaronson, S.A., and Lee, S.W. (2002). p53-mediated induction of Cox-2 counteracts p53- or genotoxic stress-induced apoptosis. EMBO J. *21*, 5635–5644.

Han, T.H., Ok, T., Kim, J., Shin, D.O., Ihee, H., Lee, H.S., and Kim, S.O. (2010). Bionanosphere Lithography via hierarchical Peptide self-assembly of aromatic triphenylalanine. Small *6*, 945–951.

Hanahan, D., and Weinberg, R.A. (2000). The hallmarks of cancer. Cell *100*, 57–70.

Hanahan, D., and Weinberg, R.A. (2011). 2000: The hallmarks of cancer. Cancer Immunol. Immunother. *60*, 319–326.

Hannafon, B.N., Sebastiani, P., de las Morenas, A., Lu, J., and Rosenberg, C.L. (2011). Expression of microRNA and their gene targets are dysregulated in preinvasive breast cancer. Breast Cancer Res. *13*, R24.

Harburger, D.S., and Calderwood, D.A. (2009). Integrin signalling at a glance. J. Cell Sci. *122*, 159–163.

Hatakeyama, H., Cheng, H., Wirth, P., Counsell, A., Marcrom, S.R., Wood, C.B., Pohlmann, P.R., Gilbert, J., Murphy, B., Yarbrough, W.G., et al. (2010). Regulation of heparin-binding EGF-like growth factor by miR-212 and acquired cetuximab-resistance in head and neck squamous cell carcinoma. PLoS One *5*, e12702.

He, L., He, X., Lim, L.P., De Stanchina, E., Xuan, Z., Liang, Y., Xue, W., Zender, L., Magnus, J., Ridzon, D., et al. (2007). A microRNA component of the p53 tumour suppressor network. Nature *447*, 1130–1134.

Hidalgo, M. (2010). Pancreatic Cancer. N. Engl. J. Med. *362*, 1605–1617.

Higashiyama, S., Abraham, J., Miller, J., Fiddes, J., and Klagsbrun, M. (1991). A heparin-binding growth factor secreted by macrophage-like cells that is related to EGF. Science *251*, 936–939.

Higashiyama, S., Lau, K., Besner, G.E., Abraham, J.A., and Klagsbrun, M. (1992). Structure of heparin-binding EGF-like growth factor. Multiple forms, primary structure, and glycosylation of the mature protein. J. Biol. Chem. *267*, 6205–6212.

Higashiyama, S., Abraham, J.A., and Klagsbrun, M. (1993). Heparin-binding EGF-like growth factor stimulation of smooth muscle cell migration: Dependence on interactions with cell surface heparan sulfate. J. Cell Biol. *122*, 933–940.

Higashiyama, S., Iwamoto, R., Goishi, K., Raab, G., Taniguchi, N., Klagsbrun, M., and Mekada, E. (1995). The membrane protein CD9/DRAP 27 potentiates the juxtacrine growth factor activity of the membrane-anchored heparin-binding EGF-like growth factor. J. Cell Biol. *128*, 929–938.

Hingorani, S.R., Petricoin, E.F., Maitra, A., Rajapakse, V., King, C., Jacobetz, M.A., Ross, S., Conrads, T.P., Veenstra, T.D., Hitt, B.A., et al. (2003). Preinvasive and invasive ductal pancreatic cancer and its early detection in the mouse. Cancer Cell *4*, 437–450.

Hingorani, S.R., Wang, L., Multani, A.S., Combs, C., Deramaudt, T.B., Hruban, R.H., Rustgi, A.K., Chang, S., and Tuveson, D.A. (2005). Trp53 R172H and Kras G12D cooperate to promote chromosomal instability and widely metastatic pancreatic ductal adenocarcinoma in mice. Cancer Cell *7*, 469–483.

Hollier, B.G., Tinnirello, A.A., Werden, S.J., Evans, K.W., Taube, J.H., Sarkar, T.R., Sphyris, N., Shariati, M., Kumar, S. V., Battula, V.L., et al. (2013). FOXC2 expression links epithelial-mesenchymal transition and stem cell properties in breast cancer. Cancer Res. *73*, 1981–1992.

Hong, Y., Liang, H., Uzair-ur-Rehman, Wang, Y., Zhang, W., Zhou, Y., Chen, S., Yu, M., Cui, S., Liu, M., et al. (2016). miR-96 promotes cell proliferation, migration and invasion by targeting PTPN9 in breast cancer. Sci. Rep. *6*, 37421.

Hoshino, A., Costa-Silva, B., Shen, T.L., Rodrigues, G., Hashimoto, A., Tesic Mark, M., Molina, H., Kohsaka, S., Di Giannatale, A., Ceder, S., et al. (2015). Tumour exosome integrins determine organotropic metastasis. Nature *527*, 329–335.

Hruban, R.H., Wilentz, R.E., and Kern, S.E. (2000). Genetic progression in the pancreatic ducts. Am. J. Pathol. *156*, 1821–1825.

Hruban, R.H., Adsay, N.V., Albores-Saavedra, J., Compton, C., Garrett, E.S., Goodman, S.N., Kern, S.E., Klimstra, D.S., Klöppel, G., Longnecker, D.S., et al. (2001). Pancreatic intraepithelial neoplasia: A new nomenclature and classification system for pancreatic duct lesions. Am. J. Surg. Pathol. *25*, 579–586.

Hu, J., Li, G., Zhang, P., Zhuang, X., and Hu, G. (2017). A CD44v+ subpopulation of breast cancer Stem-Like cells with enhanced lung metastasis capacity. Cell Death Dis. *8*, e2679.

Huang, D.W., Sherman, B.T., and Lempicki, R.A. (2009a). Bioinformatics enrichment tools: Paths toward the comprehensive functional analysis of large gene lists. Nucleic Acids Res. *37*, 1–13.

Huang, D.W., Sherman, B.T., and Lempicki, R.A. (2009b). Systematic and integrative analysis of large gene lists using DAVID bioinformatics resources. Nat. Protoc. *4*, 44–57.

Huang, L., Holtzinger, A., Jagan, I., Begora, M., Lohse, I., Ngai, N., Nostro, C., Wang, R., Muthuswamy, L.B., Crawford, H.C., et al. (2015). Ductal pancreatic cancer modeling and drug screening using human pluripotent stem cell- and patient-derived tumor organoids. Nat. Med. *21*, 1364–1371.

Hung, K.W., Huang, H.W., Cho, C.C., Chang, S.C., and Yu, C. (2014). Nuclear magnetic

resonance structure of the cytoplasmic tail of heparin binding EGF-like growth factor (proHB-EGF-CT) complexed with the ubiquitin homology domain of Bcl-2-associated athanogene 1 from Mus musculus (mBAG-1-UBH). Biochemistry *53*, 1935–1946.

Hutvágner, G., McLachlan, J., Pasquinelli, A.E., Bálint, É., Tuschl, T., and Zamore, P.D. (2001). A cellular function for the RNA-interference enzyme dicer in the maturation of the let-7 small temporal RNA. Science *293*, 834–838.

Huxley (1956). CANCER BIOLOGY: COMPARATIVE and GENETIC. Biol. Rev. *31*, 474.

Hwang, H.W., and Mendell, J.T. (2006). MicroRNAs in cell proliferation, cell death, and tumorigenesis. Br J Cancer *94*, 776–780.

Idowu, M.O., Kmieciak, M., Dumur, C., Burton, R.S., Grimes, M.M., Powers, C.N., and Manjili, M.H. (2012). CD44 +/CD24 -/low cancer stem/progenitor cells are more abundant in triple-negative invasive breast carcinoma phenotype and are associated with poor outcome. Hum. Pathol. *43*, 364–373.

Iida, N., and Bourguignon, L.Y.W. (1995). New CD44 splice variants associated with human breast cancers. J. Cell. Physiol. *162*, 127–133.

Iliopoulos, D., Lindahl-Allen, M., Polytarchou, C., Hirsch, H.A., Tsichlis, P.N., and Struhl, K. (2010). Loss of miR-200 Inhibition of Suz12 Leads to Polycomb-Mediated Repression Required for the Formation and Maintenance of Cancer Stem Cells. Mol. Cell *39*, 761–772.

Iliopoulos, D., Hirsch, H.A., Wang, G., and Struhl, K. (2011). Inducible formation of breast cancer stem cells and their dynamic equilibrium with non-stem cancer cells via IL6 secretion. Proc. Natl. Acad. Sci. U. S. A. *108*, 1397–1402.

Iorio, M. V., Ferracin, M., Liu, C.G., Veronese, A., Spizzo, R., Sabbioni, S., Magri, E., Pedriali, M., Fabbri, M., Campiglio, M., et al. (2005). MicroRNA gene expression deregulation in human breast cancer. Cancer Res. *65*, 7065–7070.

Ito, Y., Takeda, T., Higashiyama, S., Noguchi, S., and Matsuura, N. (2001). Expression of heparin-binding epidermal growth factor-like growth factor in breast carcinoma. Breast Cancer Res. Treat. *67*, 81–85.

Iwamoto, R., Yamazaki, S., Asakura, M., Takashima, S., Hasuwa, H., Miyado, K., Adachi, S., Kitakaze, M., Hashimoto, K., Raab, G., et al. (2003). Heparin-binding EGF-like growth factor and ErbB signaling is essential for heart function. Proc. Natl. Acad. Sci. U. S. A. *100*, 3221–3226.

Izumi, Y., Hirata, M., Hasuwa, H., Iwamoto, R., Umata, T., Miyado, K., Tamai, Y., Kurisaki, T., Sehara-Fujisawa, A., Ohno, S., et al. (1998). A metalloprotease-disintegrin, MDC9/meltrin-γ/ADAM9 and PKCδ are involved in TPA-induced ectodomain shedding of membrane-anchored heparin-binding EGF-like growth factor. EMBO J. *17*, 7260–7272.

Jackson, D.G., Bell, J.I., Dickinson, R., Timans, J., Shields, J., and Whittle, N. (1995). Proteoglycan forms of the lymphocyte homing receptor CD44 are alternatively spliced variants containing the v3 exon. J. Cell Biol. *128*, 673–685.

Jacobetz, M.A., Chan, D.S., Neesse, A., Bapiro, T.E., Cook, N., Frese, K.K., Feig, C., Nakagawa, T., Caldwell, M.E., Zecchini, H.I., et al. (2013). Hyaluronan impairs vascular function and drug delivery in a mouse model of pancreatic cancer. Gut *62*, 112–120.

Jain, C. V., Jessmon, P., Kilburn, B.A., Jodar, M., Sendler, E., Krawetz, S.A., and Randall Armant, D. (2016). Regulation of HBEGF by micro-RNA for survival of developing human trophoblast cells. PLoS One *11*, e0163913.

Jalkanen, S., and Jalkanen, M. (1992). Lymphocyte CD44 binds the COOH-terminal heparin-binding domain of fibronectin. J. Cell Biol. *116*, 817–825.

De Jesus-Acosta, A., Sugar, E.A., O'Dwyer, P.J., Ramanathan, R.K., Von Hoff, D.D., Rasheed, Z., Zheng, L., Begum, A., Anders, R., Maitra, A., et al. (2020). Phase 2 study of

vismodegib, a hedgehog inhibitor, combined with gemcitabine and nab-paclitaxel in patients with untreated metastatic pancreatic adenocarcinoma. Br. J. Cancer *122*, 498–505.

Ji, Q., Hao, X., Zhang, M., Tang, W., Meng, Y., Li, L., Xiang, D., DeSano, J.T., Bommer, G.T., Fan, D., et al. (2009). MicroRNA miR-34 inhibits human pancreatic cancer tumor-initiating cells. PLoS One *4*, e6816.

Jiang, F.X., Naselli, G., and Harrison, L.C. (2002). Distinct distribution of laminin and its integrin receptors in the pancreas. J. Histochem. Cytochem. *50*, 1625–1632.

John, B., Enright, A.J., Aravin, A., Tuschl, T., Sander, C., and Marks, D.S. (2004). Human microRNA targets. PLoS Biol. *3*, e264.

Jones, F.E., Welte, T., Fu, X.Y., and Stern, D.F. (1999). ErbB4 signaling in the mammary gland is required for lobuloalveolar development and Stat5 activation during lactation. J. Cell Biol. *147*, 77–88.

Jones, S., Zhang, X., Parsons, D.W., Lin, J.C.H., Leary, R.J., Angenendt, P., Mankoo, P., Carter, H., Kamiyama, H., Jimeno, A., et al. (2008). Core signaling pathways in human pancreatic cancers revealed by global genomic analyses. Science *321*, 1801–1806.

Julian, L., and Olson, M.F. (2014). Rho-associated coiled-coil containing kinases (ROCK), structure, regulation, and functions. Small GTPases *5*, e29846.

Kagara, N., Huynh, K.T., Kuo, C., Okano, H., Sim, M.S., Elashoff, D., Chong, K., Giuliano, A.E., and Hoon, D.S. (2012). Epigenetic regulation of cancer stem cell genes in triple-negative breast cancer. Am J Pathol *181*, 257–267.

Kaipparettu, B.A., Malik, S., Konduri, S.D., Liu, W., Rokavec, M., Van Der Kuip, H., Hoppe, R., Hammerich-Hille, S., Fritz, P., Schroth, W., et al. (2008). Estrogen-mediated downregulation of CD24 in breast cancer cells. Int. J. Cancer *123*, 66–72.

Kalish, E.D., Iida, N., Moffat, F.L., and Bourguignon, L.Y. (1999a). A new CD44V3-containing isoform is involved in tumor cell growth and migration during human breast carcinoma progression. Front. Biosci. *4*, a1-8.

Kalish, E.D., Iida, N., Moffat, F.L., and Bourguignon, L.Y. (1999b). A new CD44V3-containing isoform is involved in tumor cell growth and migration during human breast carcinoma progression. Front Biosci *4*, A1-8.

Kaneko, K., Satoh, K., Masamune, A., Satoh, A., and Shimosegawa, T. (2002). Expression of ROCK-1 in human pancreatic cancer: Its down-regulation by morpholino oligo antisense can reduce the migration of pancreatic cancer cells in vitro. Pancreas *24*, 251–257.

Kang, L., Mao, J., Tao, Y., Song, B., Ma, W., Lu, Y., Zhao, L., Li, J., Yang, B., and Li, L. (2015). MicroRNA-34a suppresses the breast cancer stem cell-like characteristics by downregulating Notch1 pathway. Cancer Sci. *106*, 700–708.

Kaufmann, M., von Minckwitz, G., Heider, K.H., Ponta, H., Herrlich, P., and Sinn, H.P. (1995). CD44 variant exon epitopes in primary breast cancer and length of survival. Lancet *345*, 615–619.

Kawamata, T., Seitz, H., and Tomari, Y. (2009). Structural determinants of miRNAs for RISC loading and slicer-independent unwinding. Nat. Struct. Mol. Biol. *16*, 953–960.

Ketting, R.F., Fischer, S.E.J., Bernstein, E., Sijen, T., Hannon, G.J., and Plasterk, R.H.A. (2001). Dicer functions in RNA interference and in synthesis of small RNA involved in developmental timing in C. elegans. Genes Dev. *15*, 2654–2659.

Kim, W.T., and Ryu, C.J. (2017). Cancer stem cell surface markers on normal stem cells. BMB Rep. *50*, 285–298.

Kim, S.Y., Kang, J.W., Song, X., Kim, B.K., Yoo, Y.D., Kwon, Y.T., and Lee, Y.J. (2013). Role of the IL-6-JAK1-STAT3-Oct-4 pathway in the conversion of non-stem cancer cells

into cancer stem-like cells. Cell. Signal. *25*, 961–969.

Kimura, K., Ito, M., Amano, M., Chihara, K., Fukata, Y., Nakafuku, M., Yamamori, B., Feng, J., Nakano, T., Okawa, K., et al. (1996). Regulation of myosin phosphatase by Rho and Rho-associated kinase (Rho- kinase). Science *273*, 245–248.

Kinugasa, Y., Hieda, M., Hori, M., and Higashiyama, S. (2007). The carboxyl-terminal fragment of pro-HB-EGF reverses Bcl6-mediated gene repression. J. Biol. Chem. *282*, 14797–14806.

Kiriakidou, M., Nelson, P.T., Kouranov, A., Fitziev, P., Bouyioukos, C., Mourelatos, Z., and Hatzigeorgiou, A. (2004). A combined computational-experimental approach predicts human microRNA targets. Genes Dev. *18*, 1165–1178.

Kleinman, H.K., and Martin, G.R. (2005). Matrigel: Basement membrane matrix with biological activity. Semin. Cancer Biol. *15*, 378–386.

Kleinman, H.K., McGarvey, M.L., Hassell, J.R., Star, V.L., Cannon, F.B., Laurie, G.W., and Martin, G.R. (1986). Basement Membrane Complexes with Biological Activity. Biochemistry *25*, 312–318.

Kleppe, M., and Levine, R.L. (2014). Tumor heterogeneity confounds and illuminates: assessing the implications. Nat. Med. *20*, 342–344.

Knezevic, J., Pfefferle, A.D., Petrovic, I., Greene, S.B., Perou, C.M., and Rosen, J.M. (2015). Expression of miR-200c in claudin-low breast cancer alters stem cell functionality, enhances chemosensitivity and reduces metastatic potential. Oncogene *34*, 5997–6006.

Knudson, W., Biswas, C., and Toole, B.P. (1984). Interactions between human tumor cells and fibroblasts stimulate hyaluronate synthesis. Proc. Natl. Acad. Sci. U. S. A. *81*, 6767–6771.

König, H., Ponta, H., and Herrlich, P. (1998). Coupling of signal transduction to alternative pre-mRNA splicing by a composite splice regulator. EMBO J. *17*, 2904–2913.

Korpal, M., Lee, E.S., Hu, G., and Kang, Y. (2008). The miR-200 family inhibits epithelial-mesenchymal transition and cancer cell migration by direct targeting of E-cadherin transcriptional repressors ZEB1 and ZEB2. J. Biol. Chem. *283*, 14910–14914.

Krek, A., Grün, D., Poy, M.N., Wolf, R., Rosenberg, L., Epstein, E.J., MacMenamin, P., Da Piedade, I., Gunsalus, K.C., Stoffel, M., et al. (2005). Combinatorial microRNA target predictions. Nat. Genet. *37*, 495–500.

Kreso, A., and Dick, J.E. (2014). Evolution of the cancer stem cell model. Cell Stem Cell *14*, 275–291.

Kristiansen, G., Winzer, K.J., Mayordomo, E., Bellach, J., Schlüns, K., Denkert, C., Dahl, E., Pilarsky, C., Altevogt, P., Guski, H., et al. (2003). CD24 Expression Is a New Prognostic Marker in Breast Cancer. Clin. Cancer Res. *9*, 4906–4913.

Kulemann, B., Pitman, M.B., Liss, A.S., Valsangkar, N., Fernández-Del Castillo, C., Lillemoe, K.D., Hoeppner, J., Mino-Kenudson, M., Warshaw, A.L., and Thayer, S.P. (2015). Circulating tumor cells found in patients with localized and advanced pancreatic cancer. Pancreas *44*, 547–550.

Kultti, A., Zhao, C., Singha, N.C., Zimmerman, S., Osgood, R.J., Symons, R., Jiang, P., Li, X., Thompson, C.B., Infante, J.R., et al. (2014). Accumulation of Extracellular Hyaluronan by Hyaluronan Synthase 3 Promotes Tumor Growth and Modulates the Pancreatic Cancer Microenvironment. Biomed Res. Int. e817613.

Kumazoe, M., Takai, M., Bae, J., Hiroi, S., Huang, Y., Takamatsu, K., Won, Y., Yamashita, M., Hidaka, S., Yamashita, S., et al. (2017a). FOXO3 is essential for CD44 expression in pancreatic cancer cells. Oncogene *36*, 2643–2654.

Kumazoe, M., Takai, M., Hiroi, S., Takeuchi, C., Kadomatsu, M., Nojiri, T., Onda, H., Bae, J., Huang, Y., Takamatsu, K., et al. (2017b). The FOXO3/PGC-1β signaling axis is essential for cancer stem cell properties of pancreatic ductal adenocarcinoma. J. Biol. Chem. *292*, 10813–10823.

Lai, E.C. (2002). Micro RNAs are complementary to 3′ UTR sequence motifs that mediate negative post-transcriptional regulation. Nat. Genet. *30*, 363–364.

Laklai, H., Miroshnikova, Y.A., Pickup, M.W., Collisson, E.A., Kim, G.E., Barrett, A.S., Hill, R.C., Lakins, J.N., Schlaepfer, D.D., Mouw, J.K., et al. (2016). Genotype tunes pancreatic ductal adenocarcinoma tissue tension to induce matricellular fibrosis and tumor progression. Nat. Med. *22*, 497–505.

Lapidot, T., Sirard, C., Vormoor, J., Murdoch, B., Hoang, T., Caceres-Cortes, J., Minden, M., Paterson, B., Caligiuri, M.A., and Dick, J.E. (1994). A cell initiating human acute myeloid leukaemia after transplantation into SCID mice. Nature *367*, 645–648.

Laplante, M., and Sabatini, D.M. (2009). mTOR signaling at a glance. J. Cell Sci. *122*, 3589–3594.

Lawson, D.A., Bhakta, N.R., Kessenbrock, K., Prummel, K.D., Yu, Y., Takai, K., Zhou, A., Eyob, H., Balakrishnan, S., Wang, C.Y., et al. (2015). Single-cell analysis reveals a stem-cell program in human metastatic breast cancer cells. Nature *526*, 131–135.

Lee, J.W., Komar, C.A., Bengsch, F., Graham, K., and Beatty, G.L. (2016). Genetically engineered mouse models of pancreatic cancer: The KPC model (LSL-KrasG12D/+;LSL-Trp53R172H/+;Pdx-1-Cre), its variants, and their application in immuno-oncology drug discovery. Curr. Protoc. Pharmacol. *73*, 14.39.1-14.39.20.

Lee, M.C.W., Lopez-Diaz, F.J., Khan, S.Y., Tariq, M.A., Dayn, Y., Vaske, C.J., Radenbaugh, A.J., Kim, H.J., Emerson, B.M., and Pourm, N. (2014). Single-cell analyses of transcriptional

heterogeneity during drug tolerance transition in cancer cells by RNA sequencing. Proc. Natl. Acad. Sci. U. S. A. *111*, E4726–E4735.

Lee, S.W., Fang, L., Igarashi, M., Ouchi, T., Lu, K.P., and Aaronson, S.A. (2000). Sustained activation of Ras/Raf/mitogen-activated protein kinase cascade by the tumor suppressor p53. Proc. Natl. Acad. Sci. U. S. A. *97*, 8302–8305.

Lee, Y., Jeon, K., Lee, J.T., Kim, S., and Kim, V.N. (2002). MicroRNA maturation: Stepwise processing and subcellular localization. EMBO J. *21*, 4663–4670.

Lee, Y., Ahn, C., Han, J., Choi, H., Kim, J., Yim, J., Lee, J., Provost, P., Rådmark, O., Kim, S., et al. (2003). The nuclear RNase III Drosha initiates microRNA processing. Nature *425*, 415–419.

Lee, Y., Kim, M., Han, J., Yeom, K.H., Lee, S., Baek, S.H., and Kim, V.N. (2004). MicroRNA genes are transcribed by RNA polymerase II. EMBO J. *23*, 4051–4060.

Lehmann, U., Streichert, T., Otto, B., Albat, C., Hasemeier, B., Christgen, H., Schipper, E., Hille, U., Kreipe, H.H., and Länger, F. (2010). Identification of differentially expressed microRNAs in human male breast cancer. BMC Cancer *10*, e109.

Leuschner, P.J.F., Ameres, S.L., Kueng, S., and Martinez, J. (2006). Cleavage of the siRNA passenger strand during RISC assembly in human cells. EMBO Rep. *7*, 314–320.

Levental, K.R., Yu, H., Kass, L., Lakins, J.N., Egeblad, M., Erler, J.T., Fong, S.F.T., Csiszar, K., Giaccia, A., Weninger, W., et al. (2009). Matrix Crosslinking Forces Tumor Progression by Enhancing Integrin Signaling. Cell *139*, 891–906.

Lewis, B.P., Shih, I.H., Jones-Rhoades, M.W., Bartel, D.P., and Burge, C.B. (2003). Prediction of Mammalian MicroRNA Targets. Cell *115*, 787–798.

Lewis, B.P., Burge, C.B., and Bartel, D.P. (2005). Conserved seed pairing, often flanked by

adenosines, indicates that thousands of human genes are microRNA targets. Cell *120*, 15–20.

Li, B., Lu, Y., Wang, H., Han, X., Mao, J., Li, J., Yu, L., Wang, B., Fan, S., Yu, X., et al. (2016). MiR-221/222 enhance the tumorigenicity of human breast cancer stem cells via modulation of PTEN/Akt pathway. Biomed. Pharmacother. *79*, 93–101.

Li, D., Wang, A., Liu, X., Meisgen, F., Grünler, J., Botusan, I.R., Narayanan, S., Erikci, E., Li, X., Blomqvist, L., et al. (2015). MicroRNA-132 enhances transition from inflammation to proliferation during wound healing. J. Clin. Invest. *125*, 3008–3026.

Li, P., Sheng, C., Huang, L., Zhang, H., Huang, L., Cheng, Z., and Zhu, Q. (2014a). MiR-183/-96/-182 cluster is up-regulated in most breast cancers and increases cell proliferation and migration. Breast Cancer Res. *16*.

Li, X., Lewis, M.T., Huang, J., Gutierrez, C., Osborne, C.K., Wu, M.F., Hilsenbeck, S.G., Pavlick, A., Zhang, X., Chamness, G.C., et al. (2008). Intrinsic resistance of tumorigenic breast cancer cells to chemotherapy. J. Natl. Cancer Inst. *100*, 672–679.

Li, X.L., Hara, T., Choi, Y., Subramanian, M., Francis, P., Bilke, S., Walker, R.L., Pineda, M., Zhu, Y., Yang, Y., et al. (2014b). A p21-ZEB1 Complex Inhibits Epithelial-Mesenchymal Transition through the MicroRNA 183-96-182 Cluster. Mol. Cell. Biol. *34*, 533–550.

Lim, L.P., Lau, N.C., Garrett-Engele, P., Grimson, A., Schelter, J.M., Castle, J., Bartel, D.P., Linsley, P.S., and Johnson, J.M. (2005). Microarray analysis shows that some microRNAs downregulate large numbers of-target mRNAs. Nature *433*, 769–773.

Lin, H., Dai, T., Xiong, H., Zhao, X., Chen, X., Yu, C., Li, J., Wang, X., and Song, L. (2010a). Unregulated miR-96 induces cell proliferation in human breast cancer by downregulating transcriptional factor FOXO3a. PLoS One *5*, e15797.

Lin, H., Dai, T., Xiong, H., Zhao, X., Chen, X., Yu, C., Li, J., Wang, X., and Song, L.

(2010b). Unregulated miR-96 induces cell proliferation in human breast cancer by downregulating transcriptional factor FOXO3a. PLoS One *5*.

Lin, J., Hutchinson, L., Gaston, S.M., Raab, G., and Freeman, M.R. (2001). BAG-1 is a novel cytoplasmic binding partner of the membrane form of heparin-binding EGF-like growth factor. A unique role for proHB-EGF in cell survival regulation. J. Biol. Chem. *276*, 30127–30132.

Liu, C., Kelnar, K., Liu, B., Chen, X., Calhoun-Davis, T., Li, H., Patrawala, L., Yan, H., Jeter, C., Honorio, S., et al. (2011). The microRNA miR-34a inhibits prostate cancer stem cells and metastasis by directly repressing CD44. Nat. Med. *17*, 211–216.

Liu, S., Cong, Y., Wang, D., Sun, Y., Deng, L., Liu, Y., Martin-Trevino, R., Shang, L., McDermott, S.P., Landis, M.D., et al. (2014). Breast cancer stem cells transition between epithelial and mesenchymal states reflective of their normal counterparts. Stem Cell Reports *2*, 78–91.

Liu, X., Xu, J., Zhang, B., Liu, J., Liang, C., Meng, Q., Hua, J., Yu, X., and Shi, S. (2019). The reciprocal regulation between host tissue and immune cells in pancreatic ductal adenocarcinoma: new insights and therapeutic implications. Mol. Cancer *18*, 184. https://doi.org/10.1186/s12943-019-1117–1119.

Lodygin, D., Tarasov, V., Epanchintsev, A., Berking, C., Knyazeva, T., Körner, H., Knyazev, P., Diebold, J., and Hermeking, H. (2008). Inactivation of miR-34a by aberrant CpG methylation in multiple types of cancer. Cell Cycle *7*, 2591–2600.

Loh, H.Y., Norman, B.P., Lai, K.S., Rahman, N.M.A.N.A., Alitheen, N.B.M., and Osman, M.A. (2019). The regulatory role of microRNAs in breast cancer. Int. J. Mol. Sci. *20*, e4940.

Lomberk, G., Blum, Y., Nicolle, R., Nair, A., Gaonkar, K.S., Marisa, L., Mathison, A., Sun, Z., Yan, H., Elarouci, N., et al. (2018). Distinct epigenetic landscapes underlie the

pathobiology of pancreatic cancer subtypes. Nat. Commun. *9*, e1978. https://doi.org/10.1038/s41467-018-04383-6.

Lomberk, G., Dusetti, N., Iovanna, J., and Urrutia, R. (2019). Emerging epigenomic landscapes of pancreatic cancer in the era of precision medicine. Nat. Commun. *10*, e3875. https://doi.org/10.1038/s41467-019-11812-7.

Long, W., Wagner, K.U., Lloyd, K.C.K., Binart, N., Shillingford, J.M., Hennighausen, L., and Jones, F.E. (2003). Impaired differentiation and lactational failure of Erbb4-deficient mammary glands identify ERBB4 as an obligate mediator of STAT5. Development *130*, 5257–5268.

Louie, G. V., Yang, W., Bowman, M.E., and Choe, S. (1997). Crystal structure of the complex of diphtheria toxin with an extracellular fragment of its receptor. Mol. Cell *1*, 67–78.

Loukopoulos, P., Kanetaka, K., Takamura, M., Shibata, T., Sakamoto, M., and Hirohashi, S. (2004). Orthotopic transplantation models of pancreatic adenocarcinoma derived from cell lines and primary tumors and displaying varying metastatic activity. Pancreas *29*, 192–203.

Lu, J., Getz, G., Miska, E.A., Alvarez-Saavedra, E., Lamb, J., Peck, D., Sweet-Cordero, A., Ebert, B.L., Mak, R.H., Ferrando, A.A., et al. (2005). MicroRNA expression profiles classify human cancers. Nature *435*, 834–848.

Lv, C., Li, F., Li, X., Tian, Y., Zhang, Y., Sheng, X., Song, Y., Meng, Q., Yuan, S., Luan, L., et al. (2017). MiR-31 promotes mammary stem cell expansion and breast tumorigenesis by suppressing Wnt signaling antagonists. Nat. Commun. *8*, e1036.

Määttä, M., Virtanen, I., Burgeson, R., and Autio-Harmainen, H. (2001). Comparative analysis of the distribution of laminin chains in the basement membranes in some malignant epithelial tumors: The α1 chain of laminin shows a selected expression pattern in human

carcinomas. J. Histochem. Cytochem. *49*, 711–725.

Mahlbacher, V., Sewing, A., Elsasser, H.P., and Kern, H.F. (1992). Hyaluronan is a secretory product of human pancreatic adenocarcinoma cells. Eur. J. Cell Biol. *58*, 28–34.

Mahler, A., Reches, M., Rechter, M., Cohen, S., and Gazit, E. (2006). Rigid, self-assembled hydrogel composed of a modified aromatic dipeptide. Adv. Mater. *18*, 1365–1370.

Malhotra, G.K., Zhao, X., Band, H., and Band, V. (2010). Histological, molecular and functional subtypes of breast cancers. Cancer Biol. Ther. *10*, 955–960.

Mani, S.A., Guo, W., Liao, M.J., Eaton, E.N., Ayyanan, A., Zhou, A.Y., Brooks, M., Reinhard, F., Zhang, C.C., Shipitsin, M., et al. (2008). The Epithelial-Mesenchymal Transition Generates Cells with Properties of Stem Cells. Cell *133*, 704–715.

Mantoni, T.S., Lunardi, S., Al-Assar, O., Masamune, A., and Brunner, T.B. (2011). Pancreatic stellate cells radioprotect pancreatic cancer cells through β1-integrin signaling. Cancer Res. *71*, 3453–3458.

Mao, L., Wang, H., Tan, M., Ou, L., Kong, D., and Yang, Z. (2012). Conjugation of two complementary anti-cancer drugs confers molecular hydrogels as a co-delivery system. Chem. Commun. *48*, 395–397.

Marikovsky, M., Breuing, K., Liu, P.Y., Eriksson, E., Higashiyama, S., Farber, P., Abraham, J., and Klagsbrun, M. (1993). Appearance of heparin-binding EGF-like growth factor in wound fluid as a response to injury. Proc. Natl. Acad. Sci. U. S. A. *90*, 3889–3893.

Marusyk, A., Tabassum, D.P., Altrock, P.M., Almendro, V., Michor, F., and Polyak, K. (2014). Non-cell-autonomous driving of tumour growth supports sub-clonal heterogeneity. Nature *514*, 54–58.

Matranga, C., Tomari, Y., Shin, C., Bartel, D.P., and Zamore, P.D. (2005). Passenger-strand

cleavage facilitates assembly of siRNA into Ago2-containing RNAi enzyme complexes. Cell *123*, 607–620.

Matter, N., Herrlich, P., and König, H. (2002). Signal-dependent regulation of splicing via phosphorylation of Sam68. Nature *420*, 691–695.

Mayans, E., Casanovas, J., Gil, A.M., Jiménez, A.I., Cativiela, C., Puiggalí, J., and Alemán, C. (2017). Diversity and Hierarchy in Supramolecular Assemblies of Triphenylalanine: From Laminated Helical Ribbons to Toroids. Langmuir.

Mayer, S., Zur Hausen, A., Watermann, D.O., Stamm, S., Jäger, M., Gitsch, G., and Stickeler, E. (2008). Increased soluble CD44 concentrations are associated with larger tumor size and lymph node metastasis in breast cancer patients. J. Cancer Res. Clin. Oncol. *134*, 1229–1235.

McDonald, O.G., Li, X., Saunders, T., Tryggvadottir, R., Mentch, S.J., Warmoes, M.O., Word, A.E., Carrer, A., Salz, T.H., Natsume, S., et al. (2017). Epigenomic reprogramming during pancreatic cancer progression links anabolic glucose metabolism to distant metastasis. Nat. Genet. *49*, 367–376.

Melo, S.A., Luecke, L.B., Kahlert, C., Fernandez, A.F., Gammon, S.T., Kaye, J., LeBleu, V.S., Mittendorf, E.A., Weitz, J., Rahbari, N., et al. (2015). Glypican-1 identifies cancer exosomes and detects early pancreatic cancer. Nature *523*, 177–182.

Mendell, J.T., and Olson, E.N. (2012). MicroRNAs in stress signaling and human disease. Cell *148*, 1172–1187.

Meyer, M.J., Fleming, J.M., Ali, M.A., Pesesky, M.W., Ginsburg, E., and Vonderhaar, B.K. (2009). Dynamic regulation of CD24 and the invasive, CD44posCD24negphenotype in breast cancer cell lines. Breast Cancer Res. *11*, R82. https://doi.org/10.1186/bcr2449.

Meyer, M.J., Fleming, J.M., Lin, A.F., Hussnain, S.A., Ginsburg, E., and Vonderhaar, B.K.

(2010). CD44posCD49fhiCD133/2hi defines xenograft-initiating cells in estrogen receptor-negative breast cancer. Cancer Res. *70*, 4624–4633.

Miller, B.W., Morton, J.P., Pinese, M., Saturno, G., Jamieson, N.B., McGhee, E., Timpson, P., Leach, J., McGarry, L., Shanks, E., et al. (2015). Targeting the LOX / hypoxia axis reverses many of the features that make pancreatic cancer deadly: inhibition of LOX abrogates metastasis and enhances drug efficacy. EMBO Mol. Med. *7*, 1063–1076.

Mishima, T., Sadovsky, E., Gegick, M.E., and Sadovsky, Y. (2016). Determinants of effective lentivirus-driven microRNA expression in vivo. Sci. Rep. *6*, e33345. https://doi.org/10.1038/srep33345.

Mitamura, T., Higashiyama, S., Taniguchi, N., Klagsbrun, M., and Mekada, E. (1995). Diphtheria toxin binds to the epidermal growth factor (EGF)-like domain of human heparin-binding EGF-like growth factor/diphtheria toxin receptor and inhibits specifically its mitogenic activity. J. Biol. Chem. *270*, 1015–1019.

Miyake, K., Yoshizumi, T., Imura, S., Sugimoto, K., Batmunkh, E., Kanemura, H., Morine, Y., and Shimada, M. (2008). Expression of hypoxia-inducible factor-1α, histone deacetylase 1, and metastasis-associated protein 1 in pancreatic carcinoma: Correlation with poor prognosis with possible regulation. Pancreas *36*, e1–e9.

Miyoshi, E., Higashiyama, S., Nakagawa, T., Hayashi, N., and Taniguchi, N. (1997). Membrane-anchored heparin-binding epidermal growth factor-like growth factor acts as a tumor survival factor in a hepatoma cell line. J. Biol. Chem. *272*, 14349–14355.

Miyoshi, K., Tsukumo, H., Nagami, T., Siomi, H., and Siomi, M.C. (2005). Slicer function of Drosophila Argonautes and its involvement in RISC formation. Genes Dev. *19*, 2837–2848.

Moazzeni, H., Najafi, A., and Khani, M. (2017). Identification of direct target genes of miR-7, miR-9, miR-96, and miR-182 in the human breast cancer cell lines MCF-7 and MDA-MB-

231. Mol. Cell. Probes *34*, 45–52.

Moffitt, R.A., Marayati, R., Flate, E.L., Volmar, K.E., Loeza, S.G.H., Hoadley, K.A., Rashid, N.U., Williams, L.A., Eaton, S.C., Chung, A.H., et al. (2015). Virtual microdissection identifies distinct tumor- and stroma-specific subtypes of pancreatic ductal adenocarcinoma. Nat. Genet. *47*, 1168–1178.

Molnár, V., É Rsek, B., Wiener, Z., Tömböl, Z., Szabó, P.M., Igaz, P., and Falus, A. (2012). MicroRNA-132 targets HB-EGF upon IgE-mediated activation in murine and human mast cells. Cell. Mol. Life Sci. *69*, 7993–808.

Morel, A.P., Lièvre, M., Thomas, C., Hinkal, G., Ansieau, S., and Puisieux, A. (2008). Generation of breast cancer stem cells through epithelial-mesenchymal transition. PLoS One *3*, e2888.

Morlando, M., Ballarino, M., Gromak, N., Pagano, F., Bozzoni, I., and Proudfoot, N.J. (2008). Primary microRNA transcripts are processed co-transcriptionally. Nat. Struct. Mol. Biol. *15*, 902–909.

Müller, I., Wischnewski, F., Pantel, K., and Schwarzenbach, H. (2010). Promoter- and cell-specific epigenetic regulation of CD44, Cyclin D2, GLIPR1 and PTEN by Methyl-CpG binding proteins and histone modifications. BMC Cancer *10*, e297. https://doi.org/10.1186/1471-2407-10-297.

Naglich, J.G., Metherall, J.E., Russell, D.W., and Eidels, L. (1992). Expression cloning of a diphtheria toxin receptor: Identity with a heparin-binding EGF-like growth factor precursor. Cell *69*, 1051–1061.

Nakai, K., Yoneda, K., Moriue, T., Igarashi, J., Kosaka, H., and Kubota, Y. (2009). HB-EGF-induced VEGF production and eNOS activation depend on both PI3 kinase and MAP kinase in HaCaT cells. J. Dermatol. Sci. *55*, 170–178.

Nam, S.O., Yotsumoto, F., Miyata, K., Fukagawa, S., Odawara, T., Manabe, S., Ishikawa, T., Kuroki, M., Yasunaga, S., and Miyamoto, S. (2016). Anti-tumor effect of intravenous administration of CRM197 for triple-negative breast cancer therapy. Anticancer Res. *36*, 3651–3657.

Nanba, D., Mammoto, A., Hashimoto, K., and Higashiyama, S. (2003). Proteolytic release of the carboxy-terminal fragment of proHB-EGF causes nuclear export of PLZF. J. Cell Biol. *163*, 489–502.

Naoki, I. (1990). The Vitamin A-Storing Cells in the Hnman and Rat Pancreas. Kurume Med. J. *37*, 67–81.

Narita, T., Kawakami-Kimura, N., Sato, M., Matsuura, N., Higashiyama, S., Taniguchi, N., and Kannagi, R. (1996). Alteration of integrins by heparin-binding EGF like growth factor in human breast cancer cells. Oncol. *53*, 374–381.

Navin, N.E. (2015). Delineating cancer evolution with single-cell sequencing. Sci. Transl. Med. *7*, 296fs29.

Navin, N., Krasnitz, A., Rodgers, L., Cook, K., Meth, J., Kendall, J., Riggs, M., Eberling, Y., Troge, J., Grubor, V., et al. (2010). Inferring tumor progression from genomic heterogeneity. Genome Res. *20*, 68–80.

Navin, N., Kendall, J., Troge, J., Andrews, P., Rodgers, L., McIndoo, J., Cook, K., Stepansky, A., Levy, D., Esposito, D., et al. (2011). Tumour evolution inferred by single-cell sequencing. Nature *472*, 90–94.

Neal, J.T., Li, X., Zhu, J., Giangarra, V., Grzeskowiak, C.L., Ju, J., Liu, I.H., Chiou, S.H., Salahudeen, A.A., Smith, A.R., et al. (2018). Organoid Modeling of the Tumor Immune Microenvironment. Cell *175*, 1972–1988.

Neesse, A., Bauer, C.A., Öhlund, D., Lauth, M., Buchholz, M., Michl, P., Tuveson, D.A., and

Gress, T.M. (2019). Stromal biology and therapy in pancreatic cancer: Ready for clinical translation? Gut *68*, 159–171.

Nguyen, A. V., Nyberg, K.D., Scott, M.B., Welsh, A.M., Nguyen, A.H., Wu, N., Hohlbauch, S. V., Geisse, N.A., Gibb, E.A., Robertson, A.G., et al. (2016). Stiffness of pancreatic cancer cells is associated with increased invasive potential. Integr. Biol. (United Kingdom) *8*, 1232–1245.

Nielsen, P.K., and Yamada, Y. (2001). Identification of Cell-binding Sites on the Laminin α5 N-terminal Domain by Site-directed Mutagenesis. J. Biol. Chem. *276*, 10906–10912.

Nieto, M.A., Huang, R.Y.Y.J., Jackson, R.A.A., and Thiery, J.P.P. (2016). EMT: 2016. Cell *166*, 21–45.

Nik-Zainal, S., Van Loo, P., Wedge, D.C., Alexandrov, L.B., Greenman, C.D., Lau, K.W., Raine, K., Jones, D., Marshall, J., Ramakrishna, M., et al. (2012a). The life history of 21 breast cancers. Cell *149*, 994–1007.

Nik-Zainal, S., Alexandrov, L.B., Wedge, D.C., Van Loo, P., Greenman, C.D., Raine, K., Jones, D., Hinton, J., Marshall, J., Stebbings, L.A., et al. (2012b). Mutational processes molding the genomes of 21 breast cancers. Cell *149*, 979–993.

Nobes, C.D., and Hall, A. (1995). Rho, Rac, and Cdc42 GTPases regulate the assembly of multimolecular focal complexes associated with actin stress fibers, lamellipodia, and filopodia. Cell *81*, 53–62.

Noll, E.M., Eisen, C., Stenzinger, A., Espinet, E., Muckenhuber, A., Klein, C., Vogel, V., Klaus, B., Nadler, W., Rösli, C., et al. (2016). CYP3A5 mediates basal and acquired therapy resistance in different subtypes of pancreatic ductal adenocarcinoma. Nat. Med. *22*, 278–287.

Nones, K., Waddell, N., Song, S., Patch, A.M., Miller, D., Johns, A., Wu, J., Kassahn, K.S., Wood, D., Bailey, P., et al. (2014). Genome-wide DNA methylation patterns in pancreatic

ductal adenocarcinoma reveal epigenetic deregulation of SLIT-ROBO, ITGA2 and MET signaling. Int. J. Cancer *135*, 1110–1118.

Olive, K.P., Jacobetz, M.A., Davidson, C.J., Gopinathan, A., McIntyre, D., Honess, D., Madhu, B., Goldgraben, M.A., Caldwell, M.E., Allard, D., et al. (2009). Inhibition of Hedgehog signaling enhances delivery of chemotherapy in a mouse model of pancreatic cancer. Science *324*, 1457–1461.

Olsson, E., Honeth, G., Bendahl, P.O., Saal, L.H., Gruvberger-Saal, S., Ringnér, M., Vallon-Christersson, J., Jönsson, G., Holm, K., Lövgren, K., et al. (2011a). CD44 isoforms are heterogeneously expressed in breast cancer and correlate with tumor subtypes and cancer stem cell markers. BMC Cancer *11*, e418. https://doi.org/10.1186/1471-2407-11-418.

Olsson, E., Honeth, G., Bendahl, P.O., Saal, L.H., Gruvberger-Saal, S., Ringnér, M., Vallon-Christersson, J., Jönsson, G., Holm, K., Lövgren, K., et al. (2011b). CD44 isoforms are heterogeneously expressed in breast cancer and correlate with tumor subtypes and cancer stem cell markers. BMC Cancer *11*.

Ongusaha, P.P., Kwak, J.C., Zwible, A.J., Macip, S., Higashiyama, S., Taniguchi, N., Fang, L., and Lee, S.W. (2004). HB-EGF is a potent inducer of tumor growth and angiogenesis. Cancer Res. *64*, 5283–5290.

Özdemir, B.C., Pentcheva-Hoang, T., Carstens, J.L., Zheng, X., Wu, C.C., Simpson, T.R., Laklai, H., Sugimoto, H., Kahlert, C., Novitskiy, S. V., et al. (2014). Depletion of carcinoma-associated fibroblasts and fibrosis induces immunosuppression and accelerates pancreas cancer with reduced survival. Cancer Cell *25*, 719–734.

Pagano, M., Pepperkok, R., Verde, F., Ansorge, W., and Draetta, G. (1992). Cyclin A is required at two points in the human cell cycle. EMBO J. *11*, 961–971.

Pandya, A.Y., Talley, L.I., Frost, A.R., Fitzgerald, T.J., Trivedi, V., Chakravarthy, M.,

Chhieng, D.C., Grizzle, W.E., Engler, J.A., Krontiras, H., et al. (2004). Nuclear Localization of KLF4 Is Associated with An Aggressive Phenotype in Early-Stage Breast Cancer. Clin. Cancer Res. *10*, 2709–2719.

Park, S.M., Gaur, A.B., Lengyel, E., and Peter, M.E. (2008). The miR-200 family determines the epithelial phenotype of cancer cells by targeting the E-cadherin repressors ZEB1 and ZEB2. Genes Dev. *22*, 894–907.

Perou, C.M., Sørile, T., Eisen, M.B., Van De Rijn, M., Jeffrey, S.S., Ress, C.A., Pollack, J.R., Ross, D.T., Johnsen, H., Akslen, L.A., et al. (2000). Molecular portraits of human breast tumours. Nature *406*, 747–752.

Phillips, T.M., McBride, W.H., and Pajonk, F. (2006). The response of CD24-/low/CD44+ breast cancer-initiating cells to radiation. J. Natl. Cancer Inst. *98*, 1777–1785.

Pierce, M.L., Weston, M.D., Fritzsch, B., Gabel, H.W., Ruvkun, G., and Soukup, G.A. (2008). MicroRNA-183 family conservation and ciliated neurosensory organ expression. Evol. Dev. *10*, 106–113.

Polytarchoua, C., Iliopoulosa, D., and Struhlc, K. (2012). An integrated transcriptional regulatory circuit that reinforces the breast cancer stem cell state. Proc. Natl. Acad. Sci. U. S. A. *109*, 14470–14475.

Ponta, H., Sherman, L., and Herrlich, P.A. (2003). CD44: From adhesion molecules to signalling regulators. Nat. Rev. Mol. Cell Biol. *4*, 33–45.

del Pozo Martin, Y., Park, D., Ramachandran, A., Ombrato, L., Calvo, F., Chakravarty, P., Spencer-Dene, B., Derzsi, S., Hill, C.S., Sahai, E., et al. (2015). Mesenchymal Cancer Cell-Stroma Crosstalk Promotes Niche Activation, Epithelial Reversion, and Metastatic Colonization. Cell Rep. *13*, 2456–2469.

Prat, A., Parker, J.S., Karginova, O., Fan, C., Livasy, C., Herschkowitz, J.I., He, X., and

Perou, C.M. (2010). Phenotypic and molecular characterization of the claudin-low intrinsic subtype of breast cancer. Breast Cancer Res. *12*, R68.

Prenzel, N., Zwick, E., Daub, H., Leserer, M., Abraham, R., Wallasch, C., and Ullrich, A. (1999). EGF receptor transactivation by G-protein-coupled receptors requires metalloproteinase cleavage of proHB-EGF. Nature *402*, 884–888.

Provenzano, P.P., Cuevas, C., Chang, A.E., Goel, V.K., Von Hoff, D.D., and Hingorani, S.R. (2012). Enzymatic Targeting of the Stroma Ablates Physical Barriers to Treatment of Pancreatic Ductal Adenocarcinoma. Cancer Cell *21*, 418–429.

Qiu, J., Yang, G., Feng, M., Zheng, S., Cao, Z., You, L., Zheng, L., Zhang, T., and Zhao, Y. (2018). Extracellular vesicles as mediators of the progression and chemoresistance of pancreatic cancer and their potential clinical applications. Mol. Cancer *17*, 2.

Raab, G., Higashiyama, S., Hetelekidis, S., Abraham, J.A., Damm, D., Ono, M., and Klagsbrun, M. (1994). Biosynthesis and processing by phorbol ester of the cell surface-associated precursor form of heparin-binding EGF-like growth factor. Biochem. Biophys. Res. Commun. *204*, 592–597.

Rath, N., Morton, J.P., Julian, L., Helbig, L., Kadir, S., McGhee, E.J., Anderson, K.I., Kalna, G., Mullin, M., Pinho, A. V, et al. (2017). ROCK signaling promotes collagen remodeling to facilitate invasive pancreatic ductal adenocarcinoma tumor cell growth . EMBO Mol. Med. *9*, 198–218.

Rath, N., Munro, J., Cutiongco, M.F., Jagiełło, A., Gadegaard, N., McGarry, L., Unbekandt, M., Michalopoulou, E., Kamphorst, J.J., Sumpton, D., et al. (2018). Rho kinase inhibition by AT13148 blocks pancreatic ductal adenocarcinoma invasion and tumor growth. Cancer Res. *78*, 3321–3336.

Rauscher, G.H., Kresovich, J.K., Poulin, M., Yan, L., Macias, V., Mahmoud, A.M., Al-Alem,

U., Kajdacsy-Balla, A., Wiley, E.L., Tonetti, D., et al. (2015). Exploring DNA methylation changes in promoter, intragenic, and intergenic regions as early and late events in breast cancer formation. BMC Cancer *15*, e816. https://doi.org/10.1186/s12885-015-1777-9.

Reches, M., and Gazit, E. (2003). Casting metal nanowires within discrete self-assembled peptide nanotubes. Science *300*, 625–627.

Reinke, L.M., Xu, Y., and Cheng, C. (2012). Snail represses the splicing regulator epithelial splicing regulatory protein 1 to promote epithelial-mesenchymal transition. J. Biol. Chem. *287*, 36425–36442.

Révillion, F., Lhotellier, V., Hornez, L., Bonneterre, J., and Peyrat, J.P. (2008). ErbB/HER ligands in human breast cancer, and relationships with their receptors, the bio-pathological features and prognosis. Ann. Oncol. *19*, 73–80.

Rhim, A.D., Oberstein, P.E., Thomas, D.H., Mirek, E.T., Palermo, C.F., Sastra, S.A., Dekleva, E.N., Saunders, T., Becerra, C.P., Tattersall, I.W., et al. (2014). Stromal elements act to restrain, rather than support, pancreatic ductal adenocarcinoma. Cancer Cell *25*, 735–747.

Rice, A.J., Cortes, E., Lachowski, D., Cheung, B.C.H., Karim, S.A., Morton, J.P., and Del Río Hernández, A. (2017). Matrix stiffness induces epithelial-mesenchymal transition and promotes chemoresistance in pancreatic cancer cells. Oncogenesis *6*, e352.

Ridley, A.J. (2001). Rho GTPases and cell migration. J. Cell Sci. *114*, 2713–2722.

Riese, D.J., Kim, E.D., Elenius, K., Buckley, S., Klagsbrun, M., Plowman, G.D., and Stern, D.F. (1996). The epidermal growth factor receptor couples transforming growth factor- α, heparin-binding epidermal growth factor-like factor, and amphiregulin to neu, erbB-3, and erbB-4. J. Biol. Chem. *271*, 20047–20052.

Rodriguez, C., Monges, G., Rouanet, P., Dutrillaux, B., Lefrançois, D., and Theillet, C.

(1995). CD44 expression patterns in breast and colon tumors: A pcr-based study of splice variants. Int. J. Cancer *64*, 347–354.

Rottner, K., Hall, A., and Small, J. V. (1999). Interplay between Rac and Rho in the control of substrate contact dynamics. Curr. Biol. *9*, 640–648.

Rucki, A.A., Foley, K., Zhang, P., Xiao, Q., Kleponis, J., Wu, A.A., Sharma, R., Mo, G., Liu, A., Van Eyk, J., et al. (2017). Heterogeneous stromal signaling within the tumor microenvironment controls the metastasis of pancreatic cancer. Cancer Res. *77*, 41–52.

Ryś, J., Kruczak, A., Lackowska, B., Jaszcz-Gruchała, A., Brandys, A., Stelmach, A., and Reinfuss, M. (2003). The Role of CD44v3 Expression in Female Breast Carcinomas. Polish J. Pathol. *54*, 243–247.

Sacheli, R., Nguyen, L., Borgs, L., Vandenbosch, R., Bodson, M., Lefebvre, P., and Malgrange, B. (2009). Expression patterns of miR-96, miR-182 and miR-183 in the developing inner ear. Gene Expr. Patterns *9*, 364–370.

Sakuma, T., Higashiyama, S., Hosoe, S., Hayashi, S., and Taniguchi, N. (1997). CD9 antigen interacts with heparin-binding EGF-Like growth factor through its heparin-binding domain. J. Biochem. *122*, 474–480.

Sandelin, A. (2004). JASPAR: an open-access database for eukaryotic transcription factor binding profiles. Nucleic Acids Res. *32*, D91–D94.

Sasaki, T., and Timpl, R. (2001). Domain IVa of laminin α5 chain is cell-adhesive and binds β1 and αVβ3 integrins through Arg-Gly-Asp. FEBS Lett. *509*, 181–185.

Sauer, L., Gitenay, D., Vo, C., and Baron, V.T. (2010). Mutant p53 initiates a feedback loop that involves Egr-1/EGF receptor/ERK in prostate cancer cells. Oncogene *29*, 2628–2637.

Saxena, S., Jónsson, Z.O., and Dutta, A. (2003). Small RNAs with imperfect match to

endogenous mRNA repress translation. Implications for off-target activity of small inhibitory RNA in mammalian cells. J. Biol. Chem. *278*, 44312–44319.

Scarlett, C.J., Colvin, E.K., Pinese, M., Chang, D.K., Morey, A.L., Musgrove, E.A., Pajic, M., Apte, M., Henshall, S.M., Sutherland, R.L., et al. (2011). Recruitment and activation of pancreatic stellate cells from the bone marrow in pancreatic cancer: A model of tumor-host interaction. PLoS One *6*, 1–8.

Schabath, H., Runz, S., Joumaa, S., and Altevogt, P. (2006). CD24 affects CXCR4 function in pre-B lymphocytes and breast carcinoma cells. J. Cell Sci. *119*, 314–325.

Schindelmann, S., Windisch, J., Grundmann, R., Kreienberg, R., Zeillinger, R., and Deissler, H. (2002). Expression profiling of mammary carcinoma cell lines: Correlation of in vitro invasiveness with expression of CD24. Tumor Biol. *23*, 139–145.

Schmidt, J.M., Panzilius, E., Bartsch, H.S., Irmler, M., Beckers, J., Kari, V., Linnemann, J.R., Dragoi, D., Hirschi, B., Kloos, U.J., et al. (2015). Stem-cell-like properties and epithelial plasticity arise as stable traits after transient twist1 activation. Cell Rep. *10*, 131–139.

Schroeder, J.A., and Lee, D.C. (1998). Dynamic expression and activation of ERBB receptors in the developing mouse mammary gland. Cell Growth Differ. *9*, 451–464.

Screaton, G.R., Bell, M. V., Jackson, D.G., Cornelis, F.B., Gerth, U., and Bell, J.I. (1992). Genomic structure of DNA encoding the lymphocyte homing receptor CD44 reveals at least 12 alternatively spliced exons. Proc. Natl. Acad. Sci. U. S. A. *89*, 12160–12164.

Seiter, S., Arch, R., Reber, S., Komitowski, D., Hofmann, M., Ponta, H., Herrlich, P., Matzku, S., and Zöller, M. (1993). Prevention of tumor metastasis formation by anti-variant CD44. J. Exp. Med. *177*, 443–455.

Senbanjo, L.T., and Chellaiah, M.A. (2017). CD44: A multifunctional cell surface adhesion receptor is a regulator of progression and metastasis of cancer cells. Front. Cell Dev. Biol. *5*,

10.3389/fcell.2017.00018.

Shaffer, A.L., Yu, X., He, Y., Boldrick, J., Chan, E.P., and Staudt, L.M. (2000). BCL-6 represses genes that function in lymphocyte differentiation, inflammation, and cell cycle control. Immunity *13*, 199–212.

Shapiro, I.M., Cheng, A.W., Flytzanis, N.C., Balsamo, M., Condeelis, J.S., Oktay, M.H., Burge, C.B., and Gertler, F.B. (2011). An EMT-driven alternative splicing program occurs in human breast cancer and modulates cellular phenotype. PLoS Genet. *7*, e1002218.

Sherman, M.H., Yu, R.T., Engle, D.D., Ding, N., Atkins, A.R., Tiriac, H., Collisson, E.A., Connor, F., Van Dyke, T., Kozlov, S., et al. (2014). Vitamin D receptor-mediated stromal reprogramming suppresses pancreatitis and enhances pancreatic cancer therapy. Cell *159*, 80–93.

Sherman, M.H., Yu, R.T., Tseng, T.W., Sousa, C.M., Liu, S., Truitt, M.L., He, N., Ding, N., Liddle, C., Atkins, A.R., et al. (2017). Stromal cues regulate the pancreatic cancer epigenome and metabolome. Proc. Natl. Acad. Sci. U. S. A. *114*, 1129–1134.

Shi, Y., Zhao, Y., Shao, N., Ye, R., Lin, Y., Zhang, N., Li, W., Zhang, Y., and Wang, S. (2017). Overexpression of microRNA-96-5p inhibits autophagy and apoptosis and enhances the proliferation, migration and invasiveness of human breast cancer cells. Oncol. Lett. *13*, 4402–4412.

Shimono, Y., Zabala, M., Cho, R.W., Lobo, N., Dalerba, P., Qian, D., Diehn, M., Liu, H., Panula, S.P., Chiao, E., et al. (2009). Downregulation of miRNA-200c Links Breast Cancer Stem Cells with Normal Stem Cells. Cell *138*, 592–603.

Shirakata, Y., Kimura, R., Nanba, D., Iwamoto, R., Tokumaru, S., Morimoto, C., Yokota, K., Nakamura, M., Sayama, K., Mekada, E., et al. (2005). Heparin-binding EGF-like growth factor accelerates keratinocyte migration and skin wound healing. J. Cell Sci. *118*, 2363–

2370.

Silverman, B.R., and Shi, J. (2016). Alterations of epigenetic regulators in pancreatic cancer and their clinical implications. Int. J. Mol. Sci. *17*, 2138.

Smith, A.M., Williams, R.J., Tang, C., Coppo, P., Collins, R.F., Turner, M.L., Saiani, A., and Ulijn, R. V. (2008). Fmoc-diphenylalanine self assembles to a hydrogel via a novel architecture based on π-π interlocked β-sheets. Adv. Mater. *20*, 37–41.

Song, C., Zhang, L., Wang, J., Huang, Z., Li, X., Wu, M., Li, S., Tang, H., and Xie, X. (2016). High expression of microRNA-183/182/96 cluster as a prognostic biomarker for breast cancer. Sci. Rep. *6*, 24502. https://doi.org/10.1038/srep24502.

Sørlie, T., Perou, C.M., Tibshirani, R., Aas, T., Geisler, S., Johnsen, H., Hastie, T., Eisen, M.B., Van De Rijn, M., Jeffrey, S.S., et al. (2001). Gene expression patterns of breast carcinomas distinguish tumor subclasses with clinical implications. Proc. Natl. Acad. Sci. U. S. A. *98*, 10869–10874.

Sparmann, G., Kruse, M.L., Hofmeister-Mielke, N., Koczan, D., Jaster, R., Liebe, S., Wolff, D., and Emmrich, J. (2010). Bone marrow-derived pancreatic stellate cells in rats. Cell Res. *20*, 288–298.

Stinson, S., Lackner, M.R., Adai, A.T., Yu, N., Kim, H.J., O'Brien, C., Spoerke, J., Jhunjhunwala, S., Boyd, Z., Januario, T., et al. (2011). TRPS1 targeting by miR-221/222 promotes the epithelial-to-mesenchymal transition in breast cancer. Sci. Signal. *4*, ra41.

Suzuki, M., Raab, G., Moses, M.A., Fernandez, C.A., and Klagsbrun, M. (1997). Matrix metalloproteinase-3 releases active heparin-binding EGF-like growth factor by cleavage at a specific juxtamembrane site. J. Biol. Chem. *272*, 31730–31737.

Svensson, K.J., Kucharzewska, P., Christianson, H.C., Sköld, S., Löfstedt, T., Johansson, M.C., Mörgelin, M., Bengzon, J., Ruf, W., and Belting, M. (2011). Hypoxia triggers a

proangiogenic pathway involving cancer cell microvesicles and PAR-2-mediated heparin-binding EGF signaling in endothelial cells. Proc. Natl. Acad. Sci. U. S. A. *108*, 13147–13152.

Takahashi, K., Ehata, S., Koinuma, D., Morishita, Y., Soda, M., Mano, H., and Miyazono, K. (2018). Pancreatic tumor microenvironment confers highly malignant properties on pancreatic cancer cells. Oncogene *37*, 2757–2772.

Tamamis, P., Adler-Abramovich, L., Reches, M., Marshall, K., Sikorski, P., Serpell, L., Gazit, E., and Archontis, G. (2009). Self-assembly of phenylalanine oligopeptides: Insights from experiments and simulations. Biophys. J. *96*, 5020–5029.

Tani, T., Lumme, A., Linnala, A., Kivilaakso, E., Kiviluoto, T., Burgeson, R.E., Kangas, L., Leivo, I., and Virtanen, I. (1997). Pancreatic carcinomas deposit laminin-5, preferably adhere to laminin- 5, and migrate on the newly deposited basement membrane. Am. J. Pathol. *151*, 1289–1302.

Tashiro, K., Monji, A., Yoshida, I., Hayashi, Y., Matsuda, K., Tashiro, N., and Mitsuyama, Y. (1999). An IKLLI-containing peptide derived from the laminin α1 chain mediating heparin-binding, cell adhesion, neurite outgrowth and proliferation, represents a binding site for integrin α3β1 and heparan sulphate proteoglycan. Biochem. J. *340*, 119–126.

Tempero, M.A., Van Cutsem, E., Sigal, D., Oh, D.-Y., Fazio, N., Macarulla, T., Hitre, E., Hammel, P., Hendifar, A.E., Bates, S.E., et al. (2020). HALO 109-301: A randomized, double-blind, placebo-controlled, phase 3 study of pegvorhyaluronidase alfa (PEGPH20) + nab-paclitaxel/gemcitabine (AG) in patients (pts) with previously untreated hyaluronan (HA)-high metastatic pancreatic ductal adenocarcinom. J. Clin. Oncol. *38*, 638.

Theocharis, A.D., Tsara, M.E., Papageorgacopoulou, N., Karavias, D.D., and Theocharis, D.A. (2000). Pancreatic carcinoma is characterized by elevated content of hyaluronan and

chondroitin sulfate with altered disaccharide composition. Biochim. Biophys. Acta - Mol. Basis Dis. *1502*, 201–206.

Thompson, S.A., Higashiyama, S., Wood, K., Pollitt, N.S., Damm, D., McEnroe, G., Garrick, B., Ashton, N., Lau, K., Hancock, N., et al. (1994). Characterization of sequences within heparin-binding EGF-like growth factor that mediate interaction with heparin. J. Biol. Chem. *28*, 2541–2549.

Tidcombe, H., Jackson-Fishert, A., Mathers, K., Stern, D.F., Gassmann, M., and Golding, J.P. (2003). Neural and mammary gland defects in Erbb4 knockout mice genetically rescued from embryonic lethality. Proc. Natl. Acad. Sci. U. S. A. *100*, 8281–8286.

Torres, L., Ribeiro, F.R., Pandis, N., Andersen, J.A., Heim, S., and Teixeira, M.R. (2007). Intratumor genomic heterogeneity in breast cancer with clonal divergence between primary carcinomas and lymph node metastases. Breast Cancer Res. Treat. *102*, 143–155.

Tsai, S., McOlash, L., Palen, K., Johnson, B., Duris, C., Yang, Q., Dwinell, M.B., Hunt, B., Evans, D.B., Gershan, J., et al. (2018). Development of primary human pancreatic cancer organoids, matched stromal and immune cells and 3D tumor microenvironment models. BMC Cancer *18*, 335.

Tse, G.M.K., Tan, P.H., Ma, T.K.F., Gilks, C.B., Poon, C.S.P., and Law, B.K.B. (2005). CD44s is useful in the differentiation of benign and malignant papillary lesions of the breast. J. Clin. Pathol. *58*, 1185–1188.

Underhill, C. (1992). CD44: The hyaluronan receptor. J. Cell Sci. *103*, 293–298.

Vennin, C., Chin, V.T., Warren, S.C., Lucas, M.C., Herrmann, D., Magenau, A., Melenec, P., Walters, S.N., Del Monte-Nieto, G., Conway, J.R.W., et al. (2017). Transient tissue priming via ROCK inhibition uncouples pancreatic cancer progression, sensitivity to chemotherapy, and metastasis. Sci. Transl. Med. *9*, eaai8504.

Virtanen, I., Gullberg, D., Rissanen, J., Kivilaakso, E., Kiviluoto, T., Laitinen, L.A., Lehto, V.P., and Ekblom, P. (2000). Laminin α1-chain shows a restricted distribution in epithelial basement membranes of fetal and adult human tissues. Exp. Cell Res. *257*, 298–309.

Vlaicu, P., Mertins, P., Mayr, T., Widschwendter, P., Ataseven, B., Högel, B., Eiermann, W., Knyazev, P., and Ullrich, A. (2013). Monocytes/macrophages support mammary tumor invasivity by co-secreting lineage-specific EGFR ligands and a STAT3 activator. BMC Cancer *13*, 197. doi: 10.1186/1471-2407-13–197.

Volinia, S., Calin, G.A., Liu, C.G., Ambs, S., Cimmino, A., Petrocca, F., Visone, R., Iorio, M., Roldo, C., Ferracin, M., et al. (2006). A microRNA expression signature of human solid tumors defines cancer gene targets. Proc. Natl. Acad. Sci. U. S. A. *103*, 2257–2261.

Waddell, N., Pajic, M., Patch, A.M., Chang, D.K., Kassahn, K.S., Bailey, P., Johns, A.L., Miller, D., Nones, K., Quek, K., et al. (2015). Whole genomes redefine the mutational landscape of pancreatic cancer. Nature *518*, 495–501.

Walsh, N., Clynes, M., Crown, J., and O'Donovan, N. (2009). Alterations in integrin expression modulates invasion of pancreatic cancer cells. J. Exp. Clin. Cancer Res. *28*, https://doi.org/10.1186/1756-9966-28-140.

Wang, H., Wang, L., Song, Y., Wang, S., Huang, X., Xuan, Q., Kang, X., and Zhang, Q. (2017). CD44+/CD24- phenotype predicts a poor prognosis in triple-negative breast cancer. Oncol. Lett. *14*, 5890–5898.

Wang, Y., Huang, J.W., Calses, P., Kemp, C.J., and Taniguchi, T. (2012). MiR-96 downregulates REV1 and RAD51 to promote cellular sensitivity to cisplatin and PARP inhibition. Cancer Res. *72*, 4037–4046.

Wang, Y., Waters, J., Leung, M.L., Unruh, A., Roh, W., Shi, X., Chen, K., Scheet, P., Vattathil, S., Liang, H., et al. (2014). Clonal evolution in breast cancer revealed by single

nucleus genome sequencing. Nature *512*, 155–160.

Warburg, O. (1956). Injuring of Respiration the Origin of Cancer Cells. Science *123*, 309–314.

Warburg, O., Wind, F., and Negelein, E. (1927). The metabolism of tumors in the body. J. Gen. Physiol. *8*, 519–530.

Ward, P.S., and Thompson, C.B. (2012). Metabolic Reprogramming: A Cancer Hallmark Even Warburg Did Not Anticipate. Cancer Cell *21*, 297–308.

Watari, N., Hotta, Y., and Mabuchi, Y. (1982). Morphological Studies on a Vitamin A-Storing Cell and its Complex with Macrophage Observed in Mouse Pancreatic Tissues following Excess Vitamin A Administration. Okajimas Folia Anat. Jpn. *58*, 837–858.

Weber, G.F., Ashkar, S., Glimcher, M.J., and Cantor, H. (1996). Receptor-ligand interaction between CD44 and osteopontin (Eta-1). Science *271*, 509–512.

Weg-Remers, S., Ponta, H., Herrlich, P., and König, H. (2001). Regulation of alternative pre-mRNA splicing by the ERK MAP-kinase pathway. EMBO J. *20*, 4194–4203.

Weinberg, R.A. (1995). The retinoblastoma protein and cell cycle control. Cell *81*, 323–330.

Wellner, U., Schubert, J., Burk, U.C., Schmalhofer, O., Zhu, F., Sonntag, A., Waldvogel, B., Vannier, C., Darling, D., Hausen, A. Zur, et al. (2009). The EMT-activator ZEB1 promotes tumorigenicity by repressing stemness-inhibiting microRNAs. Nat. Cell Biol. *11*, 1487–1495.

Weston, M.D., Pierce, M.L., Rocha-Sanchez, S., Beisel, K.W., and Soukup, G.A. (2006). MicroRNA gene expression in the mouse inner ear. Brain Res. *1111*, 95–104.

Weston, M.D., Pierce, M.L., Jensen-Smith, H.C., Fritzsch, B., Rocha-Sanchez, S., Beisel, K.W., and Soukup, G.A. (2011). MicroRNA-183 family expression in hair cell development and requirement of microRNAs for hair cell maintenance and survival. Dev. Dyn. *240*, 808–

819.

Whatcott, C.J., Han, H., and Von Hoff, D.D. (2015a). Orchestrating the Tumor Microenvironment to Improve Survival for Patients With Pancreatic Cancer: Normalization, Not Destruction. Cancer J. *21*, 299–306.

Whatcott, C.J., Diep, C.H., Jiang, P., Watanabe, A., Lobello, J., Sima, C., Hostetter, G., Shepard, H.M., Von Hoff, D.D., and Han, H. (2015b). Desmoplasia in primary tumors and metastatic lesions of pancreatic cancer. Clin. Cancer Res. *21*, 3561–3568.

Whatcott, C.J., Ng, S., Barrett, M.T., Hostetter, G., Von Hoff, D.D., and Han, H. (2017). Inhibition of ROCK1 kinase modulates both tumor cells and stromal fibroblasts in pancreatic cancer. PLoS One *12*, 1–18.

Witkiewicz, A.K., McMillan, E.A., Balaji, U., Baek, G.H., Lin, W.C., Mansour, J., Mollaee, M., Wagner, K.U., Koduru, P., Yopp, A., et al. (2015). Whole-exome sequencing of pancreatic cancer defines genetic diversity and therapeutic targets. Nat. Commun. *6*, e6744.

Wu, L., Fan, J., and Belasco, J.G. (2006). MicroRNAs direct rapid deadenylation of mRNA. Proc. Natl. Acad. Sci. U. S. A. *103*, 4034–4039.

Xie, D., and Xie, K. (2015). Pancreatic cancer stromal biology and therapy. Genes Dis. *2*, 133–143.

Xie, W., Sun, F., Chen, L., and Cao, X. (2018). MiR-96 promotes breast cancer metastasis by suppressing MTSS1. Oncol. Lett. *15*, 3464–3471.

Xu, S., Witmer, P.D., Lumayag, S., Kovacs, B., and Valle, D. (2007). MicroRNA (miRNA) transcriptome of mouse retina and identification of a sensory organ-specific miRNA cluster. J. Biol. Chem. *282*, 25053–25066.

Xu, Y., Gao, X.D., Lee, J.H., Huang, H., Tan, H., Ahn, J., Reinke, L.M., Peter, M.E., Feng,

Y., Gius, D., et al. (2014). Cell type-restricted activity of hnRNPM promotes breast cancer metastasis via regulating alternative splicing. Genes Dev. *28*, 1191–1203.

Yae, T., Tsuchihashi, K., Ishimoto, T., Motohara, T., Yoshikawa, M., Yoshida, G.J., Wada, T., Masuko, T., Mogushi, K., Tanaka, H., et al. (2012). Alternative splicing of CD44 mRNA by ESRP1 enhances lung colonization of metastatic cancer cell. Nat. Commun. *6*, 883.

Yamano, M., Fujii, H., Takagaki, T., Kadowaki, N., Watanabe, H., and Shirai, T. (2000). Genetic progression and divergence in pancreatic carcinoma. Am. J. Pathol. *156*, 2123–2133.

Yamashita, A., Chang, T.C., Yamashita, Y., Zhu, W., Zhong, Z., Chen, C.Y.A., and Shyu, A. Bin (2005). Concerted action of poly(A) nucleases and decapping enzyme in mammalian mRNA turnover. Nat. Struct. Mol. Biol. *12*, 1054–1063.

Yang, C., Wang, Z., Ou, C., Chen, M., Wang, L., and Yang, Z. (2014a). A supramolecular hydrogelator of curcumin. Chem. Commun. *50*, 9413–9415.

Yang, M., Pan, Y., and Zhou, Y. (2014b). MiR-96 promotes osteogenic differentiation by suppressing HBEGF-EGFR signaling in osteoblastic cells. FEBS Lett. *588*, 4761–4768.

Yang, Z., Liang, G., and Xu, B. (2006). Supramolecular hydrogels based on β-amino acid derivatives. Chem. Commun. 738–740.

Yang, Z., Xu, K., Guo, Z., Guo, Z., and Xu, B. (2007). Intracellular enzymatic formation of nanofibers results in hydrogelation and regulated cell death. Adv. Mater. *19*, 3152–3156.

Yang, Z., Chen, D., Nie, J., Zhou, S., Wang, J., Tang, Q., and Yang, X. (2016). MicroRNA-143 targets CD44 to inhibit breast cancer progression and stem cell-like properties. Mol. Med. Rep. *13*, 5193–5199.

Yarden, Y., and Sliwkowski, M.X. (2001). Untangling the ErbB signalling network. Nat. Rev. Mol. Cell Biol. *2*, 127–137.

Yates, L.R., Gerstung, M., Knappskog, S., Desmedt, C., Gundem, G., Van Loo, P., Aas, T., Alexandrov, L.B., Larsimont, D., Davies, H., et al. (2015). Subclonal diversification of primary breast cancer revealed by multiregion sequencing. Nat. Med. *21*, 751–759.

Ye, X., Tam, W.L., Shibue, T., Kaygusuz, Y., Reinhardt, F., Ng Eaton, E., and Weinberg, R.A. (2015). Distinct EMT programs control normal mammary stem cells and tumour-initiating cells. Nature *525*, 256–260.

Yeyati, P.L., Shaknovich, R., Boterashvili, S., Li, J., Ball, H.J., Waxman, S., Nason-Burchenal, K., Dmitrovsky, E., Zelent, A., and Licht, J.D. (1999). Leukemia translocation protein PLZF inhibits cell growth and expression of cyclin A. Oncogene *18*, 925–934.

Yoda, M., Kawamata, T., Paroo, Z., Ye, X., Iwasaki, S., Liu, Q., and Tomari, Y. (2010). ATP-dependent human RISC assembly pathways. Nat. Struct. Mol. Biol. *17*, 17–23.

Yotsumoto, F., Oki, E., Tokunaga, E., Maehara, Y., Kuroki, M., and Miyamoto, S. (2010). HB-EGF orchestrates the complex signals involved in triple-negative and trastuzumab-resistant breast cancer. Int. J. Cancer *127*, 2707–2717.

Yotsumoto, F., Tokunaga, E., Oki, E., Maehara, Y., Yamada, H., Nakajima, K., Nam, S.O., Miyata, K., Koyanagi, M., Doi, K., et al. (2013). Molecular Hierarchy of Heparin-Binding EGF-like Growth Factor-Regulated Angiogenesis in Triple-Negative Breast Cancer. Mol. Cancer Res. *11*, 506–517.

Yu, Q., and Stamenkovic, I. (1999). Localization of matrix metalloproteinase 9 to the cell surface provides a mechanism for CD44-mediated tumor invasion. Genes Dev. *13*, 35–48.

Yu, F., Yao, H., Zhu, P., Zhang, X., Pan, Q., Gong, C., Huang, Y., Hu, X., Su, F., Lieberman, J., et al. (2007). let-7 Regulates Self Renewal and Tumorigenicity of Breast Cancer Cells. Cell *131*, 1109–1123.

Yu, S., Geng, Q., Ma, J., Sun, F., Yu, Y., Pan, Q., and Hong, A. (2013). Heparin-binding

EGF-like growth factor and miR-1192 exert opposite effect on Runx2-induced osteogenic differentiation. Cell Death Dis. *4*, e868.

Yu, W.H., Woessner, F., McNeish, J.D., and Stamenkovic, I. (2002). CD44 anchors the assembly of matrilysin/MMP-7 with heparin-binding epidermal growth factor precursor and ErbB4 and regulates female reproductive organ remodeling. Genes Dev. *16*, 307–323.

Yuan, S., Norgard, R.J., and Stanger, B.Z. (2019). Cellular plasticity in cancer. Cancer Discov. *9*, 837–851.

Yukio, I., and Kimura, S. (1992). Peptide Self-Assembly in Phospholipid Bilayer Membrane. Proc. Japan Acad. Ser. B Phys. Biol. Sci. *68*, 121–126.

Zeng, Y., Yi, R., and Cullen, B.R. (2003). MicroRNAs and small interfering RNAs can inhibit mRNA expression by similar mechanisms. Proc. Natl. Acad. Sci. U. S. A. *100*, 9779–9784.

Zhang, H., Brown, R.L., Wei, Y., Zhao, P., Liu, S., Liu, X., Deng, Y., Hu, X., Zhang, J., Gao, X.D., et al. (2019a). CD44 splice isoform switching determines breast cancer stem cell state. Genes Dev. *33*, 166–179.

Zhang, J., Kong, X., Li, J., Luo, Q., Li, X., Shen, L., Chen, L., and Fang, L. (2014). MiR-96 promotes tumor proliferation and invasion by targeting RECK in breast cancer. Oncol. Rep. *31*, 1357–1363.

Zhang, Q.H., Sun, H.M., Zheng, R.Z., Li, Y.C., Zhang, Q., Cheng, P., Tang, Z.H., and Huang, F. (2013). Meta-analysis of microRNA-183 family expression in human cancer studies comparing cancer tissues with noncancerous tissues. Gene *527*, 26–32.

Zhang, S., Holmes, T., Lockshin, C., and Rich, A. (1993). Spontaneous assembly of a self-complementary oligopeptide to form a stable macroscopic membrane. Proc. Natl. Acad. Sci. U. S. A. *90*, 3334–3338.

Zhang, W., Qian, P., Zhang, X., Zhang, M., Wang, H., Wu, M., Kong, X., Tan, S., Ding, K., Perry, J.K., et al. (2015). Autocrine/paracrine human growth hormone-stimulated microRNA 96-182-183 cluster promotes epithelial-mesenchymal transition and invasion in breast cancer. J. Biol. Chem. *290*, 13812–13829.

Zhang, X., Marjani, S.L., Hu, Z., Weissman, S.M., Pan, X., and Wu, S. (2016). Single-Cell sequencing for precise cancer research: Progress and prospects. Cancer Res. *76*, 1305–1312.

Zhang, Y., Crawford, H.C., and Pasca di Magliano, M. (2019b). Epithelial-Stromal Interactions in Pancreatic Cancer. Annu. Rev. Physiol. *81*, 211–233.

Zhao, T., Ren, H., Li, J., Chen, J., Zhang, H., Xin, W., Sun, Y., Sun, L., Yang, Y., Sun, J., et al. (2015). LASP1 is a HIF1α target gene critical for metastasis of pancreatic cancer. Cancer Res. *75*, 111–119.

Zhou, X., Guo, X., Chen, M., Xie, C., and Jiang, J. (2018). HIF-3α promotes metastatic phenotypes in pancreatic cancer by transcriptional regulation of the RhoC-ROCK1 signaling pathway. Mol. Cancer Res. *16*, 124–134.

Zhou, Z.N., Sharma, V.P., Beaty, B.T., Roh-Johnson, M., Peterson, E.A., Van Rooijen, N., Kenny, P.A., Wiley, H.S., Condeelis, J.S., and Segall, J.E. (2014). Autocrine HBEGF expression promotes breast cancer intravasation, metastasis and macrophage-independent invasion in vivo. Oncogene *33*, 3784–3793.

Zuo, J., Yu, Y., Zhu, M., Jing, W., Yu, M., Chai, H., Liang, C., and Tu, J. (2018). Inhibition of miR-155, a therapeutic target for breast cancer, prevented in cancer stem cell formation. Cancer Biomarkers *21*, 383–392.